

2015

Phenology and allocation of belowground plant carbon at local to global scales

<https://hdl.handle.net/2144/16357>

Boston University

BOSTON UNIVERSITY
GRADUATE SCHOOL OF ARTS AND SCIENCES

Dissertation

**PHENOLOGY AND ALLOCATION OF BELOWGROUND PLANT CARBON AT
LOCAL TO GLOBAL SCALES**

by

ROSE Z. ABRAMOFF

B.A., Amherst College, 2009

Submitted in partial fulfillment of the
requirements for the degree of
Doctor of Philosophy

2015

Approved by

First Reader

Adrien C. Finzi, Ph.D.
Professor of Biology

Second Reader

Lucy Hutyra, Ph.D.
Assistant Professor of Earth & Environment

Third Reader

Jennifer Talbot, Ph.D.
Assistant Professor of Biology

ACKNOWLEDGEMENTS

I thank my thesis advisor, Adrien Finzi, whose guidance was critical to the development of my research interests, expertise, and this document. I thank him for holding my work to a high standard, and for challenging me to think broadly and critically. Because of his continuing support, I feel prepared to begin a career in research. I also thank my committee members: Lucy Hutyra, Pamela Templer, Richard Primack, Nathan Phillips, and Jennifer Talbot, for years of thoughtful discussion, advice, and encouragement. This work is also a product of their guidance.

The field work, lab work, and image analysis presented here could not have been completed without the help of the following students, who enriched my experience by allowing me to mentor them for their own independent projects, projects supporting this thesis, and in their next steps in science: Amanda Alon, Samuel Knapp, Johanna Recalde, Arline Gould, and Aubree Woods. I also thank my labmates Allison Gill, Pat Sorensen, Mustafa Saifuddin, and Marc-Andre Giasson, for field work help, invaluable discussion and advice, and all the good times. To my fellow EBE and Biogeosciences graduate students, too many to name, I thank you for your support, inspiration, friendship, cookies, and beer.

Lastly, I would like to thank my family, and especially my parents, for a creative and intellectual childhood, for the privileges they have afforded me, and for their unconditional love.

**PHENOLOGY AND ALLOCATION OF BELOWGROUND PLANT CARBON AT
LOCAL TO GLOBAL SCALES**

(Order No.)

ROSE Z. ABRAMOFF

Boston University Graduate School of Arts and Sciences, 2015

Major Professor: Adrien C. Finzi, Professor of Biology

ABSTRACT

Forests play an important role in mitigating climate change by removing carbon dioxide (CO₂) from the atmosphere via photosynthesis and storing it in plant tissues and soil organic matter (SOM). Plant roots are a major conduit for transporting recently fixed CO₂ belowground, where carbon (C) remains in SOM or returns to the atmosphere via respiration of soil microbes. Compared to aboveground plant processes related to the C cycle, there is little understanding of how belowground plant-C allocation to roots, symbiotic root fungi and secretions into the soil influence the gain or loss of C from the soil. Further, the uncertainty in the timing and amount of root growth that occurs in forests is a barrier to understanding how root activity responds to global change and feeds back to the C cycle. Therefore, the objective of my research is to quantify the timing and magnitude of C allocation to roots and soil via data compilation, field studies and modeling across broad spatial scales. Using data compilation at the global scale, I show that root and shoot phenology are often asynchronous and that evergreen trees commonly have later root growth compared to deciduous trees using meta-analysis across four

biomes. At the plot scale, field studies in a mid-latitude forest demonstrate that deciduous stands allocate more C belowground earlier in the growing season compared to a conifer stand. The difference in phenology between stands can be attributed to the timing of root growth. At the root scale, zymographic analysis demonstrates that microbial extracellular enzyme activity is concentrated near the surface of roots and that the rhizosphere can extend well beyond 2 mm from the root surface. Finally, I developed a new model of microbial physiology and extracellular enzyme activity to assess how climate change may affect plant – microbe interactions and soil organic matter decomposition. I show that increases in temperature and the quantity of C inputs substantially alter decomposition. Collectively, these results demonstrate the importance of belowground allocation to the C cycle of terrestrial ecosystems.

TABLE OF CONTENTS

ACKNOWLEDGEMENTS	iv
ABSTRACT.....	v
TABLE OF CONTENTS.....	vii
LIST OF TABLES	xii
LIST OF FIGURES	xvii
LIST OF ABBREVIATIONS.....	xxvi
CHAPTER ONE: INTRODUCTION.....	1
Dissertation Overview	7
CHAPTER TWO: ARE ABOVE AND BELOWGROUND PHENOLOGY IN SYNC? 11	
Abstract.....	11
Introduction.....	12
A compilation of available data	13
Primary Data Findings	14
Some Implications of the Data.....	16
Moving Forward	20
Acknowledgements.....	21
Supplementary Information	28
Paper selection	28

Gross and net root production.....	28
Offset.....	29
Monthly root and shoot growth.....	30
Temperature and precipitation data	30
Supplementary Information Reference Guide	46

CHAPTER THREE: SEASONALITY AND PARTITIONING OF ROOT

ALLOCATION TO RHIZOSPHERE SOILS IN A MID-LATITUDE FOREST	54
Abstract.....	54
Introduction.....	56
Materials and Methods.....	58
Study Site	58
Root Production and Biomass.....	59
Root Respiration	62
Nonstructural Carbohydrates	63
Root Exudation	63
Total Belowground C Flux	64
Data Analysis	66
Results.....	67
Root Production and Biomass.....	67
Root Respiration	69
Nonstructural Carbohydrates and Root Exudation	70
Total Belowground C Flux	70

Discussion	71
Phenology of Root Growth and Mortality	72
Environmental Controls over Root Growth and Respiration.....	73
Nonstructural Carbohydrates and Root Exudation	74
Total Belowground C Flux	76
Summary	78
Acknowledgements.....	78

CHAPTER FOUR: WHERE DOES THE RHIZOSPHERE END? SPATIALLY

RESOLVED MEASUREMENTS OF IN SITU SOIL EXTRACELLULAR ENZYME

ACTIVITY	95
Abstract	95
Introduction.....	97
Methods.....	99
Site description.....	99
Results.....	105
Visual inspection.....	105
Coarse image resolution.....	106
Fine image resolution.....	107
Very fine image resolution.....	108
Discussion	108
Rhizosphere extent across stand types and enzyme classes.....	109
Effects of image analysis resolution	109

Methodological considerations	111
Conclusions.....	113
CHAPTER FIVE: A PARSIMONIOUS MODULAR APPROACH TO BUILDING A MECHANISTIC BELOWGROUND C AND N MODEL	128
Abstract	128
Introduction.....	130
Methods.....	133
Model description	133
Model comparison	138
Root input measurements.....	139
Model simulation of microbial physiology response to C:N ratio.....	140
Model simulations of global change	140
Results.....	141
Model comparison	141
Model simulation of microbial physiology response to C:N	142
Model simulations of global change	143
Discussion.....	144
Model comparison	144
Model simulation of microbial physiology response to C:N	146
Model simulations of global change	147
Summary	149

CHAPTER SIX: CONCLUSION	168
Phenology and C allocation	168
Modeling the micro-site at global scales	171
Summary	174
LITERATURE CITED	176
CURRICULUM VITAE.....	210

LIST OF TABLES

<p>Table 2.1. Parameters for phenology and carbon allocation in terrestrial biosphere models (GDD: growing degree-days, LAI: leaf area index, PFT: plant functional type, NSC: nonstructural carbohydrate).....</p>	23
<p>Table 2.2. Regression statistics for the proportion of maximum monthly root or shoot growth as a function of median monthly temperature (MMT) or mean monthly precipitation (MMP). The slope estimate (β) for MMT are in units of growth per °C and MMP growth per mm precipitation. Significant variables and overall model significance are indicated by: NS = not significant, * P < 0.05, ** P < 0.01 and *** P < 0.001.</p>	24
<p>Table 2.S1. Phenological relationships between aboveground and belowground processes as well as potential drivers of belowground phenology, their direction and strength of effect, if given. ST, temperature; SWC, soil water content; E, endogenous.....</p>	34
<p>Table 2.S2. Measurements from literature used to quantify the offset between aboveground and belowground growth peaks in Figures 1 and 2. Methods used to measure root production varied by study (¹change in root biomass, ²minirhizotron, ³field rhizotron or root box, ⁴soil CO₂ efflux). AP, day of year aboveground peak; #AP, number of aboveground production peaks; BP, day of year belowground peak; #BP, number of belowground production peaks; H, herbaceous; W, woody, MMT, median monthly temperature (°C); MMP, mean monthly precipitation (mm); REF, reference.....</p>	38

Table 2.S3. Monthly root and shoot growth rates for each biome estimated from literature. Growth rate of roots and shoots were tabulated from each study (excluding those that did not include seasonal data [i.e. measured DOY 1 as start of experiment rather than the Julian day]) and converted to a % of the maximum growth rate. Growth rates were averaged for each month with > 5 observations. These rates do not exceed 1 because many studies with differently timed maximum growth were averaged. MMT, median monthly temperature (°C); MMP, mean monthly precipitation (mm). 43

Table 3.1. Stand-level characteristics. Total C content refers to organic and mineral horizon soil C down to 15 cm. Letters indicate a statistically significant difference in means using analysis of variance at the $P < 0.05$ level. 80

Table 3.2. Summary of multiple linear regression statistics that model log(fine root growth) for each stand as a function of soil temperature. Fine root growth was log-transformed to meet assumptions of normality. *** $P < 0.001$, ** $P < 0.01$, * $P < 0.05$, . $P < 0.1$ 81

Table 3.3. Summary of multiple linear regression statistics that model fine root growth, mortality, and mass-specific respiration as a function of soil temperature and precipitation. Growth and mortality were log-transformed to meet assumptions of normality. *** $P < 0.001$, ** $P < 0.01$, * $P < 0.05$, . $P < 0.1$ 82

Table 3.4. Median root biomass (5th percentile, 95th percentile) in g C m^{-2} estimated from minirhizotron tubes binned in 10 cm depth increments. Uppercase letters indicate

significant differences between columns, and lowercase letters indicate significant differences between rows at the $P < 0.01$ level..... 83

Table 3.5. Exudation rate (\pm SE) for samples collected in 2012 and 2013. There is a significant effect of sample date ($F_{1,106} = 8.0$, $P < 0.01$), but no differences between years or stands. The exudate rate on the April sample date (DOY = 106) was significantly lower than the exudation rate measured on June, July, and October sample dates at the $P < 0.05$ level. 84

Table 3.6. Total belowground carbon flux (TBCF, $\text{g C m}^{-2} \text{gs}^{-1}$) for each stand. TBCF_{top} is defined as $F_{\text{efflux}} + F_{\text{leaching}} - F_{\text{litter}} + \Delta(C_{\text{roots}} + C_{\text{soil}})$. $\text{TBCF}_{\text{bottom}}$ is $F_{\text{roots}} + F_{\text{resp}} + F_{\text{exudates}}$ 85

Table 3.7. Activation energy (E_a , kJ mol^{-1}), pre-exponential constant (A , $\text{nmol CO}_2 \text{s}^{-1} \text{g}^{-1}$), and R^2 of mass-specific rates of root respiration ($\text{nmol CO}_2 \text{g}^{-1} \text{s}^{-1}$) for each stand over the growing season..... 86

Table 3.8. Statistical summary of mixed-effects models with fine root growth, mortality, respiration, NSC concentration, or exudation as the dependent variable. The fixed effects were stand, sample date, and year with plot as a random effect. Growth and mortality were log-transformed to meet assumptions of normality. *** $P < 0.001$, ** $P < 0.01$, * $P < 0.05$, . $P < 0.1$87

Table 4.1. Summary of spatial error model regression coefficients estimated at coarse resolution. Enzyme activity (EU ml^{-1} or mM) is modeled as a function of distance from a root (mm) and soil depth (mm). ρ is the spatial error coefficient. AIC is the Akaike information criterion, a model-selection score that balances goodness-of-fit

<p>against the number of parameters. Regression coefficients, ρ, and AIC for each image were averaged to obtain one value for each stand and enzyme. AP = acid phosphatase, PR = aminopeptidase, BG = beta-glucosidase, NAG = N-acetyl-beta-D-glucosaminidase, F = white ash, Q = red oak, T = eastern hemlock.</p>	115
<p>Table 4.2. Summary of spatial error model regression coefficients estimated at fine resolution. Enzyme activity (EU ml^{-1} or mM) is modeled as a function of distance from a root (mm) and soil depth (mm). ρ is the spatial error coefficient. AIC is the Akaike information criterion, a model-selection score that balances goodness-of-fit against the number of parameters. Regression coefficients, ρ, and AIC for each image were averaged to obtain one value for each stand and enzyme. AP = acid phosphatase, PR = aminopeptidase, BG = beta-glucosidase, NAG = N-acetyl-beta-D-glucosaminidase, F = white ash, Q = red oak, T = eastern hemlock.</p>	116
<p>Table 4.3. Tukey's HSD test on an ANOVA model of rooted area (cm^2) per 20×20 cm panel as a function of stand. Different superscript letters denote significant differences at $P < 0.05$.</p>	117
<p>Table 5.1. DAMM-MCNiP default model parameter values.</p>	151
<p>Table 5.2. Initial pool sizes (Spin Up) and the resulting default initial pool sizes (Default) after 2000 years of spin-up.</p>	153
<p>Table 5.3. Parameter values for the C:N of litter, root inputs, and microbial biomass for two theoretical stands.</p>	154

Table 5.4. Annual C and N mineralization predicted by DAMM-MCNiP in four simulations that manipulate either temperature or soil moisture. Here θ refers to volumetric soil moisture. 155

LIST OF FIGURES

Figure 2.1. Kernel density curve of the offset in days between the maximum in root and shoot production. A kernel density curve is analogous to a histogram, but rather than showing counts of binned data, it estimates a probability density function of offset using sample data. The curve is smoothed using a kernel bandwidth of 1. Offset is defined as $DOY_{\text{maximum root}} - DOY_{\text{maximum shoot}}$, where DOY refers to day of year from 1 to 365. Data include 63 tree, shrub, and herbaceous species from 40 studies (Table 2.S2), grouped by biome. The black vertical dotted line is the grand mean of all offset values. 25

Figure 2.2. (a) Offset in days between maximum shoot and root production for 87 observations averaged across four biomes: boreal, temperate, Mediterranean and subtropical (Table 2.S2). Letters indicate a statistically significant difference in means ($\alpha = 0.05$) calculated using Tukey’s HSD after one way ANOVA (offset ~ biome + root collection method, biome: $F_{3,80} = 5.0$, $P = 0.0032$, root collection method: $F_{3,80} = 2.67$, $P = 0.053$, model $F_{6,80} = 3.83$, $P = 0.0021$). (b) Deciduous ($n = 20$) trees had a significantly smaller offset than did evergreen ($n = 14$) trees (ANOVA, $F_{1,32} = 7.52$, $P = 0.009$). 26

Figure 2.3. The proportion of maximum monthly root and shoot growth for each month in (a) boreal, (b) temperate, (c) Mediterranean, and (d) subtropical biomes (Table 2.S3). In panels a-d, dark brown corresponds to root growth and light green is shoot growth. The blue dotted line is mean monthly precipitation (mm, right side y-axis). The color bar across the top is a heat map showing seasonal temperatures ranging

from -10°C (purple) to 25°C (red), with 0°C as bright blue. Panels e-h plot the proportion of maximum monthly root vs. shoot growth. In these panels, black lines join consecutive months and the direction of the arrowheads indicates time from January to December. This approach assumes that shoot growth is a suitable proxy for the initiation of photosynthesis. Calculating the proportion of peak root or shoot growth rather than absolute growth rates enables us to plot the different types of data on the same y-axis (i.e., minirhizotron vs. soil coring). Note that these proportions are not a probability distribution function (i.e., area under the curve $\neq 1$) and that no point equals 1 because multiple studies with differently timed maximum growth were averaged. 27

Figure 2.S1. Proportion root (a) and shoot (b) growth for data in all biomes plotted against median monthly temperature (°C). Color and symbol shape indicate biome. Regression statistics are found in Table 2.2..... 32

Figure 2.S2. (a) The relationship between root growth and MMT in boreal evergreen tree roots only. Arrows indicate direction of time from April to November. (b) The relationship between root growth and MMT in boreal deciduous tree, shrub and herbaceous plant roots. Arrows indicate the direction of time from March to September. 33

Figure 3.1. Map of plot locations at the Harvard Forest’s Prospect Hill Tract. There are 6 biometry plots (circles) and 10 minirhizotron plots (stars) per stand. Colored symbols indicate stand type. Blue-green symbols are white ash (*Fraxinus*

americana), orange are red oak (*Quercus rubra*), and purple are eastern hemlock (*Tsuga canadensis*). 88

Figure 3.2. Growth (a-c), mortality (d-f), and net primary production (NPP, g-i) of fine roots. In 2012, n = 4 and n = 9 for red oak and eastern hemlock, respectively. In subsequent years, n = 10 for each stand. Error bars are standard error of the mean. There was a significant effect of year and stand on both growth and mortality (Table 3.8). The eastern hemlock stand had significantly less growth and mortality than red oak and white ash stands ($P < 0.001$), but red oak and white ash stands were not different from each other (growth was only marginally different, $P < 0.1$)..... 89

Figure 3.3. (a) Field measurements of monthly mean mass-specific fine root respiration (\pm SE) in 2013 (left y-axis). The shaded area represents soil temperature (right y-axis). (b) Relationship of fine root respiration to the temperature of the measurement chamber (n = 61). Lines are nonlinear fits of the Arrhenius function to data for each stand. (c) Fine root respiration (\pm SE) scaled to the growing season using fine root biomass from soil coring. In panels a and b, asterisk indicates that white ash had significantly higher respiration rates than red oak and eastern hemlock. In panel c, letters indicate significant differences between stands at the $P < 0.001$ level. 90

Figure 3.4. Fine root respiration measured in the lab at temperatures ranging between 16°C and 25°C, with a mean of $22.8 \pm 0.5^\circ\text{C}$. There was a significant positive relationship between fine root respiration and sample date for white ash ($\beta = 0.016$, $F_{1,11} = 15.3$, $P < 0.01$, $R^2_{\text{adj}} = 0.54$), red oak ($\beta = 0.012$, $F_{1,9} = 17.6$, $P < 0.01$, $R^2_{\text{adj}} =$

0.62), and eastern hemlock ($\beta = 0.011$, $F_{1,9} = 32.1$, $P < 0.001$, $R^2_{adj} = 0.76$). Dash lines are 95% confidence intervals around the regression fit. 91

Figure 3.5. Total nonstructural carbohydrates (\pm SE) from $n = 6$ samples from each stand.

There were significant differences between years ($F_{1,1089} = 23.7$, $P < 0.001$), sample dates ($F_{1,1089} = 66.9$, $P < 0.001$), and stands ($F_{2,1089} = 67.0$, $P < 0.001$). Each stand was significantly different from the other two stands in both years. 92

Figure 3.6. Gross primary production and belowground fluxes (litterfall, $TBCF_{bottom}$ [fine root production, root respiration, exudation], heterotrophic respiration, soil CO_2

efflux) and pools (microbial biomass, root biomass, organic horizon soil C, mineral horizon soil C) for each stand. Heterotrophic respiration is estimated as the difference between soil CO_2 efflux and root respiration. Standard error is reported in parentheses next to each pool or flux value, and all units are $g\ C\ m^{-2}\ gs^{-1}$. The growing season is defined as the six month period from May–October. 93

Figure 3.7. Time series of gross primary production estimated using data from the

Harvard Forest Environmental Measurement Site flux tower and the hemlock tower in 2012 (circles). Soil respiration for the eastern hemlock and red oak stands (squares) and $TBCF_{bottom}$ (diamonds) for red oak, eastern hemlock and white ash stands calculated using root GPP, respiration and exudation from May to October. For Jan–Apr and Nov–Dec when data were not available (shaded areas), I used the median ratio of $TBCF:GPP$ to extrapolate $TBCF$ from GPP data. This ratio (5th, 95th percentiles) was 0.42 (0.23, 0.5) for hardwoods and 0.36 (0.28, 0.57) for hemlock. The orange and pink colored bars show the maximum canopy greenness in red oak

and eastern hemlock stands, respectively, for this study period determined using PhenoCam data (http://phenocam.sr.unh.edu/).....	94
Figure 4.1. Plexiglass root box designed and constructed for this study at Boston University. Roots can be accessed by lifting a hinged panel. The second hinged panel is partially visible in the lower right hand corner.....	118
Figure 4.2. Linear relationship between enzyme activity and brightness values for the zymogram area, determined by staining the zymogram with a range of acid phosphatase, protease, or 4-MUB concentrations. AP = acid phosphatase, PR = aminopeptidase, BG = beta-glucosidase, NAG = N-acetyl-beta-D-glucosaminidase.	119
Figure 4.3. Sample size (number of pixels) in each 1 mm distance from root bin at coarse (6.7 mm) and fine (2 mm) image resolution.	120
Figure 4.4. Zymograms measuring the activity of (a) acid phosphatase, (b) aminopeptidase, (c) beta-glucosidase, and (d) N-acetyl-beta-D-glucosaminidase on the same hemlock stand root box panel. Thresholded mask of roots is overlaid on each zymogram at 70% transparency. Box 4.1 is the image subset used in very-fine-resolution analysis.....	121
Figure 4.5. Level of detail visible across a range of spatial resolution. Length of the side of one pixel is, (a) 6.7 mm, (b) 2 mm, or (c) 0.13 mm (resolution of original 8-bit image).	122
Figure 4.6. Enzyme activity (EU ml ⁻¹ or mM) versus distance from root (mm) for four extracellular enzymes: acid phosphatase (AP), aminopeptidase (PR), beta-	

glucosidase (BG), and N-acetyl-beta-D-glucosaminidase (NAG) at coarse resolution. The broken solid line is the best-fit break-point regression line. The dotted vertical line indicates the location of the break point. The shaded gray area is the interquartile range of the data. 123

Figure 4.7. Enzyme activity (EU ml⁻¹ or mM) versus distance from root (mm) for white ash, red oak, and eastern hemlock stands at coarse resolution. The broken solid line is the best-fit break-point regression line. The dotted vertical line indicates the location of the break point. The shaded gray area is the interquartile range of the data..... 124

Figure 4.8. Enzyme activity (EU ml⁻¹ or mM) versus distance from root (mm) for four extracellular enzymes, acid phosphatase (AP), aminopeptidase (PR), beta-glucosidase (BG), and N-acetyl-beta-D-glucosaminidase (NAG) at fine resolution. The broken solid line is the best-fit break-point regression line. The dotted vertical line indicates the location of the break point. The shaded gray area is the interquartile range of the data. 125

Figure 4.9. Enzyme activity (EU ml⁻¹ or mM) versus distance from root (mm) for white ash, red oak, and eastern hemlock stands at fine resolution. The broken solid line is the best-fit break-point regression line. The dotted vertical line indicates the location of the break point. The shaded gray area is the interquartile range of the data. 126

Figure 4.10. Enzyme activity (EU ml⁻¹) in a 400 × 400 pixel subsection of a high-resolution photo (1500 × 1500 pixels). Break point for this subsection is 2.6 mm. 127

Figure 5.1. Conceptual figure of the merger of DAMM (blue and orange boxes) and MCNiP (box and arrow diagram). SOM depolymerization occurs using Arrhenius and Michaelis-Menten kinetics, substrate diffusion, and a temperature-dependent V_{max} (blue box). I held K_m constant for the model runs in this study, but a linear temperature-sensitivity relationship can be applied to it if desired. DOC uptake is controlled by DAMM kinetics as well as O_2 concentration at the reaction site (orange box; see Table 5.1 for DAMM equation parameter definitions). MCNiP has four pools: SOM, DOM, Microbial biomass, and Enzymes. Litter and root inputs enter the SOM and DOM pools, respectively, and outputs are CO_2 as a product of respiration and inorganic N as a product of N mineralization. 156

Figure 5.2. Model inter-comparison of (a) DAMM (pink), (b) MCNiP (blue), (c) DAMM-MCNiP (red), and (d) DAMM-MCP (green) overlaid on soil C efflux measurements from trenched plots in Harvard Forest, MA..... 157

Figure 5.3. Relationship between predicted and measured C efflux for (a) DAMM alone, (b) MCNiP alone, (c) DAMM-MCNiP, and (d) DAMM-MCP. The solid line is the regression fit, and the dotted line is the 1:1 line. 158

Figure 5.4. (a) DAMM-MCNiP and (b) DAMM model residuals plotted as a function of soil moisture (θ). 159

Figure 5.5. DAMM-MCNiP model inputs (black), fluxes (blue) and pools (pink)..... 160

Figure 5.6. Plot of overflow C as a function of N mineralization. 161

Figure 5.7. Annual C and N mineralization in stands with narrow (pink) or wide (blue) C:N using parameters defined in Table 3. (a) C and (d) N mineralization when only

input C:N was varied between stands and microbial biomass was held at the default value. (b) C and (e) N mineralization when only microbial biomass C:N was varied and inputs were held at their default value. (c) C and (f) N mineralization when both input C:N and microbial biomass C:N were varied between stands..... 162

Figure 5.8. (a) SOC as a function of root inputs. (b) Microbial efficiency (depolymerization per unit microbial biomass) as a function of root inputs. (c) Microbial biomass as a function of the SOC pool. In panels a-c, root input C:N varies between 1 and 100 (colored lines)..... 163

Figure 5.9. Effect of 5°C warming (pink) and 5°C cooling (blue) on (a) C and (b) N mineralization. Effect of 1.5x soil moisture (pink) and 0.5x soil moisture (blue) on (c) C and (d) N mineralization. Black lines indicate C or N mineralization at ambient temperature and soil moisture conditions. 164

Figure 5.10. Absolute difference in (a) C and (b) N mineralization between ambient and 5°C of warming (pink) or cooling (blue). Absolute difference in (c) C and (d) N mineralization between ambient and 1.5x (pink) or 0.5x soil moisture (θ; blue).. 165

Figure 5.11. Cumulative sums of (a) C and (b) N mineralization rates under 5°C warming (pink) and cooling (blue). Cumulative sums of (c) C and (d) N mineralization rates with 1.5x soil moisture (pink) and 0.5x soil moisture (blue). Black lines indicate cumulative sums of C or N mineralization at ambient temperature and soil moisture conditions..... 166

Figure 5.12. C mineralization under ambient temperature and soil moisture (θ ; black line), 5°C warming with no change in soil moisture (pink line), and 5°C warming with a 10% decrease in soil moisture (0.90x; green line). 167

LIST OF ABBREVIATIONS

θ	volumetric soil moisture
2-D	two dimensional
a	proportion of the enzyme pool acting on the soil organic carbon pool
A	pre-exponential constant
AIC	Akaike information criterion
AM	arbuscular mycorrhizal
ANOVA	analysis of variance
AP	acid phosphatase
BD	bulk density
BG	beta-glucosidase
C	carbon
C_{roots}	carbon pool associated with fine roots
C_{soil}	carbon pool associated with soil
CMIP5	Fifth Coupled Model Intercomparison Project
C:N	carbon-to-nitrogen ratio
CO_2	carbon dioxide
CUE	carbon use efficiency
CV	coefficient of variation
DAMM	Dual Arrhenius and Michaelis-Menten
DEATH	microbial turnover
DEPOLY	depolymerization of soil organic matter

D _{liq}	diffusion coefficient for unprotected soil organic matter in liquid
DOC	dissolved organic carbon
DOM	dissolved organic matter
DON	dissolved organic nitrogen
DOY	day of year
E _a	activation energy
EEA	extracellular enzyme activity
EPROD	enzyme production
ELOSS	enzyme turnover rate
EU	enzyme units
F _{efflux}	soil respiration rate
F _{exudates}	root exudation rate
F _{leaching}	flux of dissolved organic carbon into streamwater
F _{litterfall}	litterfall
F _{resp}	fine and coarse root respiration rate
F _{roots}	gross fine root production rate
frac	fraction of unprotected soil organic matter
GPP	gross primary production
GROWTH	microbial biomass growth
H ₂ O	water
HWA	hemlock woolly adelgid
HSD	Honestly Significant Difference

inputDOM.....	root input to the soil
K _m	half-saturation constant
MCNiP	Microbial Carbon and Nitrogen Physiology
MCP	Microbial Carbon Physiology
MIC	microbial biomass
MICtoSOM	fraction of dead microbial biomass returned to soil organic matter
MIMICS	Microbial Mineral Carbon Stabilization
MMP	mean monthly precipitation
MMT	median monthly temperature
N.....	nitrogen
NAG.....	N-acetyl-beta-D-glucosaminidase
NEON	National Ecological Observatory Network
NPP	net primary production
NSC.....	nonstructural carbohydrate
O.....	organic
O ₂	oxygen
O ₂ airfrac	volume fraction of oxygen in air
p.....	proportion of assimilated C allocated to enzyme production
PAR.....	photosynthetically active radiation
PD	particle density
Pg	petagram
PFT	plant functional type

PR.....	aminopeptidase
$r_{enzloss}$	enzyme turnover rate
r_{death}	microbial turnover rate
q.....	proportion of assimilated N allocated to enzyme production
RMSE.....	root-mean-square error
SSE.....	sum of squared residuals
SOC.....	soil organic carbon
soilM	volumetric water content
SOM.....	soil organic matter
T	temperature
TBCF.....	total belowground carbon flux
UPT	rate of dissolved organic matter uptake
UV.....	ultraviolet
V_{max}	maximum reaction rate
W.....	spatial weights matrix

CHAPTER ONE: INTRODUCTION

For over a century, researchers have recognized the link between atmospheric carbon dioxide (CO₂) concentrations and the re-radiation of thermal energy back to the Earth's surface (Arrhenius & Sandström, 1903, Chamberlin, 1899). In 1957, Roger Revelle and Hans Seuss were among the first to suggest that the observed accumulation of fossil-fuel-derived CO₂ in the atmosphere would not only contribute to a warmer climate, but that the extent of climate change may depend on interactions between the atmosphere, biosphere, and geosphere that are not yet known (Revelle & Suess, 1957). "Thus," they write, "human beings are now carrying out a large scale geophysical experiment of a kind that could not have happened in the past nor be reproduced in the future."

From 1750 to the present, the terrestrial biosphere and ocean have mitigated climate change by sequestering 300 of the 550 Pg C released from the combustion of fossil fuels (Stocker *et al.*, 2013). There is at present substantial uncertainty regarding the size of the terrestrial sink over the coming century with continued climate change (Ahlström *et al.*, 2012). There is also debate as to whether the feedback between climate change and the land sink for atmospheric CO₂ will mitigate or exacerbate future climate change (Stocker *et al.*, 2013). On the one hand, if the growing season lengthens as a result of warming temperatures, C uptake is expected to increase because of sustained photosynthesis (Richardson *et al.*, 2009). On the other hand, extension of the growing

season may exacerbate drought, fire frequency, and stimulate decomposition resulting in a net loss of CO₂ to the atmosphere (Piao *et al.*, 2008, Wu *et al.*, 2013).

The terrestrial sink for atmospheric CO₂ is in plant biomass and soil. Typically 2- to 3-fold more C is stored in soil than biomass, increasing substantially with latitude (Ciais *et al.*, 2014). The activity of soil microbes, often referred to as heterotrophs, is temperature sensitive, with greater respiration consuming soil C and releasing CO₂ to the atmosphere. Heterotrophic respiration is expected to increase with warming temperatures, but the magnitude of this effect depends on the extent to which microbes physiologically acclimate to warm temperatures, microbial community composition is changed, or the availability of soil C declines (Bradford *et al.*, 2008, Hartley *et al.*, 2007). As a result, the long-term effect of global warming on heterotrophic respiration is unclear (Frey *et al.*, 2013, Melillo *et al.*, 2002).

The research presented in this dissertation is a continuation of the effort to understand feedbacks between plants, microbes, soil and the atmosphere. Ultimately all soil C is derived from plant matter and thus plants are intimately tied to the activity of soil microbes. The main process by which this occurs is referred to as “allocation” of C to leaves, stems, and roots.

Plant C allocation is an inherently seasonal process. The timing of seasonal events, or phenology, of aboveground plant organs and the tools used to observe it are advanced compared to studies of root growth and mortality. For example, there are records from the 9th century of cherry tree flowering in Kyoto, Japan, as well as a myriad

of historical phenological records of various plant phenomena dating back to 18th century England and 19th century United States (Aono & Kazui, 2008, Margary, 1926, Miller-Rushing & Primack, 2008). Since the 1970s, “remote sensing” technology using satellites, unmanned aerial vehicles, and mounted cameras have been instrumental in estimating growing season length and C uptake over the globe (Sharma et al. 2013, Hufkens et al. 2012).

In contrast to aboveground phenology, root dynamics are hidden from view, and there is no non-invasive technique analogous to remote-sensing that can be used to accurately assess root biomass, growth, or turnover. Root biomass has been estimated using coring and excavation for over half of a century (Lyford, 1980, Lyford & Wilson, 1964). In these and similar studies, root growth was measured by taking the difference in root biomass between two sample intervals. Beginning in the early 1980s, Vogt, Persson, Gower, and others popularized “sequential” coring in plots over a finer resolution of time and ingrowth techniques to separate rates of root growth from those of mortality (Persson, 1980, Vogt *et al.*, 1986). By the late 1980s, minirhizotron cameras were developed to capture magnified images of root growth and death along the surface of a plexiglass tube installed into the soil (Brown & Upchurch, 1987). Though root boxes and minirhizotrons have been in use for some time, only recently has the automation of image capture and annotation begun to develop (Roberti *et al.*, 2014, Zeng *et al.*, 2008).

Carbon allocated belowground is used for root production, respiration and exudation, but these fluxes are difficult to measure individually. In 1989, Raich and

Nadelhoffer proposed that calculating the difference between outputs (i.e., soil CO₂ efflux) from the soil and inputs (i.e., litterfall) to the soil provides a useful estimate of the total quantity of C allocated belowground (Davidson *et al.*, 2002, Litton *et al.*, 2007). This estimate assumes that soils are in steady state. Otherwise, it is necessary to measure the change in the C pool associated with roots and soil, as in:

$$\text{TBCF} = F_{\text{efflux}} - F_{\text{litter}} + \Delta(C_{\text{roots}} + C_{\text{soil}}) \quad [1]$$

where TBCF is the total belowground carbon flux, F_{efflux} is annual soil respiration, F_{litter} is annual litterfall, and $\Delta(C_{\text{roots}} + C_{\text{soil}})$ is the annual change in the C pool associated with roots and soil. If $\Delta(C_{\text{roots}} + C_{\text{soil}})$ is equal to zero, then it is only necessary to measure F_{efflux} and F_{litter} .

The assumption that the pool of C in roots and soil does not change over time is often violated. For example, Giardina & Ryan (2002) found that the change in the root and soil pool was about 14% of measured TBCF in a Hawaiian Eucalyptus plantation. In my study, I found that 0.2 - 40% of TBCF can be represented by the change in the root pool. The most accurate method to estimate belowground C allocation may be to compare multiple methods, such as using the difference between soil CO₂ efflux and litterfall in combination with measuring belowground allocation to roots [production, respiration, exudation] directly (Drake *et al.*, 2011).

Once C enters the soil via root exudation or turnover, it is available to the microbial community for decomposition. Soil microbes are able to utilize a diverse array

of substrates for metabolism (Bai *et al.*, 2013). Given the metabolic flexibility of microbes and the amount of energy stored in soil organic matter, it is paradoxical that there should be more than 1500 Pg of soil organic matter remaining on Earth (Ciais *et al.*, 2014). Most soil organic matter has an irregular structure and is therefore difficult to characterize by chemical or spectral analysis. Indeed, for the past several decades, the prevailing paradigm to explain the persistence of SOM was that most organic matter cannot be degraded because of its irregular chemical structure (Oades, 1989, Skjemstad *et al.*, 1996). Recent research has placed more emphasis on the physical separation of SOM from the microbial extracellular enzymes that would degrade them (Schmidt *et al.*, 2011) and the physical protection of SOM bound to or within soil aggregates (Conant *et al.*, 2011).

The wealth of research over the past century has clarified many feedbacks between the biosphere and atmosphere, by demonstrating that phenology has changed with warming, and that respiration and C allocation may also change (Bradford *et al.*, 2008, Melillo *et al.*, 2011, Richardson *et al.*, 2009). As a result, we have a greater ability to monitor and simulate C pools and fluxes at global scales than we did only two decades ago (Stocker *et al.*, 2013, Tang & Riley, 2015).

Despite these advances, many mechanisms of belowground C allocation are not yet clear. Individual studies have observed many different seasonal patterns of root growth (Bevington & Castle, 1985, Iivonen *et al.*, 2001, McCormack *et al.*, 2014), but it is not clear if particular biomes or plant types have synchronous or lagged phenology.

Because belowground C allocation data are few, we know little about the seasonal C partitioning to roots and how this varies between tree species, growth form (e.g., evergreen, deciduous), or mycorrhizal association. In part because of the paucity of data with which to parameterize models and infer process-level relationships, terrestrial biosphere models struggle to represent the soil C cycle mechanistically and often default to defining belowground C allocation as an instantaneous, fixed fraction of net C uptake at each time step (Medvigy *et al.*, 2009, Oleson *et al.*, 2010, Smith *et al.*, 2013). There is little understanding of the priority of C allocation in both plants and microbes, though some promising frameworks for determining allocation to different plant organs are emerging from evolutionary theory based on competition for light and nutrients (Craine & Dybzinski, 2013, Dybzinski *et al.*, 2011).

Microbial allocation to extracellular enzymes, biomass growth, and respiration is largely unknown, and is a major difficulty in parameterizing microbial physiology models (Averill, 2014). Fortunately, allometric relationships for microbial communities, as well as models of microbial metabolism are emerging frameworks for estimating microbial allocation to different processes (Harcombe *et al.*, 2014, Sinsabaugh *et al.*, 2014).

The interaction between plant roots and microbes is similarly data-limited. For example, including my findings, estimates of the size of the rhizosphere, defined as the zone of soil around a root where microbial exoenzyme activity is stimulated, ranges from 0.1 cm to over 7 cm (De Neergaard & Magid, 2001, Spohn & Kuzyakov, 2014). This

wide range reflects the few studies that have made these measurements, and suggests that there is either a large methodological uncertainty about how to quantify the rhizosphere extent, a large heterogeneity in the actual size of the rhizosphere, or both.

The research community is uncertain how rhizosphere and bulk soil microbes will respond to changes in temperature and substrate supply (Davidson & Janssens, 2006, Tang & Riley, 2015, Wieder *et al.*, 2013). Long-term field studies of soil warming indicate that a large initial increase in heterotrophic respiration decreases over time, suggesting some combination of acclimation, microbial community shift, or substrate limitation (Frey *et al.*, 2013, Melillo *et al.*, 2002, Melillo *et al.*, 2011). Regional climate projections also predict that some areas of North America, particularly the northeastern United States, will receive more precipitation, and others less (Melillo *et al.*, 2014). It is unclear how changes in soil moisture in combination with warming will affect microbial activity.

Dissertation Overview

The objective of the research in this dissertation is to better understand the seasonality, magnitude, and partitioning of C to root and soil processes at global-to-local scales. To achieve this objective, I used a combination of data compilation, field studies, and computer simulation. In Chapter 2, my objective was to determine the relationship between above and belowground phenology. I performed a meta-analysis, compiling data that quantified the offset between the maximum in root and shoot growth in woody and herbaceous perennial plants. Using data from 40 studies, 63 species, and 4 biomes, I

found that root and shoot phenology are often asynchronous and that evergreen trees commonly have later root growth compared to deciduous trees. I also found broad differences in phenology across biomes, finding that boreal biomes had later root growth than did temperate biomes, possibly due to the predominance of evergreen trees in boreal ecosystems.

In Chapter 3, my objective was to determine the magnitude, timing and partitioning of seasonal belowground C allocation at the plot scale, using field studies at the Harvard Forest in Petersham, MA. I recorded the total amount of C allocated belowground monthly during the growing season in three mono-dominant stands, white ash (*Fraxinus americana*), red oak (*Quercus rubra*), and eastern hemlock (*Tsuga canadensis*). I found that the red oak stand allocated more C belowground earlier in the growing season compared to the eastern hemlock stand. This difference in the phenology of belowground C allocation can be attributed to the timing of root growth, making this finding consistent with the observation in Chapter 2 that deciduous trees have earlier root growth than evergreen trees. The magnitude of the belowground C flux was highest in the red oak stand, consistent with the observed increase in aboveground biomass of red oak at the Harvard Forest over the past 20 years (Keenan *et al.*, 2012, Urbanski *et al.*, 2007). The belowground C flux was lowest in the eastern hemlock stand due to a decline in allocation to root production over the study period. This decline is coincident with the arrival and spread of the hemlock woolly adelgid in this stand.

In Chapter 4, my objective was to estimate the spatial extent of the rhizosphere at the scale of individual roots, using a recently-developed enzyme imaging, or

zymography, technique. I incubated chromatography paper soaked in the substrate of four C-, N-, or P-releasing enzymes on rooted soil surfaces. When an extracellular enzyme decomposed substrate fixed to the paper, the cleavage resulted in a colorimetric or fluorometric tag that remained on the paper. These zymograph images were digitized along with photographs of roots in the sample area. I developed a quantitative framework for analyzing these image data. I used two regression models, a spatial error model that accounted for the autocorrelation between image pixels, and a “break-point” regression model that estimated the location of a change in the slope of the relationship between extracellular enzyme activity and distance from a root. I used this break point as a proxy for the rhizosphere extent. The rhizosphere extent varied depending on the resolution of image analysis, as a result of increased sample size, background staining, or misalignment of images. Nevertheless, I found that extracellular enzyme activity was concentrated near the surface of roots. The break points that I estimated suggest that the rhizosphere can extend beyond 2 mm from the root surface, suggesting that recent estimates of rhizosphere contributions to decomposition and nutrient mineralization are very conservative (Finzi *et al.*, 2015).

In Chapter 5, my objective was to develop a combined model of microbial physiology and extracellular enzyme activity to assess how climate change may affect plant–microbe interactions, soil organic matter decomposition, and soil C storage. I merged two existing models: the Dual-Arrhenius Michaelis Menten (DAMM) model (Davidson *et al.*, 2012) and the Microbial Carbon and Nitrogen Physiology (MCNiP) model (Finzi *et al.*, 2015). The combined model reproduced heterotrophic respiration

measured in a trenched plot at the Harvard Forest in central Massachusetts. It also captured the seasonal pattern of C efflux better than MCNiP alone, and predicted C efflux during wet-up events better than both models alone. DAMM-MCNiP predicted that stands with a wide C:N ratio [litter, roots, microbial biomass] stored more C, consistent with recent empirical findings at the global scale (Averill *et al.*, 2014). When subject to a series of climate change simulations, the model predicted that C mineralization increases with either +5°C warming or a 50% increase in soil moisture. The response to added soil moisture was unexpected given that oxygen (O₂) availability limits microbial activity at high soil moisture, and suggests that in this model O₂ limitation has a small effect on microbial respiration relative to substrate diffusion.

This research demonstrates that belowground C allocation affects C balance on the plot-to-global scale. There are broad differences in root phenology across biomes and plant types, and in a mid-latitude temperate forest, there are stand-level differences in both the magnitude and partitioning of C belowground, driven primarily by allocation to root growth. A significant amount of root C is allocated to the microbial community, where it stimulates microbial activity. I demonstrate that the C:N ratio of root exudates influences both the magnitude of SOM decomposition and the mechanism by which decomposition is stimulated. These findings demonstrate the importance of plant roots to the terrestrial C cycle.

CHAPTER TWO: ARE ABOVE AND BELOWGROUND PHENOLOGY IN SYNC?

Abstract

Globally, root production accounts for 33-67% of terrestrial net primary productivity and influences decomposition via root production and turnover, carbon (C) allocation to mycorrhizal fungi and root exudation. As recognized aboveground, the timing of phenological events affects terrestrial C balance, yet there is no parallel understanding for belowground phenology. In this paper I examine the phenology of root production and its relationship to temperature, soil moisture, and aboveground phenology. Synthesizing 87 observations of whole plant phenology from 40 studies, I found that on average root growth occurs 25 ± 8 days after shoot growth but that the offset between the peak in root and shoot growth varies > 200 days across biomes (boreal, temperate, Mediterranean, and subtropical). Root and shoot growth are positively correlated with median monthly temperature and mean monthly precipitation in boreal, temperate, and subtropical biomes. However, a temperature hysteresis in these biomes leads to the hypothesis that internal controls over C allocation to roots are an equally, if not more, important driver of phenology. The specific mechanism(s) are as yet unclear but are likely mediated by some combination of photoassimilate supply, hormonal signaling, and growth form.

Introduction

It is widely acknowledged that roots play a fundamental role in terrestrial C cycling, consuming up to 70% of net primary production (Grier *et al.*, 1981, Jackson *et al.*, 1997), yet there is little understanding of the factors controlling patterns of root growth (Pregitzer *et al.*, 2000). Fine root production can occur in a single flush but often occurs in multiple flushes throughout the growing season (Bevington & Castle, 1985, Harris *et al.*, 1995, Reich *et al.*, 1980, Steinaker *et al.*, 2010). Soil temperature, moisture and nutrient availability affect the growth of roots (Fukuzawa *et al.*, 2013, Noguchi *et al.*, 2013), but there is often no temporal correlation between these abiotic factors and root growth apart from obvious growing-to-nongrowing season transitions (Hendrick & Pregitzer, 1996, Joslin *et al.*, 2001; Table 2.S1). In these cases internal signaling such as photoassimilate transport may control root growth (Sloan & Jacobs, 2008), such that roots cannot grow when shoots are consuming the majority of photoassimilate. Supporting this, several studies have observed patterns of alternating root and shoot growth (Cardon *et al.*, 2002, Drew & Ledig, 1980, Mickelbart *et al.*, 2012, Reich *et al.*, 1980).

Most conceptual and terrestrial biosphere models allocate C belowground as a fixed fraction of net C uptake, which by definition makes root phenology synchronous with aboveground growth (Table 2.1). The purpose of this review is to show that current data support asynchrony between above and belowground growth. I acknowledge that the available data are few and that inference regarding broad-scale patterns is subject to change as more data become available. I hope, however, that bringing currently available

data to light in this regard will generate the collection of new data, and refine current understanding of belowground phenology and its relevance at the ecosystem scale.

A compilation of available data

It is commonly assumed that root growth peaks early in the growing season and is therefore synchronous with aboveground growth (Medvigy *et al.*, 2009). While this can be true (Misson *et al.*, 2006, Scagel *et al.*, 2007), there are many exceptions (Lahti *et al.*, 2005, Palacio & Montserrat-Marti, 2007, Willaume & Pagès, 2006). Some studies report root growth lagging shoot growth by several weeks, an observation attributed to air temperature warming faster than soil temperature in the spring (Steinaker & Wilson, 2008). Others report root growth preceding shoot growth by several weeks to months (Broschat, 1998, Ploetz *et al.*, 1992). In a common garden study in Pennsylvania, some species such as *Acer negundo* and *Pinus strobus* had large interannual variability in root phenology while others such as *Liriodendron tulipifera* did not (McCormack *et al.*, 2014), suggesting that some trees may be environmentally cued while others are inflexible in their timing (i.e., phenological programming sensu Hendrick & Pregitzer, 1996, Joslin *et al.*, 2001).

To address broad-scale patterns in phenology, I conducted a literature survey to quantify the offset between the maximum in root and shoot growth in woody and herbaceous perennial plants. Web of Science was searched using the following keywords: belowground phenology, root phenology, root allocation, and root growth in combination with shoot phenology, aboveground, stem growth, leaf out, budburst or greenness. I considered only studies that simultaneously measured both root and shoot production. Of

the 13,934 results from the keyword search, only 40 studies had suitable data. There were a total of 87 datasets containing shoot and root growth for 63 species (see *Paper selection, Gross and net root production, Monthly root and shoot growth, and Temperature and precipitation data* in Supplementary Information for a more detailed description of the data used in this survey). The data are compiled in Tables 2.S2 and 2.S3. Each observation was classified into one of four biomes (boreal, temperate, Mediterranean and subtropical) based on Whittaker's biome classification system (1970). In order to visualize findings from the literature, I quantified the difference between peak shoot and root growth using the equation,

$$\text{Offset (days)} = \text{DOY}_{\text{maximum root}} - \text{DOY}_{\text{maximum shoot}} \quad [1]$$

where DOY is the day of year of maximum root or shoot growth as indicated. In plants with multiple root and shoot flushes, maximum root or shoot growth rate was used to calculate offset. Positive offset values therefore indicate peak shoot growth preceding the peak in root growth whereas negative values would indicate root growth preceding the peak in shoot growth. Differences in root and shoot data collection methods marginally affect offset ($F_{6,80} = 2.17$, $P = 0.055$), so they were included in stepwise model selection (see *Offset* in Supplementary Information). Soil coring methods tended to detect later root growth relative to shoot growth.

Primary Data Findings

There was wide variation in the timing of maximum shoot growth relative to root growth (Figure 2.1). In the majority of cases maximum shoot production occurred before root production (offset > 0 in 54 out of 87 observations) and the mean offset for all

studies (25 ± 8 days) was greater than zero (one sample t-test; $t = 3.15$, $df = 86$, $P < 0.01$) indicating that root and shoot growth are not synchronous on a broad geographic scale.

There was no difference in offset between tree, shrub and herbaceous growth forms.

As the data are largely from extratropical, northern hemisphere localities, there is a significant correlation between growth and temperature (Table 2.2, Figure 2.S1). At the biome scale, subtropical plants were significantly different from all other biomes, with the peak in root growth occurring 45 ± 19 ($n = 11$) days earlier than shoot growth, whereas offset in boreal, Mediterranean, and temperate biomes occurred 48 ± 8 ($n = 20$), 36 ± 19 ($n = 11$), and 28 ± 12 ($n = 45$) days after shoot production, respectively (Figure 2.2a). The generally late root relative to shoot growth in boreal biomes may, however, be confounded with tree growth form. Conifer ($n = 14$) root growth peaked 44 ± 12 days later than deciduous tree species ($n = 20$, Figure 2.2b).

Similar to temperature, there is a positive linear correlation between growth and mean monthly precipitation (MMP) in boreal and subtropical biomes (Table 2.2). In these biomes median monthly temperature (MMT) and MMP are highly correlated ($\rho = 0.89$ and $\rho = 0.85$ for boreal and subtropical climate variables respectively), so it is difficult to separate the precipitation from the temperature effect. By contrast, precipitation predicts growth poorly in temperate and Mediterranean biomes (Table 2.2). In the temperate data set precipitation did not have large seasonal variation (Figure 2.3b). In the Mediterranean data set shoot growth occurs in a large spring pulse following winter rain, whereas root growth appears to proceed at a steadily rising rate over the year (Figure 2.3c).

To visualize the phenology of root relative to shoot growth, I plotted the proportion of peak root growth as a function of peak shoot growth and generated a hysteresis plot for each biome. Deviations from the 1:1 line indicate dominance of root relative to shoot growth (or vice versa) across the year (Figure 2.3e-h). In boreal ecosystems root growth remains low throughout spring shoot expansion with the largest proportion of root growth observed in the summer through autumn (Figure 2.3e). In temperate ecosystems, however, root growth is entirely proportional to shoot growth, with all data plotting closely to the 1:1 line (Figure 2.3f). The Mediterranean observations are unlike the others. There is no clear hysteresis between root and shoot growth (Figure 2.3g). The subtropical biome is similar to the temperate biome in that root growth mirrors shoot growth not deviating from the 1:1 line (Figure 2.3h).

Some Implications of the Data

The available data suggest that root and shoot growth is largely asynchronous. At broad spatial scales temperature and precipitation influence this asynchrony, for example, the positive offset between peak shoot and root growth with decreasing annual temperatures (data not shown). As suggested by Steinaker & Wilson (2008), air temperature rises more rapidly than soil temperature in the spring and hence root growth is delayed later into the spring or summer (Figure 2.3a-d). The boreal dataset supports this hypothesis. A corollary to this observation is that thermal buffering allows soils to remain warm through the autumn and, as a result, the duration of root production can be 40% longer than shoot production (Steinaker & Wilson, 2008, Steinaker *et al.*, 2010).

Once again, this observation is strongly supported by the boreal zone data set (Figure 2.3a).

There is, however, at least as much variation in the offset between peak root and shoot growth within and between biomes as that explained by climate variables (Table 2.2). This leads to the ecologically interesting hypothesis that endogenous control of plant C allocation is an important driver of root phenology. What evidence is there in support of this hypothesis?

For the purposes of this paper, I define endogenous cuing as any factor that influences the growth of roots other than direct effects of temperature and precipitation. One of the clearest examples of endogenous root cuing is the production, storage and transport of photoassimilate (Palmroth *et al.*, 2006, Pregitzer *et al.*, 2000). There are important stores of carbohydrates in plants that can fuel production (Richardson *et al.*, 2013), and root growth depends on these stores as well as newly fixed C from aboveground organs. Isotopic labelling studies have confirmed that substantial C used in root biomass is newly fixed (Keel *et al.*, 2006, Trumbore *et al.*, 2006). Root growth stops or is greatly reduced in response to experimental manipulations such as girdling and stem chilling that cut off the supply of photoassimilates from the canopy (Högberg *et al.*, 2001, Johnsen *et al.*, 2006) and thus belowground phenology must be in part regulated by aboveground phenology (Litton *et al.*, 2007).

Does the difference in root growth phenology implicate the supply of photoassimilate? It does appear to provide a parsimonious explanation. Leaf area and photosynthetic rates in temperate deciduous forests tend to be highest in the spring and

decline through late summer and rapidly in autumn as a consequence of canopy senescence (Wu *et al.*, 2010). This seasonality is highly synchronous with the most active period of root growth, and the progressive summer decline in photosynthesis and autumnal leaf senescence correlate with reductions in root growth (Figure 2.3f). The prolonged autumnal root growth in the boreal zone may also reflect photoassimilate control in that the retention of live-needles in the canopy sustains the supply of photoassimilate even as temperatures cool and day length declines (but soils stay warm). Additional support for photoassimilate-regulated autumnal root growth is observed when separating the boreal dataset into evergreen trees vs. deciduous woody and herbaceous species. Doing so shows that autumnal root growth in evergreen trees dominates the hysteresis (Figure 2.S2a) in Figure 2.3f. Autumnal root growth in the deciduous plants follows that found in the temperate biome data (i.e., maximum root growth in the spring and very little in the autumn; Figure 2.S2b). Boreal evergreen trees may also utilize stored C during late season root growth (Nordgren *et al.*, 2003).

The subtropical and Mediterranean data are challenging to interpret. The subtropical data come from evergreen species, largely palms, in a consistently warm environment, yet there is a distinct phenology in shoot and root production with the peak in both following the wettest months of the year (Figure 2.3d). I speculate that the distinct phenology may be analogous to observations from seasonally dry Amazonian rainforests where evapotranspiration rates are highest in the dry season (Hutyra *et al.*, 2007) because of reductions in cloudiness and light-limitation of photosynthesis (Restrepo-Coupe *et al.*, 2013). It is possible that the reduction in late summer and autumnal precipitation is

sufficiently large that PAR does not limit photosynthesis during this period of time and peak growth occurs.

The Mediterranean observations are the most challenging to interpret under the assumption that the majority of C used for root growth is newly fixed. Shoot and root growth are not correlated with MMT or MMP and root growth is apparently decoupled from shoot growth (Figure 2.3g). The one exception is a concentrated pulse of vernal shoot growth following winter precipitation and the delay in peak root relative to shoot growth (Figure 2.3c). The strong asynchrony between shoot and root growth that extends across the year, however, suggests that endogenous cuing and subsequent allocation of stored carbohydrates is a dominant driver of root growth in Mediterranean plants. Root and stem nonstructural carbohydrates generally decline during the growing season and re-accumulate in autumn (Loescher *et al.*, 1990, Richardson *et al.*, 2013), as stored carbohydrates are allocated to respiration and growth during the growing season. However, limited data availability in this biome may prevent any meaningful conclusions.

Finally, I note that the time scale of the data analysis here cannot address the occurrence of alternating above and belowground growth, for example, as found in *Quercus spp.* (Cardon *et al.*, 2002, Reich *et al.*, 1980). Whether this is common is not well known, but at least these data suggest coordination of C allocation across the growing season, which may be mediated by both above and belowground plant organs. For example, roots produce and transport several shoot regulating hormones acropetally, such as abscisic acid, cytokinin and strigolactone, that can affect stomatal closure, shoot

and bud growth respectively (Domagalska & Leyser, 2011, Sharp, 2002). Roots may also control photoassimilate transport by modifying the rate that photoassimilates in the phloem are taken up by root tissues (Patrick, 1997) that feedback to genetic regulatory networks (Koch, 1996). Numerous studies provide support for shared control of C allocation (Davidson & Holbrook, 2009, Farrar & Jones, 2008).

Moving Forward

At the extreme, root and shoot phenology can be offset by ± 200 days, and both are mechanistically linked by temperature, water and C allocation. This dataset establishes possible generalizations regarding root and shoot phenology based on biome and growth form (i.e., evergreen, deciduous). Temperature and moisture are positively correlated with the phenology of both shoot and root growth in three of four biomes suggesting that abiotic factors both directly and indirectly affect root physiology. Endogenous factors (e.g., allocation of photoassimilate, source-sink dynamics, hormonal control) are also likely to be important drivers of phenology but as yet I am not able to make any broad conclusions with the possible exception that photoassimilate supply, storage and transport are key drivers of root growth phenology. The temperature hysteresis in Figure 2.3 provides support for endogenous controls—particularly the boreal and Mediterranean datasets. At the present time, there are few data available in the literature probably because of the difficulty in making measurements of seasonal root growth. Current datasets are derived from techniques that are relatively indirect (soil respiration), often destructive (coring), labor intensive (minirhizotrons) and hence expensive to implement. In addition to the paucity of data, many methods are difficult to

compare often with known biases (e.g., minirhizotron vs. isotopic methods; Guo *et al.*, 2008), and suffer from chronic under-sampling (Taylor *et al.*, 2013). However, for my purposes these methods capture temporal change in root length or biomass well enough to characterize its timing, though perhaps not its magnitude. I hope that improved scaling methods (Taylor *et al.*, 2014) and standardization across large networks (Keller, 2010) will alleviate sampling difficulties and allow for more accurate and generalizable data to emerge over time. Root growth is an important conduit for photosynthetically-fixed C into the soil with well-established feedbacks on C and N cycling (Averill *et al.*, 2014, Brzostek *et al.*, 2013, Drake *et al.*, 2011, Schmidt *et al.*, 2011). Quantitative models assume the phenology of root growth is synchronous with that of aboveground phenology despite empirical evidence to the contrary. Whether the addition of belowground phenology will affect total C efflux in terrestrial biosphere models is presently unknown. In the temperate biome where phenology is largely in sync such a change may be unnecessary, but in boreal biomes late season root allocation may explain observed fall increases in soil respiration that are currently poorly explained by temperature and soil moisture (Davidson *et al.*, 2006, Giasson *et al.*, 2013). Since both root growth and decomposition are known to be temperature-sensitive, and the latter also substrate limited, understanding the phenology and drivers of above- vs. belowground-C allocation is important for estimating ecosystem C fluxes under global change.

Acknowledgements

I would like to thank Edward Brzostek, John Drake, Allison Gill, Luke McCormack, Andrew Richardson, Andrew Reinmann, Patrick Sorensen and Anthony

Walker for helpful comments and discussion. This research was supported by the American Association of University Women (AAUW) American Dissertation Fellowship, Office of Science (BER), U.S. Department of Energy (Grant No. 10-DOE-1053) and by the National Science Foundation (DEB-0743564).

Table 2.1. Parameters for phenology and carbon allocation in terrestrial biosphere models (GDD: growing degree-days, LAI: leaf area index, PFT: plant functional type, NSC: nonstructural carbohydrate).

Model	Aboveground Phenology	Belowground Phenology	C allocation	Citation
TRIFFID	Temperature	n/a	Allometric relationships (root=leaf, stem×leaf) and partitioning into 'spreading' and 'growth' based on LAI	Cox 2001
Hyland	n/a	n/a	Fixed coefficients	Friend et al. 1997, Friend and White 2000, Levy et al. 2004
PhET-BGC	GDD	Monthly turnover rate	Linear function of foliar production	Kram et al. 1999
ORCHIDEE	GDD Soil moisture	Some root growth at leaf onset, stress can cause root death	Allocation fractions for leaves, stems, roots determined based on water, light and N availability	Krinner et al. 2005
3PG	PAR number of frost days	Stress affects root growth	Allometric relationships	Landsberg and Waring 1997
IBIS	Temperature Productivity threshold	n/a	Fixed fraction of C uptake allocated to leaves, stems, roots	Mcguire et al. 2001
TEM	Evapotranspiration	n/a	Not explicit	Mcguire et al. 2001
ED2	Logistic functions derived from MODIS data	n/a	PFT-dependent allocation relationships, root:leaf varies with water or N limitation	Medvigy et al. 2009
CLM 4.0	Soil moisture Day/length	n/a	Fixed ratios of fine root:leaf and coarse root:stem	Oleson et al. 2010, Thornton and Zimmerman 2007
LPI-GUESS	GDD Soil moisture	Stress affects root growth	Allometric relationships, PFT-dependent root:leaf biomass varies with water and N availability	Sitch et al. 2003, Smith et al. 2014
TREGRO	GDD NSC status	GDD NSC status	Allocated based on priority leaf>branch>stem>coarse roots>fine roots	Weinstein et al. 1991
BIOME-BGC	Temperature Photoperiod	n/a	PFT-dependent allometric ratios such as root:leaf and stem:leaf	White et al. 1997
Sheffield-DGVM	Temperature and soil moisture	n/a	LAI optimized to maximize C uptake, wood and roots receive a constant PFT-dependent fraction of remaining C	Woodward et al. 1995, Woodward and Lomas 2004
n/a = not applicable				

Table 2.2. Regression statistics for the proportion of maximum monthly root or shoot growth as a function of median monthly temperature (MMT) or mean monthly precipitation (MMP). The slope estimate (β) for MMT are in units of growth per °C and MMP growth per mm precipitation. Significant variables and overall model significance are indicated by: NS = not significant, * P < 0.05, ** P < 0.01 and * P < 0.001.**

Biome	Organ	MMT	R_{adj}²	MMP	R_{adj}²
<i>All biomes</i>	Root	0.02 ^{***}	0.48	0.01 [*]	0.09
	Shoot	0.01 ^{**}	0.21	0.01 ^{**}	0.17
<i>Boreal</i>	Root	0.02 ^{***}	0.79	0.01 ^{***}	0.83
	Shoot	0.02 [*]	0.47	0.01 ^{**}	0.67
<i>Temperate</i>	Root	0.02 ^{***}	0.80	0.01 ^{**}	0.01
	Shoot	0.02 ^{***}	0.75	0.011 ^{NS}	0.01
<i>Mediterranean</i>	Root	0.01 ^{NS}	0.01	0.01 ^{NS}	0.18
	Shoot	0.01 ^{NS}	0.00	0.01 ^{NS}	0.01
<i>Subtropical</i>	Root	0.05 ^{**}	0.61	0.01 [*]	0.37
	Shoot	0.04 [*]	0.38	0.01 [*]	0.31

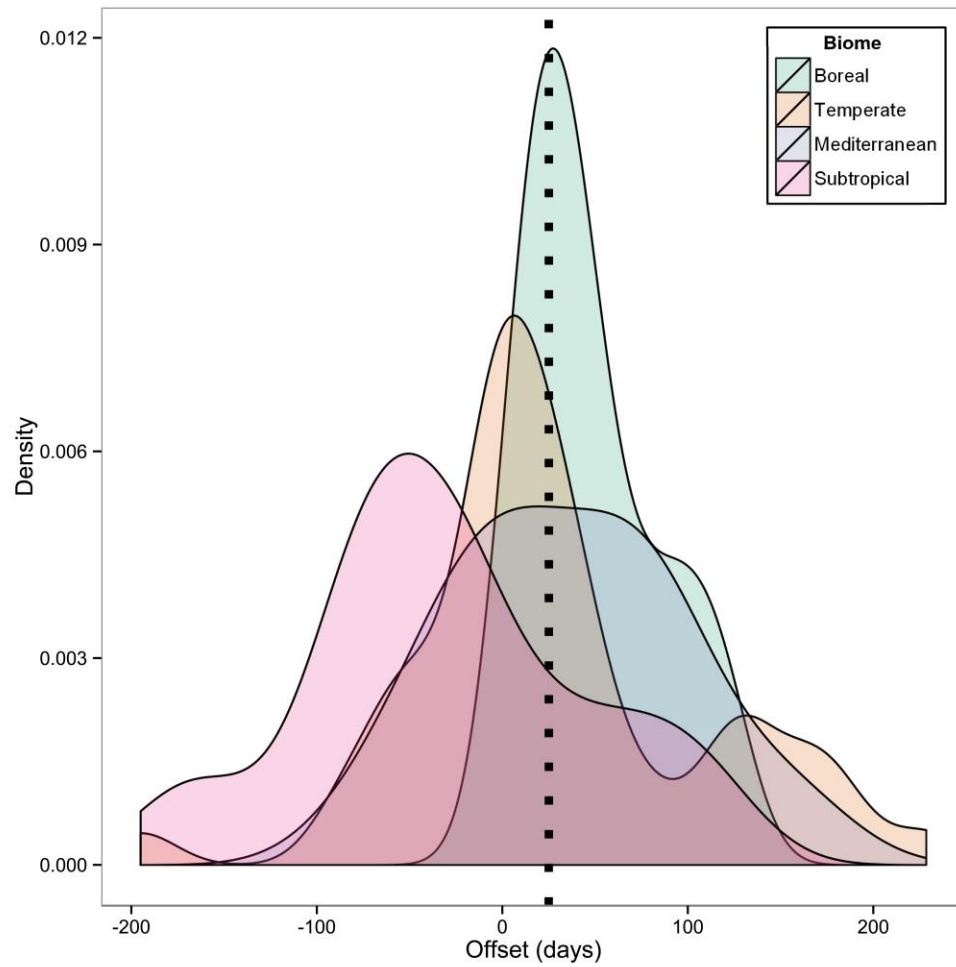


Figure 2.1. Kernel density curve of the offset in days between the maximum in root and shoot production. A kernel density curve is analogous to a histogram, but rather than showing counts of binned data, it estimates a probability density function of offset using sample data. The curve is smoothed using a kernel bandwidth of 1. Offset is defined as $DOY_{\text{maximum root}} - DOY_{\text{maximum shoots}}$ where DOY refers to day of year from 1 to 365. Data include 63 tree, shrub, and herbaceous species from 40 studies (Table 2.S2), grouped by biome. The black vertical dotted line is the grand mean of all offset values.

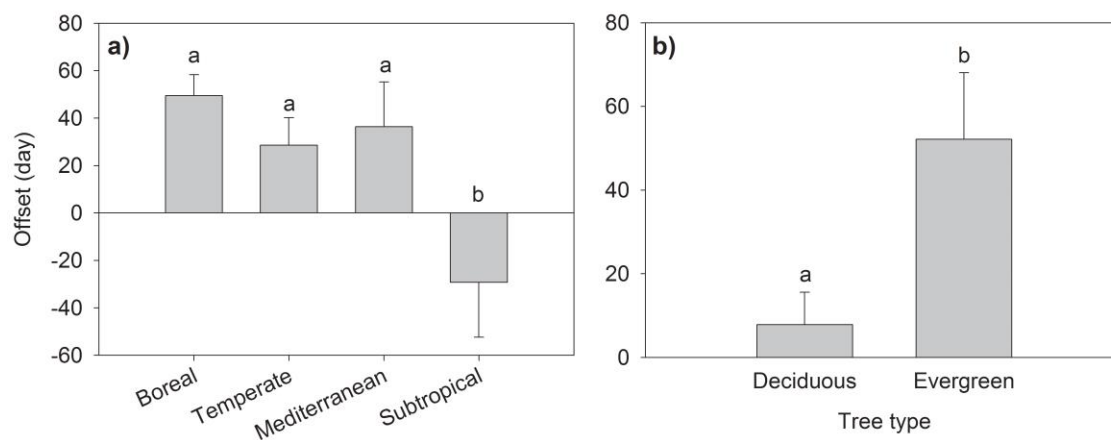


Figure 2.2. (a) Offset in days between maximum shoot and root production for 87 observations averaged across four biomes: boreal, temperate, Mediterranean and subtropical (Table 2.S2). Letters indicate a statistically significant difference in means ($\alpha = 0.05$) calculated using Tukey's HSD after one way ANOVA (offset ~ biome + root collection method, biome: $F_{3,80} = 5.0$, $P = 0.0032$, root collection method: $F_{3,80} = 2.67$, $P = 0.053$, model $F_{6,80} = 3.83$, $P = 0.0021$). (b) Deciduous ($n = 20$) trees had a significantly smaller offset than did evergreen ($n = 14$) trees (ANOVA, $F_{1,32} = 7.52$, $P = 0.009$).

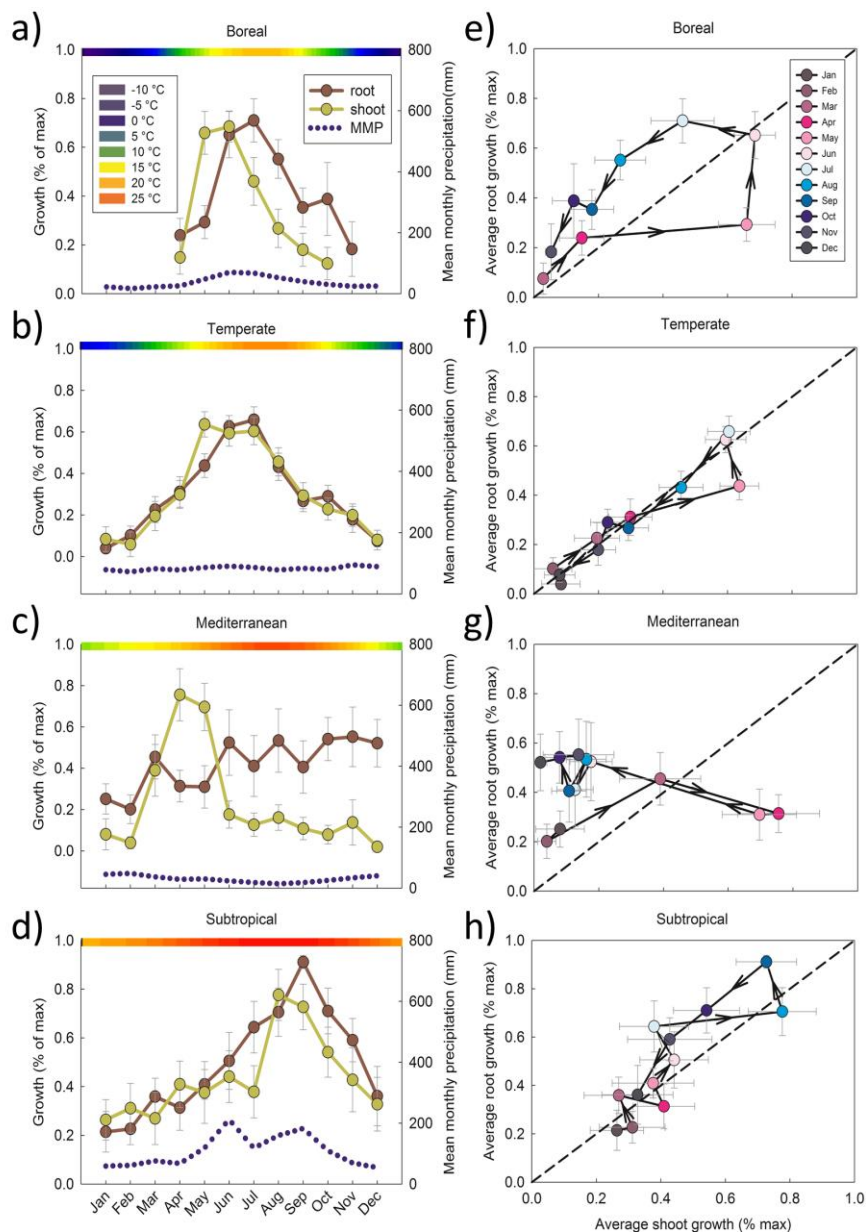


Figure 2.3. The proportion of maximum monthly root and shoot growth for each month in (a) boreal, (b) temperate, (c) Mediterranean, and (d) subtropical biomes (Table 2.S3). In panels a-d, dark brown corresponds to root growth and light green is shoot growth. The blue dotted line is mean monthly precipitation (mm, right side y-axis). The color bar across the top is a heat map showing seasonal temperatures ranging from -10°C (purple) to 25°C (red), with 0°C as bright blue. Panels e-h plot the proportion of maximum monthly root vs. shoot growth. In these panels, black lines join consecutive months and the direction of the arrowheads indicates time from January to December. This approach assumes that shoot growth is a suitable proxy for the initiation of photosynthesis. Calculating the proportion of peak root or shoot growth rather than absolute growth rates enables us to plot the different types of data on the same y-axis (i.e., minirhizotron vs. soil coring). Note that these proportions are not a probability distribution function (i.e., area under the curve $\neq 1$) and that no point equals 1 because multiple studies with differently timed maximum growth were averaged.

Supplementary Information

Paper selection

Web of Science was searched using the following keyword search: (belowground phenology OR root phenology OR root allocation OR root growth) AND (shoot phenology OR aboveground OR stem growth OR leaf out OR budburst OR greenness), in order to capture a variety of above and belowground measurements. There were 13,934 returns on Feb 3, 2014. I evaluated all papers at the abstract level for mention of seasonal root and/or shoot data. All candidate papers were read in full. Data including measurements of root and either leaf or stem production were included. Studies measuring transpiration rates, flowering, or single phenological events with no time series were not included.

Gross and net root production

In this study, offset is calculated using both gross and net root production. The phenology of net root production may be affected by seasonal variations in root mortality, especially when growth and mortality are asynchronous [1]. However, studies in temperate and boreal regions show that rates of root mortality are roughly synchronous with root growth [2, 3], implying that in these cases measurements of net root production may underestimate the magnitude of growth but not the timing of growth peaks. I found no significant difference between offset calculated using either gross or net root production (ANOVA, $F_{1,86} = 0.788$, $P = 0.38$) in the observations used in this study. These and all other analyses were performed in R [4].

Offset

Each observation was classified into one of four biomes based on Whittaker's biome classification system (1970). When median annual temperature and mean annual precipitation were close to the edge of a biome, classification was determined using USDA Natural Resources Conservation Service Major Biomes Map [5]. Day of year for peak root and shoot production was calculated as a mean of replicates with varying sample size ($n = 2-48$). For samples that produced multiple shoot and root flushes, the day of year of the largest peak was used to represent the above or belowground peak. Offset was calculated as the number of days between the peak in shoot and root production ($\text{offset} = \text{DOY}_{\text{peak root}} - \text{DOY}_{\text{peak shoot}}$). Negative offset values indicate that peak root production preceded peak shoot production. To explore possible biome-specific effects, I used analysis of variance to test for the effect of biome, root collection methods, and study on offset. Differences in root and shoot data collection methods (ANOVA: $\text{offset} \sim \text{root collection method} + \text{shoot collection method}$, $F_{6,80} = 2.17$, $P = 0.055$), and study author did not affect offset (ANOVA: $\text{offset} \sim \text{study author}$, $F_{1,85} = 0.00004$, $P = 0.99$). Stepwise model selection using explanatory variables 1) biome, 2) data collection method, and 3) study author indicated that the [biome + root collection method] model had the lowest AIC value (stepAIC[library:MASS] Initial model: $\text{offset} \sim \text{biome} + \text{shoot collection method} + \text{root collection method} + \text{study author}$, $\text{AIC} = 749.6731$; Final model: $\text{offset} \sim \text{biome} + \text{root collection method}$, $\text{AIC} = 737.1790$). Offset between the peak in root and shoot production in the subtropical biome was significantly different from other biomes (Tukey's HSD after ANOVA: $\text{offset} \sim \text{biome} + \text{root collection method}$, biome:

$F_{3,80} = 5.0$, $P = 0.0032$, root collection method: $F_{3,80} = 2.67$, $P = 0.053$, model $F_{6,80} = 3.83$, $P = 0.0021$, Figure 2.S1a). Offset was not affected by plant growth form (herbaceous, tree or shrub; ANOVA: offset~growth form, $F_{2,84} = 0.827$, $P = 0.44$).

Monthly root and shoot growth

Measurements from literature were used to estimate monthly root and shoot growth rates for each biome. Growth rate of roots and shoots were tabulated from each study (excluding those that did not include seasonal data [i.e., measured DOY 1 as start of experiment rather than the Julian day]) and converted to a % of the maximum growth rate. Growth rates were averaged for each month with > 5 observations. Most rates do not exceed 1 because multiple studies with differently timed maximum growth were averaged (Table 2.S3). For all biomes, root and shoot growth together have a positive relationship with MMT and MMP (Growth = $0.0148 \cdot \text{MMT} + 0.123$, $F_{1,85} = 41.05$, $P < 0.0001$, $R_{\text{adj}}^2 = 0.32$; Growth = $0.00190 \cdot \text{MMP} + 0.240$, $F_{1,85} = 14.19$, $P < 0.001$, $R_{\text{adj}}^2 = 0.13$). There was no significant interaction effect between MMT and MMP when both were included in a model (MAT:MAP $P = 0.15$, model $F_{3,83} = 17.22$, $P < 0.0001$, $R_{\text{adj}}^2 = 0.36$).

Temperature and precipitation data

To explore whether the seasonal variation in organ growth was the result of changes in temperature or precipitation, I obtained monthly daily maximum and minimum temperature as well as monthly mean total precipitation data for the station

located nearest each study site from the World Weather Information Service [6]. Means are based on 30 year averages from 1959-1997 (Greece), 1961–1990 (Chile, Czech Republic, Malaysia, Sweden), 1971–2000 (Canada, Finland, France, the Netherlands, Spain), or 1981-2010 (Japan, United Kingdom, United States of America). Daily maximum and minimum temperatures for each month were averaged to obtain a median monthly temperature (°C). Precipitation was reported as monthly mean total precipitation (mm). Precipitation refers to all types of precipitation in Sweden, Canada, France, Netherlands, and Spain. Only rainfall was measured in Greece, Chile, Czech Republic, Malaysia, Finland, Japan, United Kingdom, and United States of America.

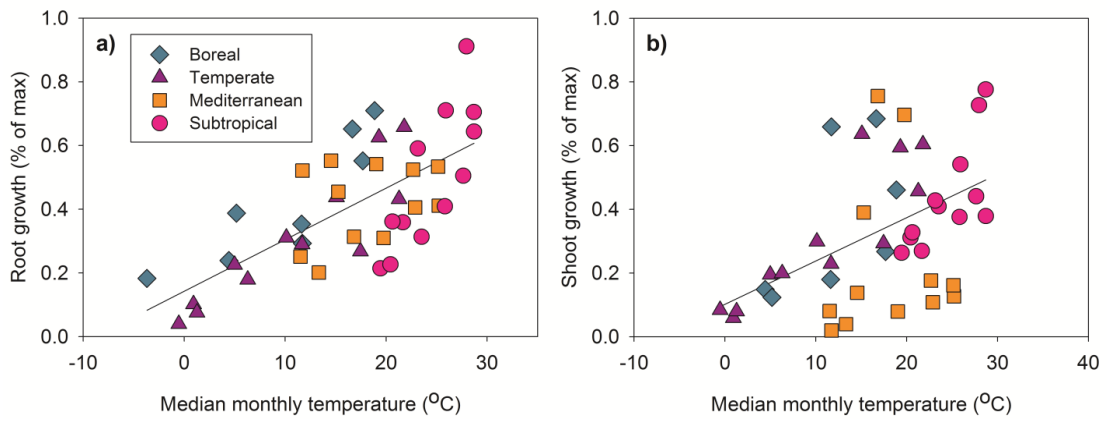


Figure 2.S1. Proportion root (a) and shoot (b) growth for data in all biomes plotted against median monthly temperature (°C). Color and symbol shape indicate biome. Regression statistics are found in Table 2.2.

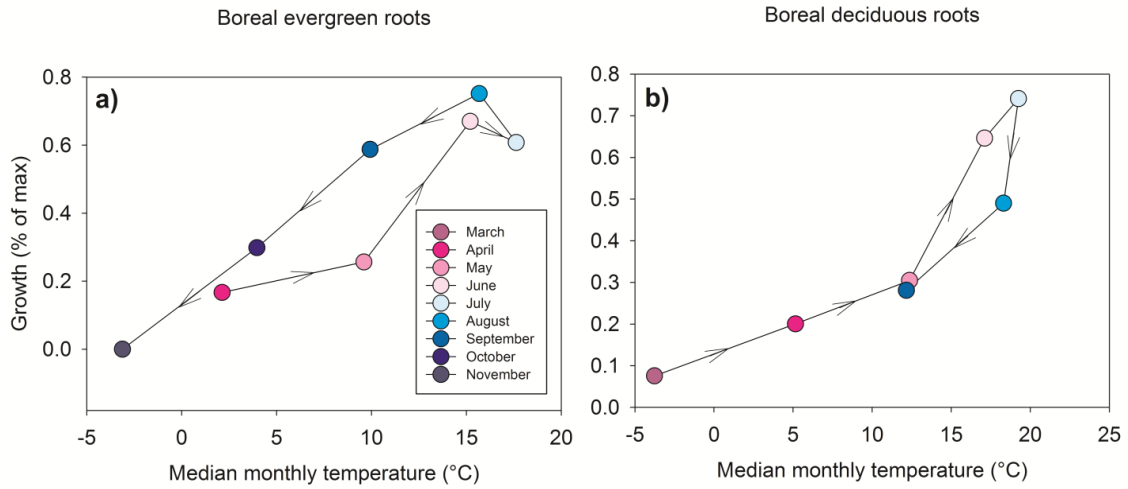


Figure 2.S2. (a) The relationship between root growth and MMT in boreal evergreen tree roots only. Arrows indicate direction of time from April to November. (b) The relationship between root growth and MMT in boreal deciduous tree, shrub and herbaceous plant roots. Arrows indicate the direction of time from March to September.

Table 2.S1. Phenological relationships between aboveground and belowground processes as well as potential drivers of belowground phenology, their direction and strength of effect, if given. ST, temperature; SWC, soil water content; E, endogenous.

Biome	Location	Species	Relationship of above- to belowground phenology	Possible Drivers	Reference
<i>Boreal</i>	Northern Savonia, Finland	<i>Pinus sylvestris</i>	Shoot elongation before peak in root production	T (+/-, hysteresis), E	[7]
	Northern Savonia, Finland	<i>Picea abies</i>	Root growth before and after shoot growth	ST (+)	[8]
	Uppland, Sweden	<i>Salix viminalis</i>	Max height growth before max change in fine root number	n/a	[9]
Saskatchewan, Canada		<i>Stipa comata</i>			
		<i>Carex spp.</i>			
		<i>Bouteloua gracilis</i>			
		<i>Agropyron spp.</i>			
		<i>Koeleria gracilis</i>	Shoot elongation before peak in root production	T (grassland: $r = -0.16$, $P < 0.05$, forest: $r = -0.20$, $P < 0.05$), SWC (grassland: $r = +0.58$, $P < 0.001$, forest: $r = +0.60$, $P < 0.0001$)	[10]
		<i>Poa spp.</i>			
		<i>Selaginella densa</i>			
		<i>Populus tremuloides</i>			
		<i>Symphoricarpos occidentalis</i>			
		<i>Rubus idaeus</i>			
Saskatchewan, Canada		<i>Festuca rubra</i>			
		<i>Koeleria gracilis</i>			
		<i>Poa compressa</i>			
		<i>Bouteloua gracilis</i>			
		<i>Schizachyrium scoparium</i>	Shoot elongation before peak in root production	T (herbaceous: $r = +0.42$ to $+0.63$, $P < 0.01$ to $P < 0.0001$, woody: $r = +0.23$ to $+0.62$, $P < 0.05$ to $P < 0.0001$), SWC (herbaceous: $r = -0.01$ to -0.78 , ns to $P < 0.0001$, woody: $r = -0.07$ to -0.40 , ns to $P < 0.01$)	[11]
		<i>Rosa woodsii</i>			
		<i>Shepherdia canadensis</i>			
		<i>Symphoricarpos occidentalis</i>			
		<i>Prunus virginiana</i>			
		<i>Picea glauca</i>			

Biome	Location	Species	Relationship of above- to belowground phenology	Possible Drivers	Reference
Boreal	Northern Savonia, Finland	<i>Pinus sylvestris</i> <i>Picea abies</i>	Synchronous for pine seedlings, root growth initiated before shoot elongation in spruce seedlings	ST (+)	[12]
Mediterranean	California, USA	<i>Pinus ponderosa</i>	Synchronous	ST = (+), SWC = (+)	[13]
	Huesca, Spain	<i>Echinopartum horridum</i> <i>Salvia lavandulifolia</i> <i>Lepidium subulatum</i> <i>Linum suffruticosum</i>	Shoot elongation before peak in root production, offset	T(+), SWC(+), E	[14]
	California, USA	<i>Pinus ponderosa</i>	Variable	ST (+)	[15]
	Nevada, USA	<i>Larrea tridentata</i> <i>Ambrosia dumosa</i> <i>Ephedra nevadensis</i> <i>Lycium pallidum</i>	n/a	SWC (r = +0.245 to +0.8, P = 0.217 to P<0.001)	[16]
Subtropical	Florida, USA	<i>Citrus sinensis</i> x <i>Citrus jambhiri</i> <i>Citrus sinensis</i> x <i>Poncirus trifoliata</i>	Alternating shoot and root flushes	ST (r = +0.74 to +0.87, P < 0.05), SWC (+)	[17]
	Florida, USA	<i>Roystonea regia</i> <i>Cocos nucifera</i> <i>Syagrus romanzoffiana</i> <i>Phoenix roebelenii</i>	Root growth before shoot growth	ST (r = +0.354 to +0.697, P < 0.0001)	[18]
	Northern Territory, Australia	<i>Eucalyptus miniata</i> <i>Eucalyptus tetradonta</i> <i>Sorghum spp.</i>	n/a	SWC (+)	[19]

Biome	Location	Species	Relationship of above- to belowground phenology	Possible Drivers	Reference	
Subtropical	Sabah, Malaysia	<i>Dipterocarpaceae</i>				
		<i>Meliaceae</i>	n/a	SWC ($r = +0.39$, $P < 0.05$)	[20]	
		<i>Tiliaceae</i> <i>Lauraceae</i> <i>Euphorbiaceae</i>				
	Florida, USA	<i>Persea americana</i>	Root elongation before shoot elongation	n/a	[21]	
	Barro Colorado Island, Panama	Tropical moist forest	n/a	SWC (+)	[22]	
Temperate	New York, USA	<i>Acer saccharum</i>				
		<i>Fagus grandifolia</i>	Initiation of root growth synchronous with budswell	T ($r = 0.871$, $P < 0.01$), E	[23]	
		<i>Betula alleghaniensis</i>				
		<i>Acer rubrum</i>				
	Connecticut, USA	<i>Quercus rubra</i>	Alternating shoot and root flushes		E	[24]
		<i>Acer saccharum</i> <i>Fagus grandifolia</i>	Offset, root growth before peak in diameter increment in one year, after in another		ST (-), SWC (+), diameter increment (-), N mineralization (-)	[25]
	Quebec, Canada	<i>Betula alleghaniensis</i> <i>Populus grandidentata</i> <i>Acer rubrum</i>				
		<i>Picea sitchensis</i>	n/a	ST, SWC (+, $P < 0.05$), E	[26]	
	Dumfries, United Kingdom			model $r = +0.608$, radiation flux (regression coefficient: $+5.75$, $P < 0.001$), surface temp (regression coefficient: $+2.86$, $P < 0.01$), air temp (regression coefficient: -2.59 , $P < 0.01$)	radiation flux ($r = +0.520$)	[28]
	Cumbria, United Kingdom	<i>Festuca ovina</i> <i>Juncus squarrosus</i> <i>Nardus stricta</i>	n/a			[27]
Grassland dominated by <i>Festuca ovina</i> and <i>Agrostis capillaris</i>		n/a				

Biome	Location	Species	Relationship of above- to belowground phenology	Possible Drivers	Reference
Temperate	Michigan, USA	<i>Quercus alba</i>	Some root production before leaf expansion, 80% of annual production before August	n/a	[29]
	Tennessee, USA	<i>Quercus alba</i> <i>Quercus prinus</i>	Offset, root production after leaf expansion, little root production after first week in August	SWC ($r = +0.25$, $P < 0.01$), E (correlation with known phenology patterns: $r = -0.4$, $P < 0.0001$)	[30]
	Washington, USA	<i>Pseudotsuga menziesii</i> <i>Abies amabilis</i> <i>Abies procera</i> <i>Pinus contorta</i> <i>Pinus ponderosa</i>	n/a	ST (optimum)	[31]
	Berkshire, United Kingdom	<i>Brassica napus</i> <i>Hordeum vulgare</i>	n/a	ST (+ with high temp asymptote)	[32]
	Missouri, USA	<i>Quercus alba</i> <i>Quercus velutina</i> <i>Quercus marilandica</i>	Alternating shoot and root flushes	E	[33]
	North Carolina, USA	<i>Glycine max</i>	n/a	root temperature (optimum)	[34]
	Missouri, USA	<i>Quercus alba</i>	n/a	ST (optimum), SWC (+)	[35]
	Bédoin, France	<i>Quercus pubescens</i>	Alternating shoot and root flushes	E	[36]

Table 2.S2. Measurements from literature used to quantify the offset between aboveground and belowground growth peaks in Figures 1 and 2. Methods used to measure root production varied by study (change in root biomass, ²minirhizotron, ³field rhizotron or root box, ⁴soil CO₂ efflux). AP, day of year aboveground peak; #AP, number of aboveground production peaks; BP, day of year belowground peak; #BP, number of belowground production peaks; H, herbaceous; W, woody; MMT, median monthly temperature (°C); MMP, mean monthly precipitation (mm); REF, reference.

Biome	Location	Species	H or W	D or E	Type of aboveground or measurement or abiotic variable	AP	#AP	Type of belowground measurement	BP	#BP	Offset	MMT	MMP	REF	
Boreal	Northern Savonia, Finland	<i>Picea abies</i>	W	E	change in seedling height (mm)	176.5	1	change in root biomass (g*time ⁻¹) ¹	273	1	96.5	3.1	608	[37]	
	North Karelia, Finland	<i>Picea abies</i>	W	E	change in height increment (cm*time ⁻¹)	142.5	1	change in root increment (cm*time ⁻¹) ¹	140	2	5	3.1	608	[8]	
	North Karelia, Finland	<i>Pinus sylvestris</i>	W	E	shoot elongation (midpoint)	321	1	root elongation (mm*time ⁻¹) ²	341	1	20	3.1	608	[38]	
	Uppland, Sweden	<i>Salix viminalis</i>	W	-	maximum shoot height (cm)	164	1	change in fine root number ²	258	3	94	6.8	539	[9]	
			<i>Populus tremuloides</i> , <i>Symphoricarpos occidentalis</i> , <i>Rubus ideaus</i>	W	-	leaf production (%)	119	1	root production (m ³ m ⁻³) ²	166	2	46.5	2.8	388	[10]
			<i>Stipa comata</i> , <i>Carex spp.</i> , <i>Bouteloua gracilis</i> , <i>Agropyron spp.</i> , <i>Koeleria gracilis</i> , <i>Poa spp.</i> , <i>Selaginella densa</i>	H	-	leaf production (%)	145	1	root production (m ³ m ⁻³) ²	166	2	21	2.8	388	[10]
			<i>Schizachyrium scoparium</i>	H	-	shoot production (%)	173	1	root production (%) ²	185	1	12	2.8	388	[11]
			<i>Festuca rubra</i>	H	-	shoot production (%)	160	2	root production (%) ²	179	1	19	2.8	388	[11]
			<i>Rosa woodsii</i>	W	-	shoot production (%)	156	1	root production (%) ²	187	3	31	2.8	388	[11]

Biome	Location	Species	H or W	D or E	Type of aboveground measurement or abiotic variable	AP	#AP	Type of belowground measurement	BP	#BP	Offset	MMT	MMIP	REF
Boreal	Saskatchewan, Canada	<i>Stephania canadensis</i>	W	-	shoot production (%)	175	1	root production (%) ²	206	2	31	2.8	388	[11]
	Saskatchewan, Canada	<i>Bouteloua gracilis</i>	H	-	shoot production (%)	187	1	root production (%) ²	223	1	36	2.8	388	[11]
	Saskatchewan, Canada	<i>Poa compressa</i>	H	-	shoot production (%)	156	1	root production (%) ²	195	2	39	2.8	388	[11]
	Saskatchewan, Canada	<i>Picea glauca</i>	W	E	shoot production (%)	140	1	root production (%) ²	184	2	44	2.8	388	[11]
	Saskatchewan, Canada	<i>Prunus virginiana</i>	W	-	shoot production (%)	129	1	root production (%) ²	186	2	57	2.8	388	[11]
	Saskatchewan, Canada	<i>Symphoricarpos occidentalis</i>	W	-	shoot production (%)	141	1	root production (%) ²	205	2	64	2.8	388	[11]
	Saskatchewan, Canada	<i>Koeleria gracilis</i>	H	-	shoot production (%)	141	1	root production (%) ²	221	1	80	2.8	388	[11]
	Northern Savonia, Finland	<i>Pinus sylvestris</i>	W	E	shoot growth (mm*time ⁻¹)	11.5	1	number ²	3.5	2	6.5	3.1	608	[39]
	Utrecht, Netherlands	<i>Carex rostrata</i>	H	-	maximum biomass increment (g*m ⁻²)	213	1	root production (%) ¹	213	1	0	9.7	793	[40]
	Utrecht, Netherlands	<i>Carex acutiformis</i>	H	-	maximum biomass increment (g*m ⁻²)	182	1	root production (%) ¹	335	1	153	9.7	793	[40]
	Utrecht, Netherlands	<i>Carex diandra</i>	H	-	maximum biomass increment (g*m ⁻²)	213	1	root production (%) ¹	335	1	122	9.7	793	[40]
	Utrecht, Netherlands	<i>Carex lasiocarpa</i>	H	-	maximum biomass increment (g*m ⁻²)	213	1	root production (%) ¹	335	1	122	9.7	793	[40]
	England, UK	<i>Populus euramericana</i>	W	D	change in stem height (mm*time ⁻¹)	63.5	1	change in apparent root length (cm*time ⁻¹) ¹	56.5	1	-7	11.0	1007	[41]
	New York, USA	<i>Acer saccharum</i>	W	D	maximum height increment (cm)	212	1	root production (%) ¹	212	1	0	9.4	1055	[42]
Temperate	Connecticut, USA	<i>Quercus rubra</i>	W	D	shoot production (cm ³ *d ⁻¹)	230	2	soil respiration ⁴	219	2	-11	10.9	1198	[24]
	Connecticut, USA	<i>Quercus rubra</i>	W	D	shoot production (cm ³ *d ⁻¹)	196	2	soil respiration ⁴	193	2	-3	10.9	1198	[24]
	Connecticut, USA	<i>Quercus rubra</i>	W	D	shoot production (cm ³ *d ⁻¹)	190	2	soil respiration ⁴	207	2	17	10.9	1198	[24]
	Connecticut, USA	<i>Quercus rubra</i>	W	D	shoot production (cm ³ *d ⁻¹)	217	2	soil respiration ⁴	236	2	19	10.9	1198	[24]

Biome	Location	Species	H W	D E	Type of aboveground or measurement or abiotic variable	AP	#AP	Type of belowground measurement	BP	#BP	Offset	MMT	MMP	REF
Temperate		<i>Acer saccharum</i> ,												
		<i>Fagus grandifolia</i> ,												
		<i>Betula</i>												
		<i>alleghaniensis</i> ,												
		<i>Populus</i>												
	Quebec, Canada	<i>grandidentata</i> , <i>Acer</i>	W	D	diameter increment (mm ³ d ⁻¹)	176	2	root growth (kg*ha ⁻¹ *d ⁻¹)	193	2	17	5.0	1065	[25]
		<i>rubrum</i>												
	Michigan, USA	<i>Populus</i>	W	D	change in stem height (cm)	218.5	1	change in root length (mm) ²	210	1	-9	5.4	837	[43]
		<i>grandidentata</i>												
		<i>Bromus inermis</i> ,												
		<i>Dactylis glomerata</i> ,												
	lowa, USA	<i>Phalaris</i>	H	-	aboveground biomass production (gC*m ⁻² *time ⁻¹)	141	1	soil respiration (gC*m ⁻² *d ⁻¹) ¹	213	1	72	10.4	915	[44]
		<i>arundinacea</i>												
	lowa, USA	<i>Panicum virgatum</i>	H	-	aboveground biomass production (gC*m ⁻² *time ⁻¹)	168.5	1	soil respiration (gC*m ⁻² *d ⁻¹) ⁴	201	1	32.5	10.4	915	[44]
		<i>Panicum virgatum</i> ,												
		<i>Sorghastrum</i>												
		<i>nutans</i> , <i>Setaria spp.</i> ,												
		<i>Echinacea purpurea</i> ,												
		<i>Solidago canadensis</i> ,												
		<i>Verbena stricta</i> ,												
	lowa, USA	<i>Desmanthus</i>	H	-	aboveground biomass production (gC*m ⁻² *time ⁻¹)	170	1	soil respiration (gC*m ⁻² *d ⁻¹) ⁴	213	1	43	10.4	915	[44]
		<i>illinoensis</i>												
lowa, USA	<i>Amaranthus spp.</i> ,	H	-	aboveground biomass production (gC*m ⁻² *time ⁻¹)	217	1	soil respiration (gC*m ⁻² *d ⁻¹) ¹	201	1	-16	10.4	915	[44]	
	<i>Xanthium</i>													
lowa, USA	<i>strumarium</i>	H	-	aboveground biomass production (gC*m ⁻² *time ⁻¹)	217	1	soil respiration (gC*m ⁻² *d ⁻¹) ¹	201	1	-16	10.4	915	[44]	
North Carolina, USA	<i>Pinus taeda</i>	W	E	shoot growth (%)	155	3	root production (%) ¹	284	2	129	13.6	940	[45]	
South Bohemia, Czech Republic	<i>Salix caprea</i>	W	-	relative growth rate (g ⁺ *g biomass ⁻¹ *d ⁻¹)	142	1	relative growth rate (g ⁺ *g biomass ⁻¹ *d ⁻¹)	176	2	165	8.9	490	[46]	
South Bohemia, Czech Republic	<i>Salix caprea</i>	W	-	relative growth rate (g ⁺ *g biomass ⁻¹ *d ⁻¹)	142	1	relative growth rate (g ⁺ *g biomass ⁻¹ *d ⁻¹)	165	1	176	8.9	490	[46]	
South Bohemia, Czech Republic	<i>Salix caprea</i>	W	-	relative growth rate (g ⁺ *g biomass ⁻¹ *d ⁻¹)	200	2	relative growth rate (g ⁺ *g biomass ⁻¹ *d ⁻¹)	196	1	-4	8.9	490	[46]	
New York, USA	<i>Corylus colurna</i>	W	D	shoot growth (%*d ⁻¹)	141	1	root growth (%*d ⁻¹) ³	165	2	24	9.4	1055	[47]	
	<i>Fraxinus</i>													
New York, USA	<i>pennsylvanica</i>	W	D	shoot growth (%*d ⁻¹)	142	1	root growth (%*d ⁻¹) ³	173	2	31	9.4	1055	[47]	
New York, USA	<i>Quercus coccinea</i>	W	D	shoot growth (%*d ⁻¹)	143	1	root growth (%*d ⁻¹) ³	195	3	52	9.4	1055	[47]	
New York, USA	<i>Syringa reticulata</i>	W	-	shoot growth (%*d ⁻¹)	140	1	root growth (%*d ⁻¹) ³	228	3	88	9.4	1055	[47]	

Biome	Location	Species	H W	D E	Type of aboveground or measurement or abiotic variable	AP	#AP	Type of belowground measurement	BP	#BP	Offset	MMT	MMP	REF
Temperate	Scotland, UK	<i>Pinus sylvestris</i>	W	E	shoot growth (m*time ⁻¹)	118.5	1	change in dry weight (g) ¹	250	1	131.5	8.5	815	[48]
	Scotland, UK Nova Scotia, Canada	<i>Sorbus aucuparia</i> <i>Vaccinium angustifolium</i>	W	-	shoot growth (m*time ⁻¹)	128.5	1	change in dry weight (g) ¹	77.5	2	-51	8.5	815	[48]
	Pennsylvania, USA	<i>Acer saccharum</i>	W	-	stem length (cm) leaf elongation	187	1	change in root biomass (g*m ⁻²) ¹	166	1	-21	6.3	1452	[49]
	Pennsylvania, USA	<i>Carya glabra</i>	W	D	(midpoint) leaf elongation	130.5	1	root production (%) ²	89	6	-41.5	11.1	1108	[50]
	Pennsylvania, USA	<i>Liriodendron tulipifera</i>	W	D	(midpoint) leaf elongation	155	1	root production (%) ²	104	3	-51	11.1	1108	[50]
	Pennsylvania, USA	<i>Pinus strobus</i>	W	-	(midpoint) leaf elongation	128.5	1	root production (%) ²	138	7	9.5	11.1	1108	[50]
	Pennsylvania, USA	<i>Prunus virginiana</i>	W	E	(midpoint) leaf elongation	178	1	root production (%) ²	124	6	-54	11.1	1108	[50]
	Pennsylvania, USA	<i>Quercus alba</i>	W	D	(midpoint) leaf elongation	173	1	root production (%) ²	89	6	-84	11.1	1108	[50]
	New York, USA	<i>Malus sylvestris</i>	W	-	shoot growth (cm*d ⁻¹)	145.5	1	root production (%) ²	89	5	-56.5	11.1	1108	[50]
	New York, USA	<i>Malus sylvestris</i>	W	-	shoot growth (cm*d ⁻¹) mean onset of shoot or leaf flush	153	1	root growth (roots*tube ⁻¹ *d ⁻¹) ²	171	1	18	9.4	1055	[51]
	Missouri, USA	<i>Quercus alba</i>	W	D	leaf flush relative growth rate	140	1	root growth (roots*tube ⁻¹ *d ⁻¹) ²	189	1	49	9.4	1055	[51]
	Oregon, USA	<i>Rhododendron</i> 'P.J.Mezzitt Compact'	W	-	relative growth rate	125	4	root growth (%*d ⁻¹) ³	121	4	4	16.0	1394	[33]
	Oregon, USA	<i>Rhododendron</i> 'English Roseum'	W	-	relative growth rate	213	1	relative growth rate (mg*g ⁻¹ *d ⁻¹) ¹	213	2	0	11.3	1171	[52]
	Oregon, USA	<i>Rhododendron</i> 'Gibraltar'	W	-	relative growth rate	213	3	relative growth rate (mg*g ⁻¹ *d ⁻¹) ¹	213	2	0	11.3	1171	[52]
	Bédoin, France North Carolina, USA	<i>Quercus pubescens</i>	W	D	leaf area production	241	2	relative growth rate (mg*g ⁻¹ *d ⁻¹) ¹	159	3	-82	11.3	1171	[52]
	North Carolina, USA	<i>Kalmia latifolia</i>	W	-	change in shoot biomass (g*time ⁻¹)	9.7	1	lateral root growth rate (cm*d ⁻¹) ³	21.4	1	11.7	15.1	555	[36]
	USA	<i>Ilex crenata</i>	W	-	change in shoot biomass (g*time ⁻¹)	354.5	2	change in root length (cm*time ⁻¹) ¹	160	2	-195	16.0	1101	[53]
	Fukuoka, Japan	<i>Eustoma grandiflorum</i>	W	-	change in shoot length	124.5	2	change in root length (cm*time ⁻¹) ¹	353	4	228.5	16.0	1101	[53]
	Fukuoka, Japan	<i>Eustoma grandiflorum</i>	H	-	(mm*time ⁻¹) change in shoot length	266.5	1	change in root length (cm*time ⁻¹) ¹	311	1	44.5	17.2	1613	[54]
	Oregon, USA	<i>Rubus spectabilis</i>	W	-	shoot growth (number active*segment ⁻¹)	266.5	1	change in root length (cm*time ⁻¹) ¹	311	1	44.5	17.2	1613	[54]
						64	1	root growth (number active*segment ⁻¹) ¹	248	1	184	11.3	1171	[55]

Biome	Location	Species	H or W	D or E	Type of aboveground measurement or abiotic variable	AP	#AP	Type of belowground measurement	BP	#BP	Offset	MMT	MMP	REF
<i>Mediterranean</i>	Cachapaol, Chile	<i>Prunus avium</i>	W	D	shoot growth (cm ³ *time ⁻¹)	339.5	1	root growth (cm ³ *time ⁻¹) ³	375	3	35	15.4	313	[56]
	California, USA	<i>Persea americana</i>	W	-	shoot growth rate (%)	107	1	root growth rate (%) ³	162	2	55	18.6	379	[57]
	California, USA	<i>Persea americana</i>	W	-	shoot growth rate (%)	107	2	root growth rate (%) ³	260	2	153	18.6	379	[57]
	California, USA	<i>Pinus ponderosa</i>	W	E	shoot growth (%)	157	1	root growth (%) ²	157	1	0	16.4	378	[13]
	Huesca, Spain	<i>Lepidium subulatum</i>	H	-	phenophase occurrence (%)	138	1	root growth (%) ¹	74	2	-64	15.0	317	[14]
	Huesca, Spain	<i>Salvia lavandulifolia</i>	H	-	phenophase occurrence (%)	159.5	2	root growth (%) ¹	138	2	-21.2	15.0	317	[14]
	Huesca, Spain	<i>Echinopsartum horridum</i>	H	-	phenophase occurrence (%)	88	1	root growth (%) ¹	68	1	-20	15.0	317	[14]
	Huesca, Spain	<i>Linus suffruticosum</i>	H	-	phenophase occurrence (%)	23	1	root growth (%) ¹	97	3	74	15.0	317	[14]
	Greek Macedonia, Greece	<i>Quercus coccifera</i>	W	D	shoot production (g ³ *m ² *time ⁻¹)	136	2	change in dry weight (g ³ *m ⁻² *time ⁻¹) ¹	228	3	92	15.0	449	[58]
	California, USA	<i>Pinus ponderosa</i>	W	E	height increment (cm)	129	1	new root area density (mm ² *mm ⁻²)	140	1	11	16.1	471	[15]
	California, USA	<i>Pinus ponderosa</i>	W	E	height increment (cm)	133	1	new root area density (mm ² *mm ⁻²)	218	1	85	16.1	471	[15]
	Florida, USA	<i>Citrus sinensis</i> x <i>Citrus jambhiri</i>	W	-	shoot growth (cm*d ⁻¹)	229	5	root growth (cm ³ *d ⁻¹)	297	5	68	22.9	1350	[17]
	Florida, USA	<i>Citrus sinensis</i> x <i>Poncirus trifoliata</i>	W	-	shoot growth (cm*d ⁻¹)	219	5	root growth (cm ³ *d ⁻¹)	247	5	28	22.9	1350	[17]
	Florida, USA	<i>Cocos nucifera</i>	W	-	shoot growth (mm ³ *week ⁻¹)	270	1	root growth (mm ³ *week ⁻¹) ³	249	1	-21	24.9	1272	[18]
Florida, USA	<i>Phoenix roebelenii</i>	W	-	shoot growth (mm ³ *week ⁻¹)	289	2	root growth (mm ³ *week ⁻¹) ³	231	3	-58	24.9	1272	[18]	
Florida, USA	<i>Roystonea regia</i>	W	-	shoot growth (mm ³ *week ⁻¹)	272	1	root growth (mm ³ *week ⁻¹) ³	202	2	-70	24.9	1272	[18]	
Florida, USA	<i>Syagrus romanzoffiana</i>	W	-	shoot growth (mm ³ *week ⁻¹)	269	1	root growth (mm ³ *week ⁻¹) ³	102	1	-167	24.9	1272	[18]	
Sarawak, Malaysia	<i>Dipterocarp forest</i>	W	-	leaf production (mgC*ha ⁻¹ *month ⁻¹)	365	1	root production (mgC*ha ⁻¹ *month ⁻¹) ¹	332	1	-33	27.9	1985	[59]	
Sarawak, Malaysia	<i>Dipterocarp forest</i>	W	-	leaf production (mgC*ha ⁻¹ *month ⁻¹)	217	3	root production (mgC*ha ⁻¹ *month ⁻¹) ¹	201	1	-16	27.9	1985	[59]	
Florida, USA	<i>Litchi chinensis</i>	W	-	stem growth (mm*d ⁻¹)	136	4	root growth (mm ³ *d ⁻¹)	69	2	-67	24.9	1272	[60]	
Florida, USA	<i>Persea americana</i>	W	-	shoot growth (mm*d ⁻¹)	248	2	root growth (mm ³ *d ⁻¹)	179	2	-69	24.9	1272	[21]	
Florida, USA	<i>Persea americana</i>	W	-	shoot growth (mm*d ⁻¹)	247	2	root growth (mm ³ *d ⁻¹)	156	3	-91	24.9	1272	[21]	

Table 2.S3. Monthly root and shoot growth rates for each biome estimated from literature. Growth rate of roots and shoots were tabulated from each study (excluding those that did not include seasonal data [i.e. measured DOY 1 as start of experiment rather than the Julian day]) and converted to a % of the maximum growth rate. Growth rates were averaged for each month with > 5 observations. These rates do not exceed 1 because many studies with differently timed maximum growth were averaged. MMT, median monthly temperature (°C); MMP, mean monthly precipitation (mm).

Biome	Month	Growth (% max)			Organ	MMT	MMP
<i>Boreal (n=17)</i>	Jan	-	±	-	root	-13.229	22.38
	Feb	-	±	-	root	-10.221	16.85
	Mar	0.08	±	0.06	root	-3.9353	22.51
	Apr	0.24	±	0.07	root	4.4382	25.75
	May	0.29	±	0.07	root	11.7118	47.65
	Jun	0.65	±	0.09	root	16.6588	69.85
	Jul	0.71	±	0.09	root	18.8676	67.5
	Aug	0.55	±	0.08	root	17.6882	52.41
	Sep	0.35	±	0.08	root	11.6382	39.82
	Oct	0.39	±	0.15	root	5.1824	30.59
	Nov	0.18	±	0.11	root	-3.6735	24.36
	Dec	-	±	-	root	-10.506	25.04
	Jan	-	±	-	shoot	-13.229	22.38
	Feb	-	±	-	shoot	-10.221	16.85
	Mar	0.03	±	0.01	shoot	-3.9353	22.51
	Apr	0.15	±	0.07	shoot	4.4382	25.75
	May	0.66	±	0.09	shoot	11.7118	47.65
	Jun	0.68	±	0.06	shoot	16.6588	69.85
	Jul	0.46	±	0.10	shoot	18.8676	67.5
	Aug	0.27	±	0.08	shoot	17.6882	52.41
	Sep	0.18	±	0.07	shoot	11.6382	39.82
	Oct	0.12	±	0.07	shoot	5.1824	30.59
	Nov	0.05	±	0.02	shoot	-3.6735	24.36
	Dec	-	±	-	shoot	-10.506	25.04
<i>Mediterranean (n=20)</i>	Jan	0.25	±	0.07	root	11.525	45.2
	Feb	0.20	±	0.07	root	13.335	48.42
	Mar	0.45	±	0.11	root	15.27	36.89

Biome	Month	Growth (% max)			Organ	MMT	MMP	
<i>Mediterranean (n=20)</i>	Apr	0.31	±	0.08	root	16.82	29.02	
	May	0.31	±	0.10	root	19.745	30.3	
	Jun	0.52	±	0.16	root	22.67	23.62	
	Jul	0.41	±	0.15	root	25.215	18.31	
	Aug	0.53	±	0.15	root	25.145	14.35	
	Sep	0.41	±	0.13	root	22.875	18.28	
	Oct	0.54	±	0.10	root	19.025	25.17	
	Nov	0.55	±	0.14	root	14.555	33.7	
	Dec	0.52	±	0.11	root	11.725	40.38	
	Jan	0.08	±	0.08	shoot	11.525	45.2	
	Feb	0.04	±	0.03	shoot	13.335	48.42	
	Mar	0.39	±	0.13	shoot	15.27	36.89	
	Apr	0.76	±	0.13	shoot	16.82	29.02	
	May	0.70	±	0.11	shoot	19.745	30.3	
	Jun	0.18	±	0.07	shoot	22.67	23.62	
	Jul	0.13	±	0.06	shoot	25.215	18.31	
	Aug	0.16	±	0.06	shoot	25.145	14.35	
	Sep	0.11	±	0.05	shoot	22.875	18.28	
	Oct	0.08	±	0.05	shoot	19.025	25.17	
	Nov	0.14	±	0.11	shoot	14.555	33.7	
	Dec	0.02	±	0.02	shoot	11.725	40.38	
	<i>Subtropical (n=11)</i>	Jan	0.21	±	0.08	root	19.4333	59.1
		Feb	0.23	±	0.07	root	20.4222	61.63
		Mar	0.36	±	0.08	root	21.6611	75.92
Apr		0.31	±	0.09	root	23.5111	67.56	
May		0.41	±	0.06	root	25.8111	118.6	
Jun		0.51	±	0.12	root	27.6333	212.4	
Jul		0.64	±	0.11	root	28.7	118.5	
Aug		0.71	±	0.10	root	28.6889	159.7	
Sep		0.91	±	0.03	root	27.95	182.8	
Oct		0.71	±	0.09	root	25.9056	109.7	
Nov		0.59	±	0.09	root	23.1333	69.36	
Dec		0.36	±	0.12	root	20.6222	54.36	
Jan		0.26	±	0.08	shoot	19.4333	59.1	
Feb		0.31	±	0.10	shoot	20.4222	61.63	
Mar		0.27	±	0.11	shoot	21.6611	75.92	
Apr		0.41	±	0.10	shoot	23.5111	67.56	
May		0.38	±	0.13	shoot	25.8111	118.6	
Jun		0.44	±	0.11	shoot	27.6333	212.4	

Biome	Month	Growth (%max)		Organ	MMT	MMP
<i>Subtropical (n=11)</i>	Jul	0.38	± 0.11	shoot	28.7	118.5
	Aug	0.78	± 0.11	shoot	28.6889	159.7
	Sep	0.73	± 0.09	shoot	27.95	182.8
	Oct	0.54	± 0.10	shoot	25.9056	109.7
	Nov	0.43	± 0.13	shoot	23.1333	69.36
	Dec	0.33	± 0.11	shoot	20.6222	54.36
<i>Temperate (n=38)</i>	Jan	0.04	± 0.02	root	-0.5392	79.24
	Feb	0.10	± 0.04	root	0.9284	72.46
	Mar	0.23	± 0.06	root	4.9851	82.22
	Apr	0.31	± 0.07	root	10.1203	78.32
	May	0.44	± 0.06	root	15.0743	86.3
	Jun	0.63	± 0.05	root	19.2946	90.63
	Jul	0.66	± 0.06	root	21.7824	86.54
	Aug	0.43	± 0.07	root	21.2757	78.34
	Sep	0.27	± 0.05	root	17.4554	83.59
	Oct	0.29	± 0.05	root	11.6743	79.73
	Nov	0.18	± 0.06	root	6.2986	94.68
	Dec	0.08	± 0.03	root	1.273	89.37
	Jan	0.08	± 0.06	shoot	-0.5392	79.24
	Feb	0.06	± 0.06	shoot	0.9284	72.46
	Mar	0.20	± 0.07	shoot	4.9851	82.22
	Apr	0.30	± 0.07	shoot	10.1203	78.32
	May	0.64	± 0.06	shoot	15.0743	86.3
	Jun	0.59	± 0.06	shoot	19.2946	90.63
	Jul	0.60	± 0.07	shoot	21.7824	86.54
	Aug	0.46	± 0.07	shoot	21.2757	78.34
	Sep	0.29	± 0.06	shoot	17.4554	83.59
	Oct	0.23	± 0.05	shoot	11.6743	79.73
	Nov	0.20	± 0.05	shoot	6.2986	94.68
	Dec	0.08	± 0.05	shoot	1.273	89.37

Supplementary Information Reference Guide

1. López B, Sabaté S, Gracia C (2001) Annual and seasonal changes in fine root biomass of a *Quercus ilex* L. forest. *Plant and Soil*, **230**, 125-134.
2. Majdi H, Andersson P (2005) Fine root production and turnover in a Norway spruce stand in northern Sweden: effects of nitrogen and water manipulation. *Ecosystems*, **8**, 191-199.
3. Pritchard SG, Strand AE, McCormack ML *et al.* (2008) Fine root dynamics in a loblolly pine forest are influenced by free-air-CO₂-enrichment: a six-year-minirhizotron study. *Global Change Biology*, **14**, 588-602.
4. R Development Core Team (2013) R: A language and environment for statistical computing., Vienna, Austria, R Foundation for Statistical Computing.
5. Reich P (1999) World Biomes Map. In: *Soil climate map*. Washington D.C., USDA-NRCS, Soil Science Division, World Soil Resources.
6. World Weather Information Service. (2013) World Meteorological Organization.
7. Iivonen S, Rikala R, Vapaavuori E (2001) Seasonal root growth of Scots pine seedlings in relation to shoot phenology, carbohydrate status, and nutrient supply. *Canadian Journal of Forest Research-Revue Canadienne De Recherche Forestiere*, **31**, 1569-1578.
8. Lahti M, Aphalo P, Finér L, Ryppö A, Lehto T, Mannerkoski H (2005) Effects of soil temperature on shoot and root growth and nutrient uptake of 5-year-old Norway spruce seedlings. *Tree Physiology*, **25**, 115-122.

9. Rytter R-M (2001) Biomass production and allocation, including fine-root turnover, and annual N uptake in lysimeter-grown basket willows. *Forest Ecology and Management*, **140**, 177-192.
10. Steinaker DF, Wilson SD (2008) Phenology of fine roots and leaves in forest and grassland. *Journal of Ecology*, **96**, 1222-1229.
11. Steinaker DF, Wilson SD, Peltzer DA (2010) Asynchronicity in root and shoot phenology in grasses and woody plants. *Global Change Biology*, **16**, 2241-2251.
12. Vapaavuori E, Iivonen S, Rikala R (2001) Seasonal root growth of Scots pine seedlings in relation to shoot phenology, carbohydrate status, and nutrient supply. *Canadian Journal of Forest Research-Revue Canadienne De Recherche Forestiere*, **31**, 1569-1578.
13. Misson L, Gershenson A, Tang J, Mckay M, Cheng W, Goldstein A (2006) Influences of canopy photosynthesis and summer rain pulses on root dynamics and soil respiration in a young ponderosa pine forest. *Tree Physiology*, **26**, 833-844.
14. Palacio S, Montserrat-Marti G (2007) Above and belowground phenology of four Mediterranean sub-shrubs. Preliminary results on root-shoot competition. *Journal of Arid Environments*, **68**, 522-533.
15. Tingey DT, Johnson MG, Phillips DL, Johnson DW, Ball JT (1996) Effects of elevated CO₂ and nitrogen on the synchrony of shoot and root growth in ponderosa pine. *Tree Physiology*, **16**, 905-914.

16. Wilcox CS, Ferguson JW, Fernandez GC, Nowak RS (2004) Fine root growth dynamics of four Mojave Desert shrubs as related to soil moisture and microsite. *Journal of Arid Environments*, **56**, 129-148.
17. Bevington KB, Castle WS (1985) Annual root growth pattern of young citrus trees in relation to shoot growth, soil temperature, and soil water content. *Journal of the American Society for Horticultural Science*, **110**, 840-845.
18. Broschat TK (1998) Root and shoot growth patterns in four palm species and their relationships with air and soil temperatures. *HortScience*, **33**, 995-998.
19. Chen XY, Eamus D, Hutley LB (2004) Seasonal patterns of fine-root productivity and turnover in a tropical savanna of northern Australia. *Journal of Tropical Ecology*, **20**, 221-224.
20. Green IJ, Dawson LA, Proctor J, Duff EI, Elston DA (2005) Fine root dynamics in a tropical rain forest is influenced by rainfall. *Plant and Soil*, **276**, 23-32.
21. Ploetz RC, Ramos JL, Parrado JL, Lovatt C (1992) Shoot and root growth phenology of grafted avocado. In: *Proc. Second World Avocado Congress. University of California, Riverside, USA. [Links]*. pp 215-220.
22. Yavitt JB, Wright SJ (2001) Drought and irrigation effects on fine root dynamics in a tropical moist forest, Panama. *Biotropica*, **33**, 421-434.
23. Burke MK, Raynal DJ (1994) Fine-Root Growth Phenology, Production, and Turnover in a Northern Hardwood Forest Ecosystem. *Plant and Soil*, **162**, 135-146.

24. Cardon ZG, Czaja AD, Funk JL, Vitt PL (2002) Periodic carbon flushing to roots of *Quercus rubra* saplings affects soil respiration and rhizosphere microbial biomass. *Oecologia*, **133**, 626-626.
25. Côté B, Hendershot WH, Fyles JW, Roy AG, Bradley R, Biron PM, Courchesne F (1998) The phenology of fine root growth in a maple-dominated ecosystem: relationships with some soil properties. *Plant and Soil*, **201**, 59-69.
26. Deans J (1979) Fluctuations of the soil environment and fine root growth in a young Sitka spruce plantation. *Plant and Soil*, **52**, 195-208.
27. Fitter A, Graves J, Self G, Brown T, Bogie D, Taylor K (1998) Root production, turnover and respiration under two grassland types along an altitudinal gradient: influence of temperature and solar radiation. *Oecologia*, **114**, 20-30.
28. Fitter A, Self G, Brown T, Bogie D, Graves J, Benham D, Ineson P (1999) Root production and turnover in an upland grassland subjected to artificial soil warming respond to radiation flux and nutrients, not temperature. *Oecologia*, **120**, 575-581.
29. Hendrick RL, Pregitzer KS (1996) Applications of minirhizotrons to understand root function in forests and other natural ecosystems. *Plant and Soil*, **185**, 293-304.
30. Joslin JD, Wolfe MH, Hanson PJ (2001) Factors controlling the timing of root elongation intensity in a mature upland oak stand. *Plant and Soil*, **228**, 201-212.
31. Lopushinsky W, Max T (1990) Effect of soil temperature on root and shoot growth and on budburst timing in conifer seedling transplants. *New Forests*, **4**, 107-124.

32. Macduff J, Wild A, Hopper M, Dhanoa M (1986) Effects of temperature on parameters of root growth relevant to nutrient uptake: measurements on oilseed rape and barley grown in flowing nutrient solution. *Plant and Soil*, **94**, 321-332.
33. Reich PB, Teskey RO, Johnson PS, Hinckley TM (1980) Periodic root and shoot growth in oak. *Forest Science*, **26**, 590-598.
34. Rufty TW, Raper CD, Jackson WA (1981) Nitrogen assimilation, root growth and whole plant responses of soybean to root temperature, and to carbon dioxide and light in the aerial environment. *New Phytologist*, **88**, 607-619.
35. Teskey RO, Hinckley TM (1981) Influence of Temperature and Water Potential on Root-Growth of White Oak. *Physiologia Plantarum*, **52**, 363-369.
36. Willaume M, Pagès L (2006) How periodic growth pattern and source/sink relations affect root growth in oak tree seedlings. *Journal of Experimental Botany*, **57**, 815-826.
37. Kaakinen S, Jolkkonen A, Iivonen S, Vapaavuori E (2004) Growth, allocation and tissue chemistry of *Picea abies* seedlings affected by nutrient supply during the second growing season. *Tree Physiology*, **24**, 707-719.
38. Repo T, Lehto T, Finér L (2008) Delayed soil thawing affects root and shoot functioning and growth in Scots pine. *Tree Physiology*, **28**, 1583-1591.
39. Vapaavuori E, Rikala R, Ryyppö A (1992) Effects of root temperature on growth and photosynthesis in conifer seedlings during shoot elongation. *Tree Physiology*, **10**, 217-230.

40. Aerts R, De Caluwe H, Konings H (1992) Seasonal allocation of biomass and nitrogen in four *Carex* species from mesotrophic and eutrophic fens as affected by nitrogen supply. *Journal of Ecology*, 653-664.
41. Bosac C, Gardner S, Taylor G, Wilkins D (1995) Elevated CO₂ and hybrid poplar: a detailed investigation of root and shoot growth and physiology of *Populus euramericana*, 'Primo'. *Forest Ecology and Management*, **74**, 103-116.
42. Burke MK, Raynal DJ, Mitchell MJ (1992) Soil nitrogen availability influences seasonal carbon allocation patterns in sugar maple (*Acer saccharum*). *Canadian Journal of Forest Research*, **22**, 447-456.
43. Curtis PS, Zak DR, Pregitzer KS, Teeri JA (1995) Above- and belowground response of *Populus grandidentata* to elevated atmospheric CO₂ and soil N availability. In: *Belowground Responses to Rising Atmospheric CO₂: Implications for Plants, Soil Biota, and Ecosystem Processes*. pp 45-51. Springer.
44. Dornbush ME, Raich JW (2006) Soil temperature, not aboveground plant productivity, best predicts intra-annual variations of soil respiration in central Iowa grasslands. *Ecosystems*, **9**, 909-920.
45. Drew AP, Ledig FT (1981) Seasonal patterns of CO₂ exchange in the shoot and root of loblolly pine seedlings. *Botanical Gazette*, 200-205.
46. Dušek J, Květ J (2006) Seasonal dynamics of dry weight, growth rate and root/shoot ratio in different aged seedlings of *Salix caprea*. *Biologia*, **61**, 441-447.

47. Harris JR, Bassuk NL, Zobel RW, Whitlow TH (1995) Root and shoot growth periodicity of green ash, scarlet oak, turkish hazelnut, and tree lilac. *Journal of the American Society for Horticultural Science*, **120**, 211-216.
48. Hester AJ, Millard P, Baillie GJ, Wendler R (2004) How does timing of browsing affect above-and below-ground growth of *Betula pendula*, *Pinus sylvestris* and *Sorbus aucuparia*? *Oikos*, **105**, 536-550.
49. Kaur J, Percival D, Hainstock LJ, Prive J-P (2012) Seasonal growth dynamics and carbon allocation of the wild blueberry plant (*Vaccinium angustifolium* Ait.). *Canadian Journal of Plant Science*, **92**, 1145-1154.
50. McCormack ML, Adams TS, Smithwick EaH, Eissenstat DM (2014) Variability in root production, phenology, and turnover rate among 12 temperate tree species. *Ecology*, **95**, 2224-2235.
51. Psarras G, Merwin IA, Lakso AN, Ray JA (2000) Root Growth Phenology, Root Longevity, and Rhizosphere Respiration of Field Grown Mutsu' Apple Trees on Malling 9' Rootstock. *Journal of the American Society for Horticultural Science*, **125**, 596-602.
52. Scagel CF, Bi G, Fuchigami LH, Regan RP (2007) Seasonal variation in growth, nitrogen uptake and allocation by container-grown evergreen and deciduous rhododendron cultivars. *HortScience*, **42**, 1440-1449.
53. Wright AN, Warren SL, Blazich FA, Blum U (2004) Root and Shoot Growth Periodicity of *Kalmia latifolia* Sarah' and *Ilex crenata* Compacta'. *HortScience*, **39**, 243-247.

54. Yamashita M, Imamura H (2007) Shoot and Root Growth and Lysigenous Aerenchyma Formation in Rosetted and Stem-extensional Plants of *Eustoma grandiflorum* (Raf.) Shinn. *園芸学会雑誌*, **76**, 54-59.
55. Zasada JC, Tappeiner Iii JC, Maxwell BD, Radwan M (1994) Seasonal changes in shoot and root production and in carbohydrate content of salmonberry (*Rubus spectabilis*) rhizome segments from the central Oregon Coast Ranges. *Canadian Journal of Forest Research*, **24**, 272-277.
56. Bonomelli C, Bonilla C, Acuña E, Artacho P (2012) Seasonal pattern of root growth in relation to shoot phenology and soil temperature in sweet cherry trees (*Prunus avium*): A preliminary study in central Chile. *Ciencia e Investigación Agraria*, **39**, 127-136.
57. Mickelbart MV, Robinson PW, Witney G, Arpaia ML (2012) 'Hass' avocado tree growth on four rootstocks in California. II. Shoot and root growth. *Scientia Horticulturae*, **143**, 205-210.
58. Papatheodorou EM, Pantis JD, Stamou GP (1998) The effect of grazing on phenology and biomass allocation in *Quercus coccifera* (L.). *Acta Oecologica*, **19**, 339-347.
59. Kho LK, Malhi Y, Tan SKS (2013) Annual budget and seasonal variation of aboveground and belowground net primary productivity in a lowland dipterocarp forest in Borneo. *Journal of Geophysical Research: Biogeosciences*, **118**, 1282-1296.
60. Marler TE, Willis LE (1996) Root and Stem Growth Patterns of YoungMauritius' Lychee Trees. *HortScience*, **31**, 815-818.

**CHAPTER THREE: SEASONALITY AND PARTITIONING OF ROOT
ALLOCATION TO RHIZOSPHERE SOILS IN A MID-LATITUDE FOREST**

Abstract

Fine roots are a seasonally dynamic carbon (C) pool that accounts for a large proportion of net primary production. Roots affect the composition and function of the soil microbial community through turnover of root tissues, exudation of labile organic compounds and allocation of C to mycorrhizal fungi. As such root growth, mortality, and exudation are important components of biogeochemical cycles, yet data on the timing and partitioning of C to these processes are rare. The objective of this study is to estimate the seasonality, magnitude, and partitioning of C allocated belowground across the growing season in three mid-latitude hardwood and conifer stands at Harvard Forest in central Massachusetts using a minirhizotron camera, infrared gas analyzer, and cuvette collection to measure root production, respiration and exudation, respectively.

Fine root growth and respiration were both positively correlated with temperature, but differed in their phenology. Root phenology was characterized by multiple flushes of growth and mortality, whereas root respiration was unimodal across the growing season. Deciduous hardwood stands allocated C belowground earlier in the season compared to a conifer-dominated stand. Total belowground C flux (TBCF) was highest in the red oak stand, consistent with the observed increase in aboveground biomass of red oak at Harvard Forest over the past 20 years. TBCF was lowest in the eastern hemlock stand due to a decline in allocation to root production over the study period. This decline is coincident with the arrival and spread of the hemlock woolly adelgid in this stand. This

study elucidates the seasonal partitioning of belowground C within the context of long-term stand dynamics.

Introduction

Fine roots are a dynamic carbon (C) pool that accounts for 10-60% of net primary production (NPP, Keyes & Grier 1981, Helmisaari *et al.*, 2002, Ostonen *et al.*, 2005).

Allocation of C to roots is the main conduit by which C is transported belowground and incorporated into soil organic matter (SOM). Roots affect the composition and function of the soil microbial community through tissue turnover, exudation of labile organic compounds and allocation of C to mycorrhizal fungi. Root exudation stimulates microbial biomass growth and extracellular enzyme activity, thereby increasing the decomposition rate of SOM, liberating plant available nitrogen (N), and releasing carbon dioxide (CO₂) to the atmosphere (Kuzyakov, 2010, Phillips *et al.*, 2011). As such root growth, mortality and exudation are important components of biogeochemical cycles (Finzi *et al.*, 2015).

Root respiration can account for up to 70% of total belowground C allocation and over half of soil CO₂ efflux (Burton *et al.*, 2008, Drake *et al.*, 2011, Fahey *et al.*, 2005).

Soil respiration is a large flux that integrates information about autotrophic and heterotrophic processes that together follow the seasonal cycle of air temperature and photosynthesis, and as a result it is relatively easy to detect the seasonal pattern of soil respiration. In contrast, measuring individual processes that contribute to belowground C allocation and soil respiration, such as autotrophic respiration, is far more challenging because of disturbance effects associated with sampling, small sample volume and small fluxes. A compromise approach measures the rate of root respiration indirectly by subtracting soil respiration rates in trenched and untrenched plots. While seasonally resolved, this method may over- or under-estimate autotrophic respiration as a result of

root death and decomposition (Drake *et al.*, 2012, Savage *et al.*, 2013) or the loss of priming effects (Finzi *et al.*, 2015). Perhaps as a result of these difficulties, few studies assess seasonal patterns of belowground C allocation, making it difficult to understand how the belowground C flux is partitioned among roots, exudates, and mycorrhizal fungi (Drake *et al.*, 2011). There are a handful of studies that have included seasonally resolved measurements of root respiration using chamber measurements on intact or excavated roots (Burton *et al.*, 2002, Davidson & Holbrook, 2009, Davidson *et al.*, 2006). Similarly, there are few seasonally-resolved measurements of fine root nonstructural carbohydrates (NSC) pools despite their potential importance to ecosystem-scale C cycling (Boldingh *et al.*, 2000, Li *et al.*, 1996). Even less is known about the seasonality of root exudation (Phillips *et al.*, 2008, Pritchard *et al.*, 2008).

Despite the paucity of process-level data, there are sufficient studies that document notable variations in the phenology of belowground C allocation. For example, Cardon *et al.* (2002) report multiple flushes of root production in oak species throughout the growing season. There are also observations of differences in the phenology of root growth between different tree species in the same geographical location, indicating that belowground phenology depends in part on internal cues (McCormack *et al.*, 2014). At the biome scale, root production is commonly asynchronous with aboveground growth, particularly where coniferous tree species are present (Abramoff & Finzi, 2015).

In previous work I found that the phenology of belowground autotrophic activity is sensitive to variations in temperature, precipitation, and substrate supply (Abramoff & Finzi, 2015, Giasson *et al.*, 2013). One observation common to both studies is a peak in

soil respiration or maximum root growth occurring after the peak in ecosystem respiration and maximum shoot growth, respectively. Neither of these studies, however, directly measured the components of belowground C allocation and their phenology using the same methods through time.

The objective of this study is to assess the phenology, magnitude, and partitioning of C allocated belowground across the growing season in mid-latitude, hardwood and conifer stands at the Harvard Forest in central Massachusetts. Based on the results of my previous work, I hypothesize that (1) deciduous stands allocate C belowground earlier in the growing season than the conifer stand; (2) root growth, mortality and respiration are positively correlated with soil temperature and precipitation; and the (3) total belowground C flux (TBCF) is highest overall in the red oak stand compared to the white ash and eastern hemlock stand, consistent with the observed increase in red oak aboveground biomass throughout the Harvard Forest over the past 20 years (Urbanski *et al.*, 2007), and consistent with the arrival of the invasive pest the hemlock woolly adelgid to the hemlock stand (Ellison *et al.*, 2015).

Materials and Methods

Study Site

This study was conducted in the Prospect Hill tract of the Harvard Forest Long Term Ecological Research site, a 120+-year-old secondary-growth forest located in Petersham, MA (42°N, 72°W, elevation 340 m; Wofsy *et al.*, 1993, Goulden *et al.*, 1996). The dominant species are northern red oak (*Quercus rubra*) and red maple (*Acer rubrum*), with smaller populations of eastern hemlock (*Tsuga canadensis*), white ash

(*Fraxinus americana*), white pine (*Pinus strobus*) and red pine (*Pinus resinosa*). The site is located on former agricultural land that was abandoned in the mid-1800s allowing forest regrowth beginning late in the 19th century (Foster *et al.*, 2003). Forest uptake of C has increased since 1990 from $\sim 2 \text{ Mg C ha}^{-1} \text{ yr}^{-1}$ to $\sim 5 \text{ Mg C ha}^{-1} \text{ yr}^{-1}$ (Keenan *et al.*, 2012, Urbanski *et al.*, 2007). Soils are Typic Distrochrepts derived from glacial deposits of granite, schist and gneiss.

Plots were established in three mono-dominant stands: white ash, red oak, and eastern hemlock (Figure 3.1). Each stand occupies an area of 3.4, 8.3, and 10.9 hectares, respectively. I established 6 biometry plots per stand ($N = 18$) and 10 minirhizotron tube plots per stand ($N = 30$). The basal area in each 8-m-radius biometry plot is composed of 80% dominant tree species, with the inner 5-m basal area containing only the dominant species. The three stands differ in soil chemistry and biogeochemistry (Brzostek & Finzi, 2012). The white ash stand has a lower ratio of C-to-N content in the soil than the oak and hemlock stand (Table 3.1).

Root Production and Biomass

Root production and turnover were measured April–December 2012, March–November 2013, and April–November 2014 using a BTC-100x high magnification minirhizotron camera system (Bartz Technology Company, Carpinteria, CA). Measurements were made bi-weekly during the growing season in 2012 and monthly in 2013, 2014, and during the snow-free dormant season of each of the three years. There was no sampling from December 2012 to March 2013 and November 2013 to April 2014.

The camera system was inserted into cellulose acetate butyrate tubes installed at a 45° angle to a vertical soil depth of 40 cm. Thirteen tubes were installed in the center of each minirhizotron tube plot at Harvard Forest 10+ years ago (n = 4 in red oak, n = 9 in eastern hemlock). Seventeen tubes were installed in November 2012 (n = 6 in red oak, n = 1 in eastern hemlock, and n = 10 in white ash) for a sample size of n = 10 for each stand in 2013 and 2014. Minirhizotron tubes installed in November 2012 likely severed existing roots during placement and may have increased root growth rates in the following seasons. To test for this effect I conducted an analysis of variance using growth or mortality as the dependent variable and sample date and whether or not the sample came from a recently installed minirhizotron tube as fixed effects for 2013 and 2014.

The camera captures thirty-nine sequential images that are 13.5 x 17 mm in size along the upper axis of each tube at each sampling interval. The resulting images were processed using the open source imaging software Rootfly (Rootfly Development Team, Version 2.0.2, GNU General Public License). In each image, every root or root segment's length and diameter was annotated. Length (mm) and diameter (mm) were scaled to mass (g) using a site-specific relationship based on n = 20 per species. For each root sample I recorded length and diameter, and dried it to constant mass at 60°C for 4 days. The polynomial fit to mass as a function of length and diameter was of the form:

$$mass = length*[a*(diameter)^2 - b*(diameter)] \quad [1]$$

where the coefficients [a, b] were [$3 \cdot 10^{-4}$, $1 \cdot 10^{-5}$], [$6 \cdot 10^{-4}$, $5 \cdot 10^{-5}$], and [$4 \cdot 10^{-4}$, $9 \cdot 10^{-5}$], for white ash, red oak, and eastern hemlock respectively. The R^2 value for this relationship was greater than 0.94 for each species. Root biomass was estimated from the

images assuming that the viewing depth is 0.7848 mm and calculating the diameter of the imaged root using the method of Taylor *et al.* (2014). Assuming that roots are cylindrical, the relationship between the true diameter (D) and diameter perceived (p) at depth (f) is:

$$D = \frac{(f^2 + \frac{1}{4}p^2)}{f} \quad [2]$$

Daily fine root growth and mortality (g root d⁻¹) in each minirhizotron image for each sampling interval were calculated as:

$$Growth (g root d^{-1}) = \frac{m_{t_2} - m_{t_1}}{t_2 - t_1} \text{ when } m_{t_2} - m_{t_1} > 0 \quad [3]$$

$$Mortality (g root d^{-1}) = \frac{m_{t_2} - m_{t_1}}{t_2 - t_1} \text{ when } m_{t_2} - m_{t_1} < 0 \quad [4]$$

where m is the total mass of roots traced on day of year (DOY) t_1 and t_2 . Gross root production refers to total fine root growth summed over an interval of time. Net root production is the sum of growth and mortality for that interval. Root production measurements were scaled to g C m⁻² d⁻¹ using the assumption that each minirhizotron image is representative of a 0.173 cm³ (13 mm x 17 mm x 0.7848 mm) volume of soil (Taylor *et al.*, 2014).

The standing biomass of roots was estimated from field samples. I collected three 10 x 10 cm samples of the organic horizon and three 5 cm diameter mineral soil samples to a depth of 15 cm monthly in each plot. Roots were removed and sorted into fine (< 2 mm), coarse (> 2 mm), live and dead pools. Roots were then dried and weighed to obtain standing biomass for live fine roots (g m⁻²). Subsamples of roots from monthly soil coring were assayed for carbon content (%C) using an elemental analyzer (model NC2500; CE Instruments, Milan, Italy). Fine root standing biomass for the organic

horizon down to a depth of 15 cm in the mineral soil was scaled up to g C m^{-2} by adjusting for the horizontal area of the soil core, the carbon content of roots in each stand, and rock content.

Root Respiration

CO_2 efflux was measured directly on recently severed roots using an infrared gas analyzer (LI6400, LiCor Biosciences, Lincoln, NE). Measurements were made monthly from March to October 2013 on three samples per stand. Respiration rates have been measured successfully using severed roots in previous studies (Burton *et al.*, 2012, Burton & Pregitzer, 2003). Furthermore, I compared respiration measurements of an attached and severed root system for each stand on three separate days and confirmed that respiration rates were similar between the two types of roots (correlation coefficient = 0.78) and stable up to approximately 7 hours.

Two measurements per sample were made on each sample date within 7 hours of collection, one in the field at ambient temperature and one in the lab at a constant temperature. Field measurements of CO_2 efflux were fit to the Arrhenius equation,

$$R_S = A * e^{(-E_a/RT)} \quad [6]$$

where R_S is the respiration rate ($\mu\text{mol CO}_2 \text{ s}^{-1} \text{ g}^{-1}$), E_a is the activation energy (kJ mol^{-1}), A is a pre-exponential factor ($\mu\text{mol CO}_2 \text{ s}^{-1} \text{ g}^{-1}$), T is temperature (Kelvin) and R is the gas constant ($\text{kJ Kelvin}^{-1} \text{ mol}^{-1}$). The parameters E_a and A were estimated using non-linear curve fitting in SigmaPlot (Version 10.0, Systat Software, San Jose, CA). I then estimated growing season rates of R_S using daily soil temperature measured at 10 cm depth from HOBO data loggers installed in March 2013 in each stand. Mass-specific R_S

($\mu\text{mol CO}_2 \text{ g root}^{-1} \text{ s}^{-1}$) was scaled to $\text{g C m}^{-2} \text{ s}^{-1}$ using the mass of root per square meter ground surface area and converting from μmol to μg .

Nonstructural Carbohydrates

The pool of NSC was estimated as the sum of the concentration of sugars (assumed to be glucose:fructose:galactose in 1:1:1 ratio) and starch using the method of Chow & Landhausser (2004). I collected three ~1- 2 g root samples from each biometry plot monthly from May to November 2011 and four times from March to November 2012. Roots were excavated, washed, and frozen in liquid nitrogen until analysis. Sugars were extracted from dried and finely ground root tissue using a 12:5:3 methanol:chloroform:water solution before being developed with 2% phenol and concentrated sulfuric acid. Absorbance was measured at 490 nm using a digital spectrophotometer (Spectronic 20D+, Thermo Scientific). Starch was extracted using a 0.005 N sulfuric acid solution at 95°C and developed as described above.

Root Exudation

Root exudates were collected from six root systems per stand in June and August 2012, and April, May, July and October 2013 following the method of Phillips *et al.* (2008, 2011). In brief, roots were excavated 48 hours prior to collection, washed, and incubated in a moist soil-sand mixture. Roots were placed into cuvettes with glass beads and a C-free nutrient solution 24 hours prior to collection. At the time of collection, exudate-containing nutrient solution was extracted with two additional flushes of C-free nutrient solution to ensure that exudates adhering to glass beads were flushed into

solution. Samples were transported back to the lab on ice and analyzed for non-purgeable organic carbon content using an elemental analyzer (Shimadzu TOC-VCSH analyzer, New Haven, CT). Exudation rate ($\text{g C g root}^{-1} \text{ d}^{-1}$) was scaled to $\text{g C m}^{-2} \text{ d}^{-1}$ using root biomass (g root m^{-2}) from soil cores.

Total Belowground C Flux

To estimate the quantity of C allocated belowground during the growing season (herein abbreviated as “gs”), I define a simplified belowground C flux budget (sensu Litton *et al.*, 2007, Drake *et al.*, 2011) using two different approaches. First, a top-down estimate of total belowground C flux (TBCF_{top} , $\text{g C m}^{-2} \text{ gs}^{-1}$) is defined as:

$$\text{TBCF}_{\text{top}} = F_{\text{efflux}} + F_{\text{leaching}} - F_{\text{litter}} + \Delta(C_{\text{roots}} + C_{\text{soil}}) \quad [7]$$

where F_{efflux} is the growing season rate of soil respiration, F_{leaching} is the flux of dissolved organic C into streamwater, F_{litter} is litterfall, and $\Delta(C_{\text{roots}} + C_{\text{soil}})$ is the growing season change in the C pool associated with fine roots and soil. F_{efflux} is estimated from a 22-year synthesis of soil CO_2 efflux data using a range of methods across multiple stand types (Giasson *et al.*, 2013). F_{litter} is measured using litter baskets (Barker Plotkin, 2010, Brzostek, 2012, Frey & Ollinger, 1999, Hadley, 2009, Lemos, 2013, Munger & Wofsy, 1999). I estimated ΔC_{roots} using net root production from this paper. I set $\Delta C_{\text{soil}} = 0$, assuming that it is small relative to the timescale of this study (Gaudinski *et al.*, 2000).

Second, a bottom-up estimate ($\text{TBCF}_{\text{bottom}}$, $\text{g C m}^{-2} \text{ gs}^{-1}$) is defined as:

$$\text{TBCF}_{\text{bottom}} = F_{\text{roots}} + F_{\text{resp}} + F_{\text{exudates}} \quad [8]$$

where F_{roots} is gross fine root production, F_{resp} is fine and coarse root respiration, and F_{exudates} is root exudation. F_{roots} , F_{exudates} , and fine root respiration are estimated using

measurements from this study. Coarse root respiration is estimated using the observation that mass-specific rates of coarse root respiration are ca. 70% lower than fine root respiration rates in the same stand (Desrochers *et al.*, 2002, Fahey *et al.*, 2005, Pregitzer *et al.*, 1998). Coarse root respiration ($\mu\text{mol CO}_2 \text{ g root}^{-1} \text{ s}^{-1}$) was scaled to $\text{g C m}^{-2} \text{ s}^{-1}$ using coarse root biomass to 15 cm from soil pits in evergreen and hardwood stands at Harvard Forest and the Harvard Conservation Trust (Harvard, MA, 42°31'N 71°32'W), respectively (Lemos, 2013).

I did not include transpiration of dissolved inorganic C, fungal production or throughfall leaching in the calculation of C outputs or inputs as these terms are generally < 5% of the C budget in other mid-latitude forest stands (Fahey *et al.*, 2005, Drake *et al.*, 2011). Coarse root production may account for 5-10% of total C inputs (Fahey *et al.* 2005; Drake *et al.* 2011), but I had no data on coarse root production at Harvard Forest and therefore did not include it.

Belowground C pools were derived from the Harvard Forest Data Archive and this study. Soil C content data were from both published (Bowden *et al.*, 2009, Brzostek, 2012, Frey *et al.*, 2014, Lemos, 2013, Nadelhoffer *et al.*, 1999, Orwig & Foster, 2009) and unpublished sources (Drake, *unpublished data*; Sorensen, *unpublished data*). Standing biomass of roots was estimated using data from this study as well as a previous study conducted on the same plots (Lemos, 2013). Soil microbial biomass in the hemlock stand was measured in June, July, August, and September of 2012 (Averill, *unpublished data*). Soil microbial biomass in the ash stand was measured in July of 2011 (Averill,

unpublished data). Microbial biomass data in oak-dominated hardwoods stands were taken from Drake *et al.* (2013) and more recent studies (Sorensen, *unpublished data*).

Monthly values of gross primary production (GPP) were estimated using partitioned NPP measured in 2012 at the eddy-covariance towers located in a mixed hardwood stand and a hemlock stand at Harvard Forest (ORNL-DAAC, 2013). Data were not available for ash stand GPP or soil CO₂ efflux; for the purpose of this budget I assumed these values were equivalent to oak-dominated hardwoods, although I recognize this makes the ash belowground C budget less certain. I used PhenoCam data (<http://phenocam.sr.unh.edu/>) to determine maximum canopy greenness in red oak and eastern hemlock stands.

Data Analysis

All statistical analyses were performed in R Statistical Software (R Development Core Team, 2013). Stand-specific and seasonal-to-interannual variations in fine root growth, mortality, respiration, NSC concentration, and exudation were modeled using a mixed-effects model with stand, sample date, and year as fixed effects and plot as a random effect. A Tukey's HSD post-hoc test was used to test for differences between stands. Analysis of variance (ANOVA) was used to test for the effect of newly installed tubes on root growth and mortality, to test for the effect of stand on root tissue [N], to test for the effect of stand and soil horizon on root biomass, and to test for a significant difference between TBCF_{bottom} and TBCF_{top}. I also used ANOVA to test for differences in C content, N content, and organic horizon mass between stands, averaging across

subsamples. All mixed effects and ANOVA models were constructed using the *aov* function in base R.

Linear regression was used to correlate root growth with root mortality, and to correlate root growth with temperature for each stand separately. Multiple linear regression was used to model mass-specific respiration as a function of soil temperature, precipitation, and stand. I used a linear-mixed-effects model to model root mortality as a function of temperature, precipitation, stand, year, and day of year with tube as a random effect. Precipitation and day of year were not significant effects and were dropped from the final model. I also used a linear-mixed-effects model to model root growth as a function of temperature, precipitation, stand, year, and day of year with tube as a random effect using the *lmer* function in the *lme4* package in R (Bates *et al.*, 2014). In mixed-effects, ANOVA, and regression models, fine root growth and mortality were log-transformed to meet assumptions of normality.

Results

Root Production and Biomass

There was a measurable but transient effect of tube installation on root production in red oak. In 2013, mean red oak root growth was $0.34 \text{ g C m}^{-2} \text{ d}^{-1}$ higher in newly installed tubes compared to tubes established a decade earlier ($F_{2,79} = 2.7$, $P = 0.07$), but this difference diminished in 2014 to $0.09 \text{ g C m}^{-2} \text{ d}^{-1}$ ($P = 0.12$). There was no detectable installation effect on red oak root mortality or on the single hemlock tube installed. All white ash tubes were newly installed in November 2012 so it was not possible to establish an effect of installation on white ash root production.

Root growth was positively correlated with soil temperature in each stand ($P < 0.001$, Table 3.2), but was not correlated with precipitation (Table 3.3). As a result root growth was concentrated in mid-summer, but with distinct stand-level differences (Figure 3.2, a-f). Red oak root growth occurred in 1–3 flushes over the growing season, with highest mortality in mid to late-summer (Figure 3.2, a-c). Root mortality was not correlated either with soil temperature ($P = 0.13$) or precipitation ($P = 0.76$). Hemlock root growth was low throughout the growing season with smaller production peaks occurring in the fall in 2013 and 2014. White ash root growth peaked in mid-summer with high mortality in late-summer. In red oak and white ash stands the peak in maximum canopy greenness (*data not shown*) occurred ~20 days earlier than in the eastern hemlock stand, but the peak in root growth occurred ~50 days earlier. As a result, the deciduous stands had a smaller offset between maximum canopy greenness and peak root growth than did the hemlock stand. Similar to the phenology of gross production, net fine root production increased in early to mid-summer in the deciduous stands. In 2012 hemlock fine root NPP was positive but in 2013 and 2014 there was no net production of fine roots.

Root biomass was significantly higher in the red oak ($P < 0.001$) and eastern hemlock ($P < 0.1$) stand compared to ash, largely because of a surface organic horizon ($F_{1,111} = 47.9$, $P < 0.001$). White ash stands at Harvard Forest lack an organic horizon, possibly the result of bioturbation by exotic earthworms that are not present in the red oak or eastern hemlock stands. In this stand, surface litter is incorporated directly into the

mineral soil horizon in less than 1 year. As a result, there is relatively little variation in the root depth profile in this stand (Table 3.4).

In all years, red oak and white ash stands allocated more C to fine roots compared to eastern hemlock (Figure 3.2, g-i). Averaged across growing seasons $301 \pm 76 \text{ g C m}^{-2} \text{ gs}^{-1}$ and $133 \pm 42 \text{ g C gs}^{-1}$ were allocated to fine roots in red oak and white ash stands, respectively. C allocation to gross fine root production in eastern hemlock was $42 \pm 13 \text{ g C m}^{-2} \text{ gs}^{-1}$.

Root Respiration

The phenology of fine root respiration was similar between stands, with highest mass-specific respiration rates in mid-summer (Figure 3.3a). This follows from a positive correlation with soil temperature (Figure 3.3b, $R^2_{\text{adj}} = 0.68$, $P < 0.001$). Mass-specific rates of fine root respiration were significantly higher in the white ash stand than in oak and hemlock (Figure 3.3b). Arrhenius fits to mass-specific data indicate that white ash root respiration had a lower apparent activation energy ($E_a = 20 \text{ kJ mol}^{-1}$) across the growing season compared to that of red oak ($E_a = 40 \text{ kJ mol}^{-1}$) and eastern hemlock ($E_a = 29 \text{ kJ mol}^{-1}$). The pre-exponential constant A ($\text{umol CO}_2 \text{ g}^{-1} \text{ s}^{-1}$) varied over three orders of magnitude between stands and was highly correlated with E_a ($R^2 > 0.99$).

Root respiration measured in the lab increased across the growing season (Figure 3.4). The average rate of fine root respiration for the six month growing season was 191 ± 24 , 167 ± 33 , and $205 \pm 27 \text{ g C m}^{-2} \text{ gs}^{-1}$ for red oak, eastern hemlock, and white ash, respectively (Figure 3.3c).

Nonstructural Carbohydrates and Root Exudation

There was large inter-annual variability in the concentration of NSC in fine roots (Figure 3.5). In 2012, there was a decline in NSC concentration mid-summer relative to the spring and fall. In 2011, there was a slight but significant increase in NSC concentration across the growing season ($P < 0.001$). Red oak roots had significantly lower NSC concentration than white ash and eastern hemlock ($P < 0.001$, Figure 3.5).

Exudation rate was highly variable and there was no clear stand level difference or seasonal pattern, although there were significantly lower exudation rates in early spring (DOY = 106) compared to summer and fall (Table 3.5). Exudation rates for red oak, eastern hemlock, and white ash were 47 ± 24 , 55 ± 25 , and 46 ± 11 g C m⁻² gs⁻¹, respectively.

Total Belowground C Flux

In the red oak stand, total belowground C flux was 577 ± 85 g C m⁻² gs⁻¹ based on TBCF_{bottom}. Of this, 52% was allocated to root production, 40% to root respiration, and 8% to exudation (Figure 3.6, orange bars). TBCF_{top} was 791 ± 94 g C m⁻² gs⁻¹. In the eastern hemlock stand, TBCF_{bottom} was 340 ± 51 g C m⁻² gs⁻¹. Approximately 13% of this flux was allocated to root production, 71% to root respiration, and 16% to exudation (Figure 3.6, purple bars). TBCF_{top} was 474 ± 29 g C m⁻² gs⁻¹. In the white ash stand, TBCF_{bottom} was 449 ± 57 g C m⁻² gs⁻¹. Thirty percent of TBCF_{bottom} was allocated to root production, 60% to root respiration, and 10% to exudation (Figure 3.6, blue-green bars). TBCF_{top} was 633 ± 58 g C m⁻² gs⁻¹.

TBCF_{top} was larger than TBCF_{bottom} in all of the stands, but this difference was not significant (Table 3.6). In the red oak stand, TBCF_{top} was $214 \pm 127 \text{ g C m}^{-2} \text{ gs}^{-1}$ larger than TBCF_{bottom}.

The phenology of TBCF_{bottom} differed between stands (Figure 3.7). Red oak stands allocated more C belowground earlier in the growing season compared to white ash and eastern hemlock. The peak in TBCF_{bottom} in red oak was coincident with the spring ramp-up of GPP. In eastern hemlock stands, the phenology of TBCF_{bottom} was not pronounced. In both oak and hemlock stands, soil respiration peaked later in the season than either GPP or TBCF_{bottom}.

Discussion

Data on timing and partitioning of C to belowground processes are rare (Dohleman *et al.*, 2012, Fahey *et al.*, 2013). This paper provides a first look at the seasonal dynamics of multiple root processes over 2-3 years in a mid-latitude forest. I observed significant stand-level differences in belowground C flux and its partitioning to root growth, exudation and respiration. The phenology of TBCF also differed broadly between stands, especially in the evergreen hemlock stands compared to the deciduous red oak and ash stands where the peak in TBCF was coincident with the peak in GPP. I found broad support for my three hypotheses (discussed below) and a proximate explanation for the increase in the biomass of red oak throughout the Harvard Forest over the last two decades. The emergence of a forest pest, the hemlock woolly adelgid, during the course of this study negatively affected belowground C allocation and root production in hemlock from 2012 to 2014. The data reported here suggest that belowground C flux is

sensitive to variations in temperature and C supply. Follow up studies are needed to assess the impact of belowground phenology on soil biogeochemistry.

Phenology of Root Growth and Mortality

In a recent meta-analysis I found that deciduous trees have more synchronous above- and belowground phenology than evergreen trees (Abramoff & Finzi, 2015). Consistent with the meta-analysis, I found that the offset between maximum canopy greenness, a proxy for aboveground phenology, and root growth was about 30 days shorter in the deciduous stands. Consistent with my first hypothesis, fine root growth was initiated earlier in the growing season in the hardwood stands compared to the hemlock stand (Figure 3.2, a-c).

There was not a strong correspondence between root growth and mortality despite statistical significance (Figure 3.2, $R^2_{\text{adj}} = 0.01$, $P < 0.05$). At best, a visual inspection of the data suggests a lag in mortality relative to growth for most stands and years. A more striking observation was the multiple flushes of root growth observed in red oak, particularly in 2012 (Figure 3.2a). The direct observation of multiple root flushes confirm the results inferred by Cardon *et al.* (2002), who based their inference on a negative correlation between shoot elongation and soil respiration in a common garden experiment with red oak saplings. There were fewer flushes in the 2013 and 2014 data that may reflect sampling intensity. The minirhizotrons were sampled biweekly in 2012 and monthly in 2013 and 2014. It is possible that the lower sampling frequency missed flushing episodes. Alternatively, there may have been fewer flushes in these years.

Environmental Controls over Root Growth and Respiration

Consistent with hypothesis 2, root growth and respiration were sensitive to variations in soil temperature (Table 3.3). Contrary to my second hypothesis, there was no effect of precipitation on growth or respiration, and mortality was unrelated to variations in temperature or precipitation. The positive correlation between root growth and temperature observed here has been observed in a variety of ecosystems using both observational (Bevington & Castle, 1985, Teskey & Hinckley, 1981) and experimental approaches (Lahti *et al.*, 2005, Tryon & Chapin III, 1983). The positive relationship between root growth and temperature reflects a number of processes including enhanced C supply due to photosynthesis, increases in the rate of cell division and lower resistance to water uptake favoring cell expansion (Lambers *et al.*, 2008). Though very high temperatures (> 30°C) can inhibit root growth, I did not observe soil temperatures greater than 24°C (Barney, 1951, Graves *et al.*, 1991).

There was a strongly seasonal cycle to the rate of fine root respiration that reflected the sensitivity of respiration to temperature (Figure 3.3a,b). The apparent temperature sensitivity (E_a) of root respiration was lowest in the ash stands and highest in the red oak stand (Table 3.7). The measurement of temperature sensitivity reported here convolves many potential sources of variability such as differences in root chemistry and substrate supply. Thus it is difficult to ascribe control(s) for the greater temperature sensitivity in red oak compared to the other species.

When incubated at a common temperature the rate of root respiration increased across the growing season in all three species (Figure 3.4). This suggests an increase in

photosynthate allocation to roots through time and that the decline of respiration rates in the fall is related to temperature rather than acclimation of root respiration or substrate limitation. This observation is qualitatively similar to that of Burton & Pregitzer (2003) who did not find acclimation of root respiration across the growing season in sugar maple stands in Michigan. Both studies contrast with the apparent acclimation of root respiration in response to experimental soil warming at the Harvard Forest (Burton *et al.*, 2008).

Fine root respiration in ash was significantly higher than oak and hemlock and appears to be the result of high root [N]. The rate of N mineralization is high in ash compared to oak and hemlock stands (Brzostek & Finzi, 2012, Finzi *et al.*, 1998). The presence of the invasive European earthworm *Lumbricus terrestris* in these plots further accelerates the rate of N cycling because they rapidly incorporate leaf litter into the mineral soil and decrease the turnover time of organic matter (Marhan & Scheu, 2005, Scheu, 1987). High N availability is most likely the reason root [N] is significantly higher in ash compared to oak and hemlock ($F_{2,68} = 90.3$, $P < 0.001$). Given that root N concentration is correlated with respiration rate (Burton *et al.*, 2002, Reich *et al.*, 2002), the high mass-specific rates of root respiration in this species are most likely explained by their high [N]. Notably at the plot scale, total fine root respiration ($\text{g C m}^{-2} \text{gs}^{-1}$) was highest in the ash stand despite it having ~50% lower biomass than that in red oak.

Nonstructural Carbohydrates and Root Exudation

Root NSC concentrations varied significantly between stands, years, and within each growing season (Figure 3.5). In 2012, there was a strong apparent seasonal decline

in root NSC mid-summer, which may reflect the metabolism of NSC for root growth and maintenance respiration (Lynch *et al.*, 2013). In 2011, there was no evidence for a seasonal decline. The difference between years may reflect inter-annual variation in allocation to root NSC pools. It is also possible that NSC concentrations vary over timescales finer than the monthly sampling interval used here, in contrast to stemwood NSC, for which monthly sampling appears sufficient to capture the seasonal trend in the NSC pool (Richardson *et al.*, 2013).

In contrast to root NSC there was no significant difference in exudation rate among stands (Table 3.8). Brzostek *et al.* (2013) similarly found no difference in the rate of root exudation among four stand types, including the hemlock and ash plots studied here. Exudation did, however, vary significantly at the seasonal time-scale with the main distinction being significantly lower rates in the spring compared to summer and fall collection dates (Table 3.5). This pattern of exudation mirrors the seasonal increase in mass-specific rates of root respiration and supports the idea of a progressive increase in C allocation belowground across the growing season (Figure 3.4).

I caution that the detectability of variations in exudation may prove difficult given the methods presently available for research in the field. The collection of exudation requires the physical extraction of intact root systems from the soil that necessarily disrupts microbial interactions (Phillips *et al.*, 2008). Similarly, sample collection requires submerging root tips in a liquid medium with a chemical composition different from the soil solution. This may affect the rate at which C is released from roots into the

solution. Indeed, other studies of exudation across the growing season did not detect a clear seasonal pattern (Phillips *et al.*, 2008, Phillips *et al.*, 2011).

Total Belowground C Flux

TBCF varied between 28 and 35% of GPP (Table 3.6). Consistent with my third hypothesis, red oak had the highest rate of TBCF and the greatest proportional allocation to fine root production (Figure 3.6). Eddy-covariance estimates of net ecosystem production at the Harvard Forest mixed hardwood tower site suggest a near doubling of C uptake from the atmosphere over the last 20 years (Keenan *et al.*, 2012, Urbanski *et al.*, 2007). The increase in C uptake is correlated with an increase in red oak productivity and biomass. Of the dominant species within the tower footprint, the concentration of N in red oak foliage is among the highest, and this species has the most rapid rate of light-saturated net photosynthesis (Bassow & Bazzaz, 1997). Foliar [N] concentration in red oak remains unchanged throughout, suggesting that the rate of annual N uptake from the soil has also increased. Given that belowground C allocation is required to acquire soil N, this analysis suggests that high TBCF in this red oak stand relative to hemlock, the second most dominant tree species in the tower footprint, has facilitated its emergence as the dominant species at this site (Figure 3.6, Table 3.6).

The modest C investment in root production in hemlock stands may be an attribute of this species in particular or evergreen trees in general, which allocate a substantial fraction of C to ectomycorrhizal symbionts (Clemmensen *et al.*, 2013, Hobbie, 2006). Confounding this interpretation of the results, however, is the recent infestation of the invasive pest hemlock woolly adelgid (HWA), which became

widespread at the Harvard Forest in 2012 with visible signs of crown thinning and HWA-induced tree mortality recorded in 2014. Compared to 2012, the allocation of C to root production in hemlock stands dropped by 11% in 2013 and 72% in 2014, suggesting a negative effect of the HWA on root C allocation. Surveys of hemlock roots in infested stands in Connecticut found that ectomycorrhizal colonization, bacterial abundance in the adjacent rhizosphere, and root C:N all declined (Vendettuoli *et al.*, 2015).

The phenology of $TBCF_{\text{bottom}}$ differs between stands and relative to that of GPP or soil respiration (Figure 3.7). In the deciduous red oak stand, the peak in $TBCF_{\text{bottom}}$ precedes the peak in soil respiration and coincides with spring ramp-up of GPP. This suggests that belowground C allocation in oak is strongly dependent upon the supply of photosynthate. This result is consistent with pulse-chase experiments demonstrating rapid transfer of C belowground (Hogberg *et al.*, 2008) and girdling experiments showing steep declines in springtime soil respiration owing to the absence of active roots (Högberg *et al.*, 2001).

$TBCF_{\text{top}}$ was consistently greater than $TBCF_{\text{bottom}}$. This suggests an over-estimate of ΔC_{root} in $TBCF_{\text{top}}$, an underestimate of root GPP, respiration, or exudation in $TBCF_{\text{bottom}}$, or a combination of both. The largest difference between $TBCF_{\text{top}}$ and $TBCF_{\text{bottom}}$ ($\sim 240 \text{ gC m}^{-2} \text{ gs}^{-1}$) was observed in the red oak stand. The differences were smaller in the ash and hemlock stands. Root NPP was estimated from minirhizotron images and was highest in red oak (Figure 3.2, g-i). High NPP contributes to a large estimate of ΔC_{root} and hence the estimate of $TBCF_{\text{top}}$ (equation [1]). In contrast to the high minirhizotron estimate of root NPP, there was no significant change in root biomass in

soil cores collected across the growing season in 2012 (*data not shown*). Because of high spatial variability (Taylor *et al.*, 2013), the absence of a change in root biomass in one year does not exclude the possibility of high root NPP. However, the three-growing-season average root NPP of 225 g C m⁻² estimated from minirhizotron imaging is about one-half of the standing crop (Figure 3.3c), and should be measurable in soil cores. TBCF in red oak is therefore likely to reside between the two estimates.

Summary

Climatic and atmospheric perturbations alter the magnitude of C inputs belowground (e.g., Drake *et al.*, 2011) and thus at the inter-annual time-scale it is likely that changes in the quantity and phenology of belowground C inputs will influence soil biogeochemical cycling. Warming-induced increases in growing season length have significantly increased annual ecosystem C uptake at Harvard Forest, a large portion of which is hypothesized to be allocated belowground (Keenan *et al.*, 2014). Whether and how this enhanced allocation belowground will affect long-term soil-C cycling and C storage remains an open question.

Acknowledgements

I would like to thank Colin Averill, John Drake, William Munger, and Patrick Sorensen for use of data. I also thank Andrew Richardson for making data from the PhenoCam network publicly available. Development of the PhenoCam network has been supported through the National Science Foundation (award EF-1065029). This research was supported by the American Association of University Women (AAUW) American

Dissertation Fellowship, the Office of Science (BER), the US Department of Energy (grant no. 10-DOE-1053) and the National Science Foundation (DEB-0743564).

Table 3.1. Stand-level characteristics. Total C content refers to organic and mineral horizon soil C down to 15 cm. Letters indicate a statistically significant difference in means using analysis of variance at the $P < 0.05$ level.

Stand	Total C content (g m⁻²)	Total N content (g m⁻²)	O horizon mass (g m⁻²)	pH	Soil C:N Ratio
White ash	5989 ± 330 ^b	431 ± 24 ^a	-	5.1	13.9 ± 0.17 ^b
Red oak	7709 ± 438 ^a	354 ± 23 ^b	131 ± 8 ^a	5.2	21.8 ± 0.72 ^a
Eastern hemlock	6922 ± 246 ^a	290 ± 13 ^b	105 ± 7 ^b	3.7	23.9 ± 0.70 ^a

Table 3.2. Summary of multiple linear regression statistics that model log(fine root growth) for each stand as a function of soil temperature. Fine root growth was log-transformed to meet assumptions of normality. * P < 0.001, ** P < 0.01, * P < 0.05, . P < 0.1**

Log (fine root growth)	Soil temperature			
	β	F	R²_{adj}	P-value
<i>White ash</i>	0.08	48.9	0.26	***
<i>Red oak</i>	0.11	89.2	0.30	***
<i>Eastern hemlock</i>	0.08	43.8	0.15	***

Table 3.3. Summary of multiple linear regression statistics that model fine root growth, mortality, and mass-specific respiration as a function of soil temperature and precipitation. Growth and mortality were log-transformed to meet assumptions of normality. * P < 0.001, ** P < 0.01, * P < 0.05, . P < 0.1**

	Soil temperature				Precipitation
	β	F	R²_{adj}	P-value	P - value
Growth	1.5	202.9	0.47	***	ns
Mortality	1.3	3.4	0.19	*	ns
Respiration	0.29	32.2	0.68	***	ns

Table 3.4. Median root biomass (5th percentile, 95th percentile) in g C m⁻² estimated from minirhizotron tubes binned in 10 cm depth increments. Uppercase letters indicate significant differences between columns, and lowercase letters indicate significant differences between rows at the P < 0.01 level.

Depth	White ash	Red oak	Eastern hemlock
O horizon	-	3.46 (2.29, 6.65) ^{Aa}	2.82 (0.80, 7.33) ^{ABa}
0 - 10 cm	0.98 (0.20, 1.84) ^{Bb}	3.03 (0.71, 6.17) ^{Ab}	1.17 (0.53, 1.46) ^{ABb}
10 - 20 cm	0.79 (0.45, 1.08) ^{Bb}	0.77 (0.38, 1.66) ^{Ab}	1.16 (0.42, 3.24) ^{ABb}
20 - 30 cm	0.79 (0.41, 2.62) ^{Bb}	0.49 (0.25, 4.19) ^{Ab}	0.50 (0.01, 1.29) ^{ABb}
30 - 40 cm	0.45 (0.16, 2.22) ^{Bb}	0.71 (0.08, 2.01) ^{Ab}	0.65 (0.06, 1.92) ^{ABb}
40 - 50 cm	0.19 (0.07, 0.66) ^{Bb}	-	-

Table 3.5. Exudation rate (\pm SE) for samples collected in 2012 and 2013. There is a significant effect of sample date ($F_{1,106} = 8.0$, $P < 0.01$), but no differences between years or stands. The exudate rate on the April sample date (DOY = 106) was significantly lower than the exudation rate measured on June, July, and October sample dates at the $P < 0.05$ level.

Stand	Date	N	Exudation Rate (mg C g root⁻¹ day⁻¹)
White ash	6/19/2012	6	1.35 (0.43)
	8/26/2012	6	1.14 (0.25)
	4/16/2013	6	0.29 (0.23)
	5/30/2013	7	1.03 (0.07)
	7/27/2013	7	2.69 (0.68)
	10/7/2013	6	1.39 (0.34)
Red oak	6/19/2012	7	2.65 (1.34)
	8/26/2012	7	0.26 (0.10)
	4/16/2013	7	-0.47 (0.33)
	5/30/2013	6	0.52 (0.09)
	7/27/2013	6	1.37 (0.54)
	10/7/2013	6	0.70 (0.24)
Eastern hemlock	6/19/2012	5	0.78 (0.35)
	8/26/2012	6	0.36 (0.07)
	4/16/2013	6	0.02 (0.17)
	5/30/2013	6	0.56 (0.25)
	7/27/2013	6	2.23 (0.99)
	10/7/2013	6	3.59 (1.77)

Table 3.6. Total belowground carbon flux (TBCF, $\text{g C m}^{-2} \text{gs}^{-1}$) for each stand. TBCF_{top} is defined as $F_{\text{efflux}} + F_{\text{leaching}} - F_{\text{litter}} + \Delta(C_{\text{roots}} + C_{\text{soil}})$. $\text{TBCF}_{\text{bottom}}$ is $F_{\text{roots}} + F_{\text{resp}} + F_{\text{exudates}}$.

Flux	White ash	Red oak	Eastern Hemlock
TBCF_{top}	633 (58)	791 (94)	474 (29)
$\text{TBCF}_{\text{bottom}}$	449 (57)	577 (85)	340 (51)

Table 3.7. Activation energy (E_a , kJ mol^{-1}), pre-exponential constant (A , $\text{nmol CO}_2 \text{ s}^{-1} \text{ g}^{-1}$), and R^2 of mass-specific rates of root respiration ($\text{nmol CO}_2 \text{ g}^{-1} \text{ s}^{-1}$) for each stand over the growing season.

	E_a	A	R^2
White ash	20	20872	0.60
Red oak	40	36498539	0.81
Eastern hemlock	29	572865	0.56

Table 3.8. Statistical summary of mixed-effects models with fine root growth, mortality, respiration, NSC concentration, or exudation as the dependent variable. The fixed effects were stand, sample date, and year with plot as a random effect. Growth and mortality were log-transformed to meet assumptions of normality. *** P < 0.001, ** P < 0.01, * P < 0.05, . P < 0.1

	Growth			Mortality			Respiration			[NSC]			Exudation		
	df	MS	F	df	MS	F	df	MS	F	df	MS	F	df	MS	F
Stand	2	147.7	40.4 ***	2	106.5	27 ***	2	4.4*10 ⁻⁵	13.1 ***	2	2.2*10 ⁻²	67.0 ***	2	2.9*10 ⁻⁶	0.9
Day of Year	1	13.8	3.8 *	1	0.01	0	1	1.3*10 ⁻⁶	0.54	1	2.2*10 ⁻²	66.9 ***	1	2.6*10 ⁻⁵	8.0 **
Year	1	274.7	75.2 ***	1	25.3	6.3 **	-	-	-	1	7.8*10 ⁻³	23.7 ***	1	9.8*10 ⁻⁷	0.6
Error	584	3.65		497	4.0		57	3.3*10 ⁻⁶		1089	3*10 ⁻⁴		106	3.2*10 ⁻⁶	

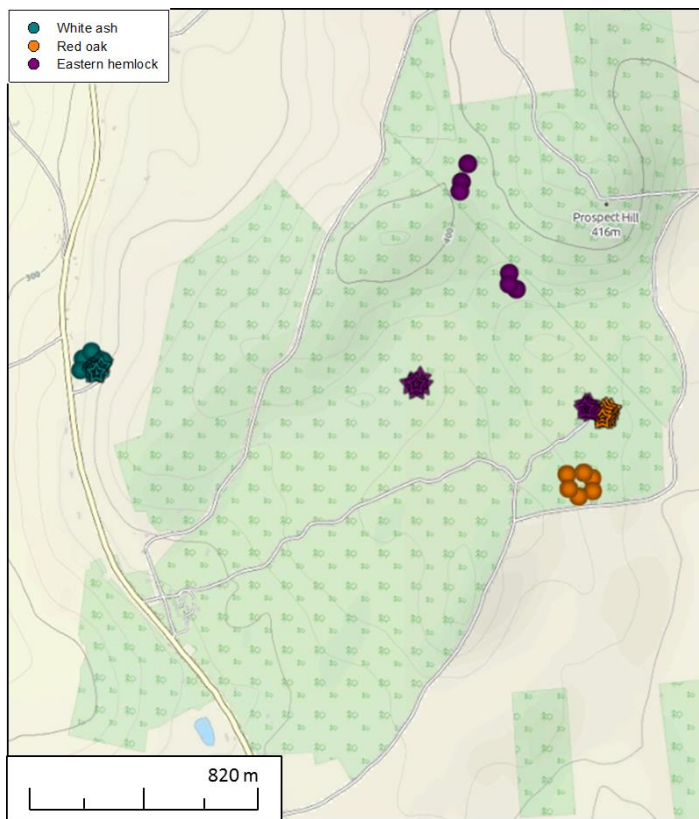


Figure 3.1. Map of plot locations at the Harvard Forest's Prospect Hill Tract. There are 6 biometry plots (circles) and 10 minirhizotron plots (stars) per stand. Colored symbols indicate stand type. Blue-green symbols are white ash (*Fraxinus americana*), orange are red oak (*Quercus rubra*), and purple are eastern hemlock (*Tsuga canadensis*).

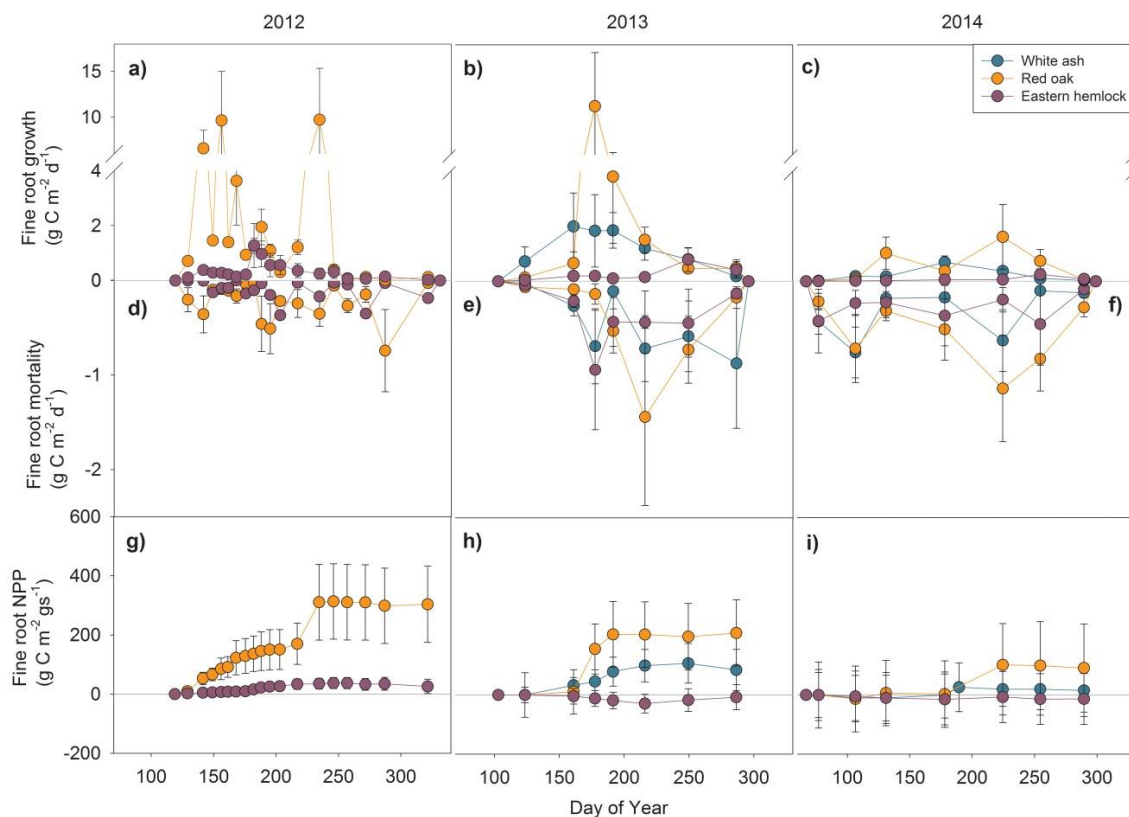


Figure 3.2. Growth (a-c), mortality (d-f), and net primary production (NPP, g-i) of fine roots. In 2012, $n = 4$ and $n = 9$ for red oak and eastern hemlock, respectively. In subsequent years, $n = 10$ for each stand. Error bars are standard error of the mean. There was a significant effect of year and stand on both growth and mortality (Table 3.8). The eastern hemlock stand had significantly less growth and mortality than red oak and white ash stands ($P < 0.001$), but red oak and white ash stands were not different from each other (growth was only marginally different, $P < 0.1$).

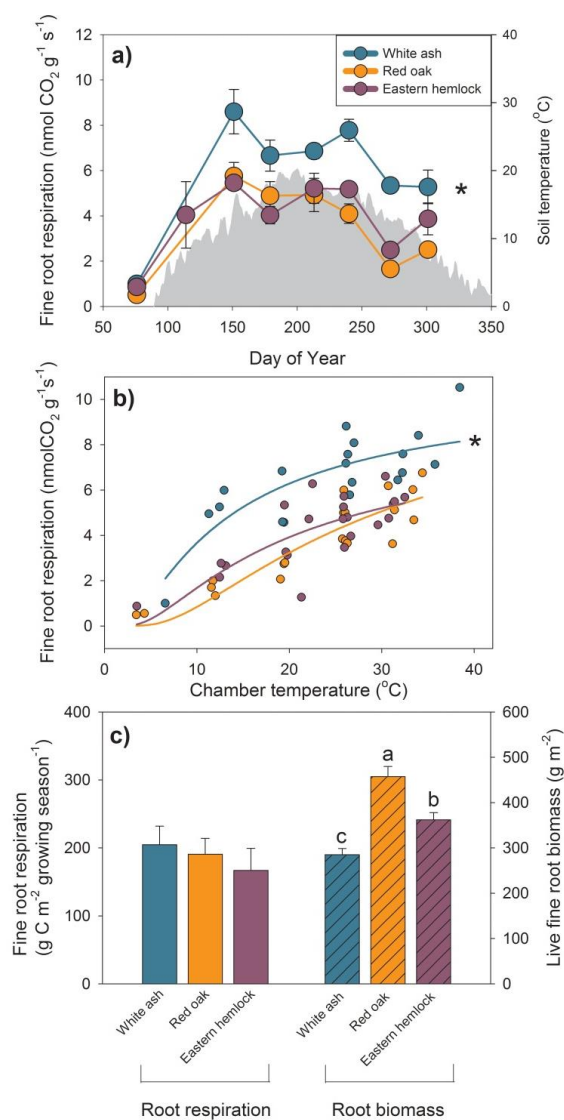


Figure 3.3. (a) Field measurements of monthly mean mass-specific fine root respiration (\pm SE) in 2013 (left y-axis). The shaded area represents soil temperature (right y-axis). (b) Relationship of fine root respiration to the temperature of the measurement chamber ($n = 61$). Lines are nonlinear fits of the Arrhenius function to data for each stand. (c) Fine root respiration (\pm SE) scaled to the growing season using fine root biomass from soil coring. In panels a and b, asterisk indicates that white ash had significantly higher respiration rates than red oak and eastern hemlock. In panel c, letters indicate significant differences between stands at the $P < 0.001$ level.

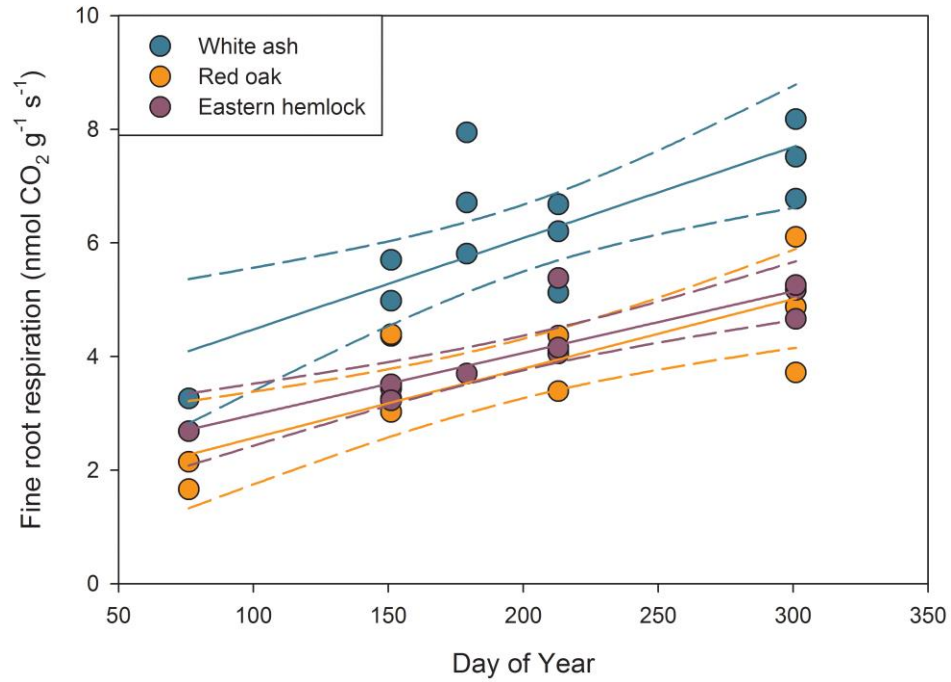


Figure 3.4. Fine root respiration measured in the lab at temperatures ranging between 16°C and 25°C, with a mean of $22.8 \pm 0.5^\circ\text{C}$. There was a significant positive relationship between fine root respiration and sample date for white ash ($\beta = 0.016$, $F_{1,11} = 15.3$, $P < 0.01$, $R^2_{\text{adj}} = 0.54$), red oak ($\beta = 0.012$, $F_{1,9} = 17.6$, $P < 0.01$, $R^2_{\text{adj}} = 0.62$), and eastern hemlock ($\beta = 0.011$, $F_{1,9} = 32.1$, $P < 0.001$, $R^2_{\text{adj}} = 0.76$). Dash lines are 95% confidence intervals around the regression fit.

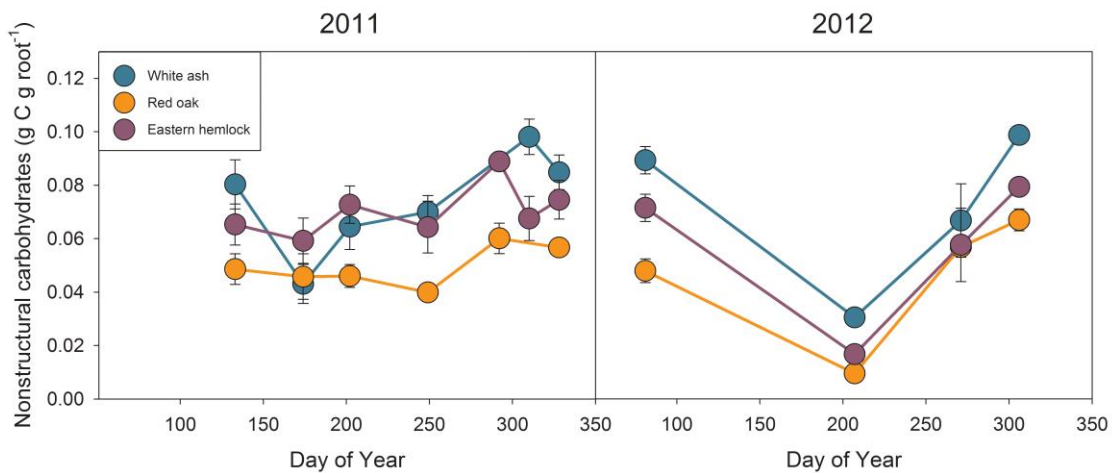


Figure 3.5. Total nonstructural carbohydrates (\pm SE) from $n = 6$ samples from each stand. There were significant differences between years ($F_{1,1089} = 23.7$, $P < 0.001$), sample dates ($F_{1,1089} = 66.9$, $P < 0.001$), and stands ($F_{2,1089} = 67.0$, $P < 0.001$). Each stand was significantly different from the other two stands in both years.

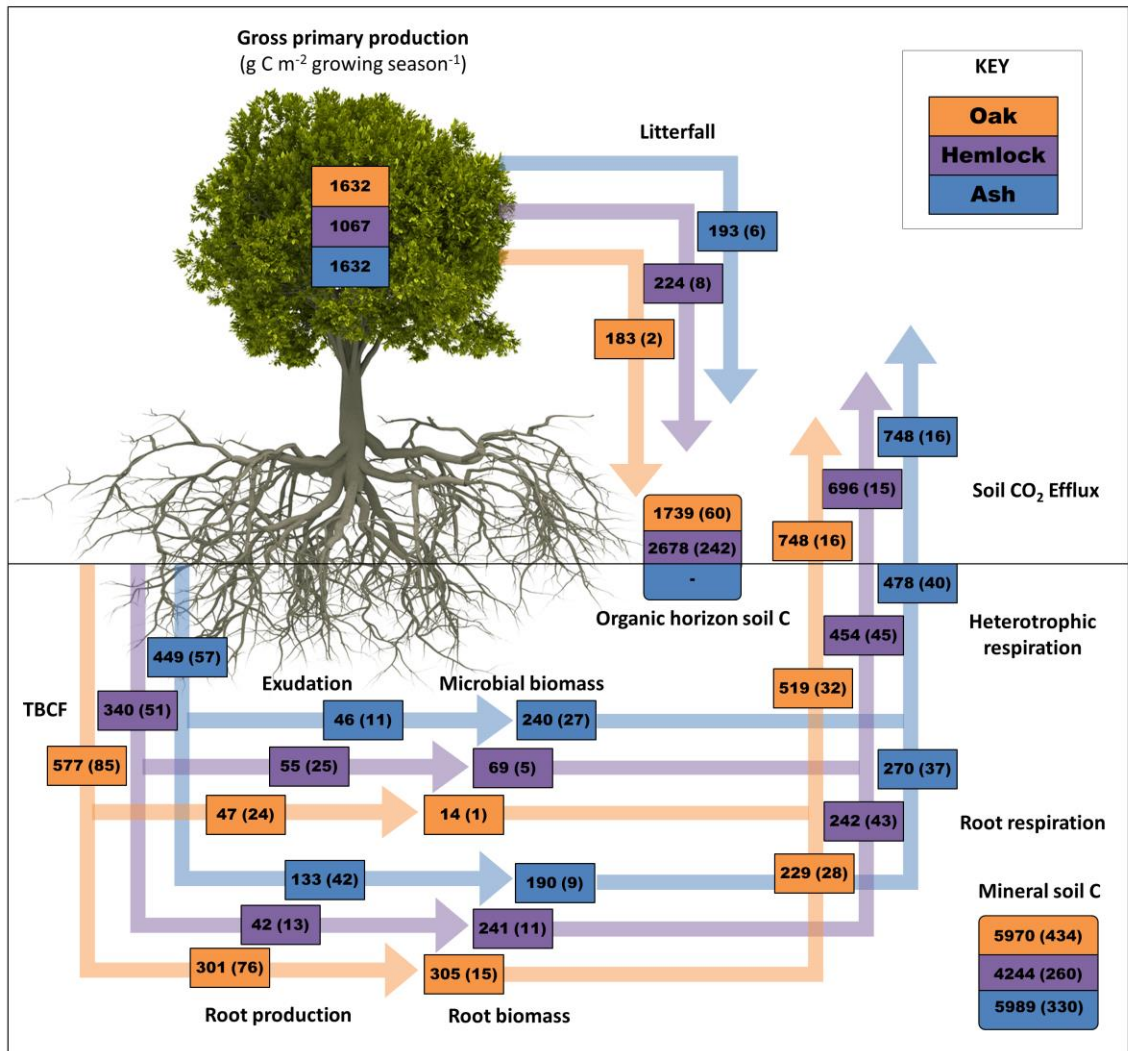


Figure 3.6. Gross primary production and belowground fluxes (litterfall, TBCF_{bottom} [fine root production, root respiration, exudation], heterotrophic respiration, soil CO₂ efflux) and pools (microbial biomass, root biomass, organic horizon soil C, mineral horizon soil C) for each stand. Heterotrophic respiration is estimated as the difference between soil CO₂ efflux and root respiration. Standard error is reported in parentheses next to each pool or flux value, and all units are g C m⁻² gs⁻¹. The growing season is defined as the six month period from May-October.

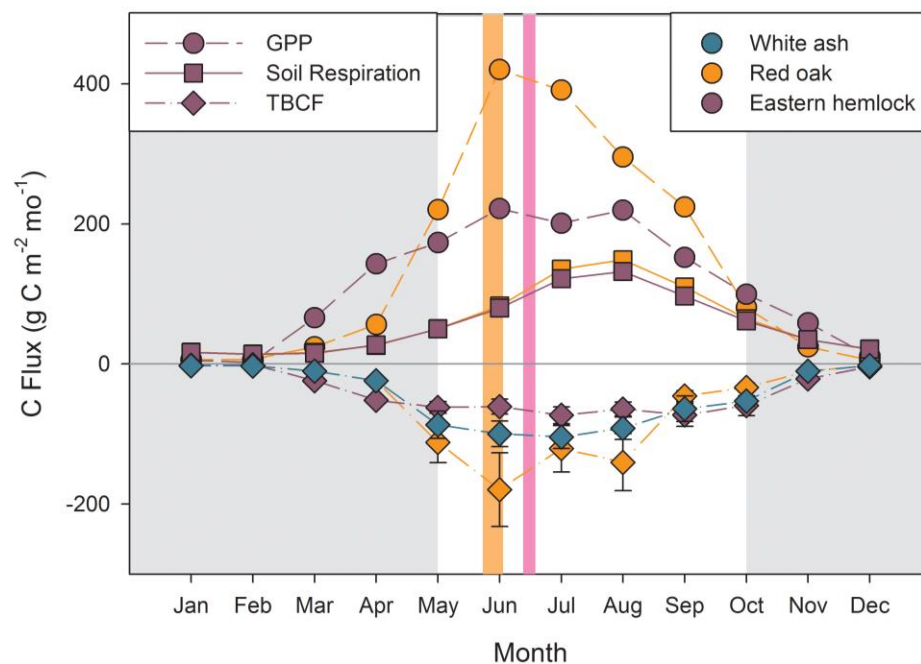


Figure 3.7. Time series of gross primary production estimated using data from the Harvard Forest Environmental Measurement Site flux tower and the hemlock tower in 2012 (circles). Soil respiration for the eastern hemlock and red oak stands (squares) and $\text{TBCF}_{\text{bottom}}$ (diamonds) for red oak, eastern hemlock and white ash stands calculated using root GPP, respiration and exudation from May to October. For Jan–Apr and Nov–Dec when data were not available (shaded areas), I used the median ratio of $\text{TBCF}:\text{GPP}$ to extrapolate TBCF from GPP data. This ratio (5th, 95th percentiles) was 0.42 (0.23, 0.5) for hardwoods and 0.36 (0.28, 0.57) for hemlock. The orange and pink colored bars show the maximum canopy greenness in red oak and eastern hemlock stands, respectively, for this study period determined using PhenoCam data (<http://phenocam.sr.unh.edu/>).

**CHAPTER FOUR: WHERE DOES THE RHIZOSPHERE END? SPATIALLY
RESOLVED MEASUREMENTS OF IN SITU SOIL EXTRACELLULAR
ENZYME ACTIVITY**

Abstract

Rhizosphere soils are hotspots for soil organic matter decomposition, with soil decomposing enzymes stimulated up to 100%, but there are few estimates of rhizosphere spatial extent in the field. Zymography (i.e., 2-D visualization of enzyme activity) allows for spatially resolved *in situ* measurements of soil extracellular enzyme activity (EEA), but there has been no quantitative analysis of the relationship between EEA and distance from a root. The objective of this work is to develop a quantitative framework for zymogram image analysis as a means for estimating the spatial extent of the rhizosphere. My analysis utilizes a spatial error model and break-point regression analysis to estimate the scale over which four enzymes – beta-glucosidase, N-acetyl-beta-D-glucosaminidase, aminopeptidase, and acid phosphatase – vary as a function of distance from a root. This analysis compares two different types of enzyme substrates (i.e., colorimetric and fluorometric) at three different image resolutions. For each assay, it was possible to visualize and estimate the size of the rhizosphere. The resolution of image analysis did not affect the estimate of the rhizosphere extent for fluorometric assays, but did affect the estimate of rhizosphere extent for colorimetric assays, where the break-point regression was only significant at very-fine-image resolution. I also note methodological concerns specific to the type of enzyme substrate, such as uneven background staining in the colorimetric assay and diffusion of the substrate in the fluorometric assay, and provide

recommendations to improve the method. Zymography is a promising methodology with the potential to increase the spatial resolution of rhizosphere studies compared to methods that measure enzyme activity by physically removing soil.

Introduction

Soil is the largest terrestrial carbon (C) pool, storing more C than the atmosphere and terrestrial vegetation combined (Schlesinger & Bernhardt, 2013). A substantial portion of this pool is associated with plant roots. In the root-associated zone, or rhizosphere, soil-organic-matter-decomposing enzymes are stimulated up to 100% relative to surrounding bulk soil (Kourtev *et al.*, 2002, Tscherko *et al.*, 2004). Though the rhizosphere occupies a small soil volume relative to bulk soil, up to 40% of heterotrophic respiration can be attributed to the rhizosphere (Finzi *et al.*, 2015). As a result, the rhizosphere has a disproportionate effect on biogeochemical cycling.

Roots exude low-molecular-weight C compounds such as organic acids and amino acids into the soil (Jones, 1998, Phillips *et al.*, 2004). This labile C stimulates microbial growth and nutrient demand, resulting in the production of extracellular enzymes that decompose soil organic matter (SOM; Brzostek & Finzi, 2011). Previous research shows that root exudates can be found anywhere from 0.1 to 1.2 cm from the root surface (De Neergaard & Magid, 2001, Jones, 1998, Sauer *et al.*, 2006, zu Schweinsberg-Mickan *et al.*, 2010). Where root exudates are present, microbial biomass, respiration, enzyme activity, N mineralization, and soil organic matter decomposition are all increased relative to soil that is unaffected by roots (Finzi *et al.*, 2015, Phillips *et al.*, 2012).

At present, measurements of microbial and extracellular enzyme activity (EEA) use coarse approaches to separate rhizosphere and bulk soil. For example, some studies consider the rhizosphere to be the soil adhering to the root after gentle shaking or soil that

is ≤ 2 mm from the root surface (Landi *et al.*, 2006, Phillips & Fahey, 2006). Of the studies that try to estimate diffusion distance of exudates in order to determine the rhizosphere extent (Darrah, 1991a,b, Kuzyakov *et al.*, 2003, Raynaud *et al.*, 2003), most assay exudate concentration at up to 10 distances from the root surface by cutting the soil into sections of $\sim 1 - 2$ mm and analyzing the homogenized soil sample (Nuruzzaman *et al.*, 2006, Sauer *et al.*, 2006, zu Schweinsberg-Mickan *et al.*, 2010).

Two methods represent a recent advance in the visualization of enzyme activity using zymography, and allow for spatially resolved *in situ* measurements of soil EEA at finer resolution than traditional studies (Dong *et al.*, 2007, Spohn *et al.*, 2013). These methods produce an image where the brightness, hue, or intensity of coloration or fluorescence corresponds to the amount of enzyme activity in a given area of the image, and provide the opportunity to quantify the relationship between EEA and distance from a root at a very fine spatial resolution, without compromising the integrity of root-microbe interactions. To date, where these methods have been applied, there has been no quantitative analysis of the relationship between EEA and distance from a root (Dong *et al.*, 2007, Spohn *et al.*, 2013).

The objective of this study is to develop a quantitative framework for analyzing zymograms, in order to determine the relationship between EEA and distance from a root. This is part of a longer-term objective of quantifying rhizosphere volume for different species and ecosystems. Here I propose two statistical methods to quantify this relationship. The first is linear regression with a spatially autocorrelated error term in order to account for the lack of independence between neighboring pixels in an image.

The second is “break-point” regression analysis, which determines the location of a change in the slope of the linear regression. Within this context, I also compare enzyme substrates that leave either a visual or fluorescent tag when degraded. Colorimetric substrates, such as that for acid phosphatase and aminopeptidase, leave behind a colored stain following reaction with an enzyme, whereas fluorometric substrates, such as that for beta-glucosidase and N-acetyl-beta-D-glucosaminidase leave behind a fluorescent stain. The previous study that used both colorimetric and fluorescent substrates found qualitative differences in the staining pattern of the assays (Dong *et al.*, 2007). Both types of assays were applied to rooted soil surfaces in three mono-dominant stands at the Harvard Forest in central Massachusetts. To determine whether image resolution affects the scaling of EEA and distance from a root, I compared images analyzed at three spatial scales.

Methods

Site description

The field portion of this study was conducted at the Harvard Forest Long Term Ecological Research Site in Petersham, MA (42°N, 72°W, elevation 340 m). The site is located on former agricultural land that was abandoned in the mid-1800s allowing forest regrowth beginning late in the 19th century (Foster *et al.*, 2003). Soils are Typic Distrochrepts derived from glacial deposits of granite, schist and gneiss. The dominant tree species in this tract are northern red oak (*Quercus rubra*) and red maple (*Acer rubrum*), with smaller populations of eastern hemlock (*Tsuga canadensis*), white ash (*Fraxinus americana*), white pine (*Pinus strobus*) and red pine (*Pinus resinosa*).

Twelve root boxes were constructed at Boston University and installed in the field in March 2012. Each root box was built from 0.9 cm thick clear polycarbonate sheeting. Each side is 40 × 40 cm, with two sides beveled out at 15° to form a rhomboid. Root boxes were set in soil pits and backfilled with excavated soil, maintaining the mineral and organic horizon delineation. Each box was equipped with two 20 × 20 cm removable panels that allow for access to the rooted soil surface (Figure 4.1). Four root boxes (n = 8 panels) were installed in each of three monodominant stands: white ash, red oak, and eastern hemlock. I assume that the > 2 years between root box installation and data collection allowed sufficient time for soils to recover from disturbance and form dense root networks.

Each root box panel (n = 24) was assessed for the activity and spatial extent of four extracellular enzymes: acid phosphatase (AP), aminopeptidase (PR), beta-glucosidase (BG), and N-acetyl-beta-D-glucosaminidase (NAG) in late June – early July 2014. EEA was measured using zymograms prepared following Dong *et al.* (2007). Briefly, a 20 × 20 cm sheet of chromatography paper was soaked in a buffer solution containing colorimetrically (AP, PR) or fluorescently (BG, NAG) labeled substrate for each enzyme, alpha naphthyl phosphate (AP), L-leucyl 2-naphthylamide (PR), 4-methylumbelliferyl-beta-glucopyranoside dehydrate (BG), or 4-methylumbelliferyl-N-acetyl-beta-glucosaminide (NAG). Standards were made by applying acid phosphatase from wheat germ (AP), aminopeptidase from *Aspergillus oryzae* (PR), or fluorescent 4-methylumbelliferone (BG, NAG) to prepared zymograms. The units for acid phosphatase and aminopeptidase activity are enzyme units per milliliter (EU ml⁻¹), defined as the

amount of enzyme in one milliliter that is needed to convert 1 μmol of substrate per minute, and for fluorescent 4-methylumbelliferone, millimolar (mM). Each zymogram (N = 96; 8 root box panels \times 3 stands \times 4 enzymes) was incubated against the soil surface for 30 minutes (BG, NAG) to 1 hour (AP, PR) depending on the type of assay. Immediately following incubation, zymograms were transported back to Boston University where they were dried, and imaged using a Ricoh 907Ex 600dpi color scanner (AP, PR; Ricoh Electronics, Inc., Tustin, CA) or an AlphaImager HP UV gel scanner (BG, NAG; ProteinSimple, San Jose, CA).

All image processing was done in the open source software ImageJ (Rasband, 1997). Digital photographs of open root box panels taken at the time of incubation were cropped, corrected for image distortion, and converted to 8-bit black and white. The background of each image was detected using a rolling ball algorithm (Sternberg, 1983). This algorithm averages over a 50 pixel area around each pixel to compute a local background value which is then subtracted from that pixel. Roots were selected by pixel brightness and false positives (e.g., light colored soil aggregates, insects, rocks) were removed manually using the selection tool. The selection of rooted area was converted to a thresholded mask, where pixels containing roots were given a value of 0 (i.e., black) and non-root pixels were given a value of 255 (i.e., white). The zymogram images were also converted to 8-bit black and white. Digital photographs and zymogram images were compressed to 30×30 , 100×100 , or 1500×1500 pixels using bilinear interpolation, corresponding to an effective pixel length of 6.7 mm, 2 mm, or 0.13 mm, respectively. The x - and y -coordinate position of each pixel was used to overlay the root threshold

image onto zymogram images. Image pixel brightness values and their x - and y -coordinate position were output to R Statistical Software (R Development Core Team, 2013), where all subsequent analyses took place.

In order to determine the relationship between EEA (EU ml^{-1} or mM) and distance from a root (mm), Euclidian distance from the nearest root was determined for each pixel in the zymogram image by creating a vector with the location of each root-containing pixel, and finding the element in this vector with the minimum distance to each pixel. Image pixel brightness values were converted to EU ml^{-1} or mM using a linear relationship between the standards and their pixel brightness values for AP ($\beta = -4.9$, $F_{1,3} = 28.0$, $R^2_{\text{adj}} = 0.87$, $P < 0.05$), PR ($\beta = -1.3$, $F_{1,3} = 15.9$, $R^2_{\text{adj}} = 0.79$, $P < 0.05$), NAG ($\beta = -45$, $F_{1,3} = 60.5$, $R^2_{\text{adj}} = 0.93$, $P < 0.01$), and BG ($\beta = -47$, $F_{1,2} = 22.3$, $R^2_{\text{adj}} = 0.88$, $P < 0.05$; Figure 4.2). High brightness values correspond to low enzyme activity due to the convention of setting brightness values to 0 for black and 255 for white pixels. I considered the total area of all pixels containing roots to be the rooted area for each stand. I used ANOVA and Tukey's HSD to test for differences in rooted area among the three stands.

I tested for the presence of spatial autocorrelation between neighboring pixels using the Moran's I statistic. I used the *moran.test* function in the *spdep* package for R Statistical Software (Bivand *et al.*, 2014). To establish a relationship between EEA and distance from a root while accounting for spatial autocorrelation between pixels and their neighbors, I used a spatial simultaneous autoregressive error model of the form:

$$Y = \beta_1 x_1 + \beta_2 x_2 + \beta_3 + \varepsilon, \text{ and} \quad [1]$$

$$\varepsilon = \rho W e + u \quad [2]$$

where Y is EEA (EU ml^{-1} or mM), x_1 is distance from root (mm), x_2 is depth (mm), and β_1 , β_2 , and β_3 are linear regression coefficients. The error term, ε , contains a spatially structured error term, $\rho W e$, where ρ is a fit coefficient, W is the spatial weight matrix, e is the spatial error term, and u is a random residual. This model assumes that neighboring pixels are not independent of one another, and as a result the predicted value for a given pixel depends in part on the value of its neighbors. The fit parameter ρ corresponds to the strength of autoregression between neighboring pixels on model residuals. I fit the spatial error model to data from each image using the *errorsarlm* function in the *spdep* package for R Statistical Software (Bivand *et al.*, 2014).

To test for the location of a change in the slope of the relationship, or break point, between EEA and the distance from a root, I used a weighted “break-point” regression. I used the break point as a proxy for the rhizosphere extent. EEA was fit as a function of distance from a root using the equation:

$$Y = \beta_1 x + \beta_2 (x - c) + \gamma I(x > c) \quad [3]$$

where x is the Euclidian distance from the root (mm), β_1 and β_2 are slope and intercept parameters, c is the break point, and $I(x > c)$ is an index variable that is equal to zero when $x < c$. The model minimizes γ , a measure of the distance between the two segments in order to constrain the segments to be close to continuous.

I observed that the sample size (i.e., number of pixels represented at each root distance) decreased as distance from a root increased (Figure 4.3). As a result, rather than

minimizing the sum of squared residuals (SSE) as in ordinary least squares, I minimized the weighted SSE:

$$\text{Weighted SSE} = \sum_{i=1}^n w_i (y_i - \hat{y}_i)^2 \quad [4]$$

where w_i is a vector of weights proportional to the sample size such that

$$w_i = \frac{N_i}{\sum_{i=1}^n N_i} \quad [5]$$

and N_i is the number of pixels at each root distance i to n . This model was fit using the *segmented* function in the *segmented* package for R statistical software (Muggeo, 2008).

I used the spatial autoregressive error model (Eq. [1]) on images at coarse and fine resolution in order to determine if there was an effect of image resolution on the relationship between EEA and distance from a root. At coarse image resolution (30×30 pixels) each pixel was 6.7 mm in length, corresponding to an area of 0.44 cm^2 per pixel. At fine image resolution (100×100 pixels) each pixel was 2 mm in length, corresponding to an area of 0.04 cm^2 per pixel.

I used break-point regression (Eq. [3]) on images at coarse, fine, and very fine resolution in order to determine if there was a relationship between pixel size and break-point value. For very-fine-resolution image analysis, I examined a subsection of a 1500×1500 pixel-resolution image focusing on a rooted area in hemlock soil (Figure 4.4a, Box 4.1). In this image, the length of each pixel was 0.13 mm, corresponding to an area of $1.7 \times 10^{-4} \text{ cm}^2$.

Results

Visual inspection

White ash and red oak stands were more sparsely rooted than eastern hemlock with $14 \pm 1.0 \text{ cm}^2$ and $15 \pm 1.1 \text{ cm}^2$ of rooted area out of the 400 cm^2 sample area, respectively ($F_{2,93} = 34.5$, $P < 0.001$, Table 4.3). Eastern hemlock images contained $27 \pm 1.7 \text{ cm}^2$ of rooted area. The mean area covered by roots across the three stands is 18.7 cm^2 , approximately 5% of the sample area.

The staining pattern on scanned zymogram images was visibly different for colorimetric compared to fluorometric assays. The colorimetric acid phosphatase assay had the most localized staining (Figure 4.4a). Aminopeptidase zymograms developed the least amount of staining (60% of pixels had no detectable EEA) compared to AP (10%), BG (1.7%), or NAG (3.2%). However, when PR did stain, it was 20–40% brighter than the other zymograms (Figure 4.4b). Beta-glucosidase and N-acetyl-beta-D-glucosaminidase were fluorometrically assayed. I found this assay to be relatively diffuse, often with large areas of high EEA covering >50% of the zymogram (Figure 4.4c,d).

At coarse image resolution, clusters of roots and EEA were visible, but not fine root morphology (Figure 4.5a). At fine resolution, individual fine roots were visible (Figure 4.5b), but it was not possible to determine the diameter of fine roots $< 2 \text{ mm}$. At both image resolutions, there appeared to be fewer pixels with high EEA at 0 – 10 mm from the top of the image in BG and NAG images (*data not shown*). At very fine resolution, it was possible to distinguish between small- and large-diameter roots (Figure

4.5c). There was visible overlap in many images between locations of rooted pixels and locations with high enzyme activity at fine resolution. However, in some cases there was a < 1 – 5 mm misalignment of images, where EEA associated with a root was offset from the thresholded mask of the root as a result of manual error in the image analysis steps that were not fully automated (i.e., root thresholding, image distortion correction).

Coarse image resolution

EEA ranged between 0–10 EU ml⁻¹ for AP, 0–40 EU ml⁻¹ for PR, and 0–4.9 mM for BG and NAG. EEA generally declined as distance from a root increased (Figure 4.6). For all images, there was significant spatial autocorrelation (Moran's I, $P < 0.05$). Of the 96 images analyzed, 54 had a significant relationship between EEA and distance from a root, including 51 which had a significant negative relationship (Table 4.1). Red oak had the greatest proportion of significant negative relationships between EEA and root distance (78%) of the three stands. Acid phosphatase had the greatest proportion (88%) of significant negative relationships of the four enzymes, and aminopeptidase had the fewest (25%). Forty-three out of 48 significant spatial error models predicted that EEA declined with depth (Table 4.1). Eastern hemlock had the greatest proportion of significant and negative relationships with depth (60%) of the three stands.

In the break-point regression model, the relationship between EEA and distance from a root was not significant for the colorimetrically assayed enzymes (AP, PR).

Fluorometrically assayed enzymes (BG, NAG) had break points of 7.5 cm and 1.8 cm, respectively (Figure 4.6). Averaging across the enzymes with a significant relationship between EEA and distance to a root (BG, NAG), I identified break points at 5.8 cm and

4.7 cm for white ash and red oak (Figure 4.7). The break-point regression model for eastern hemlock was not significant.

Fine image resolution

At fine image resolution, computing time increased 72-fold compared to coarse resolution. The increased resolution allowed us to observe a greater range of brightness values compared to coarse resolution. EEA ranged between 0-30 EU ml⁻¹ for AP, 0-170 EU ml⁻¹ for PR, and 0-5.3 mM for BG and NAG. The break point was closer to the root surface than at coarse resolution, reflecting the closer association between pixel size and root size (Figure 4.8).

A spatially autoregressive error model fit to the data found 84 of 96 significant relationships between EEA and distance from a root, of which 39 were negative (Table 4.2). BG and NAG images had the greatest number of negative regression coefficients, while AP and PR had a majority of positive coefficients, indicating that EEA increased with distance from a root. Sixty-eight of 96 images had a significant relationship with depth. Of these, 57 were positive relationships.

In the break-point regression model, the relationship between EEA and root distance was not significant for AP and PR. The break points for BG and NAG were 6.7 and 1.5 cm, respectively (Figure 4.8). The break-point regression between EEA and distance from a root for eastern hemlock was not significant. Break points for white ash and red oak were identified at 7.1 and 1.2 cm, respectively (Figure 4.9).

Very fine image resolution

In a very-fine-resolution subsection of an acid phosphatase assay in the hemlock stand (Figure 4.4, Box 4.1), the maximum observable EEA was 36 EU ml^{-1} , compared to 32 EU ml^{-1} in the fine resolution and 9 EU ml^{-1} in the coarse resolution analysis of the same enzyme. The median EEA (1.6 EU ml^{-1}) was identical to that at coarse resolution. EEA was high within 10 mm of the root, but declined quickly thereafter. Break-point regression placed the break-point location at 2.6 mm (Figure 4.10).

Discussion

There were differences in the localization of EEA in colorimetric compared to fluorometric assays, with colorimetric assays resulting in more specific staining compared to fluorometric assays. This is likely the result of the fluorometric tag's ability to diffuse when wet (Spohn & Kuzyakov, 2013). The colorimetric aminopeptidase assay resulted in an average of 60% of the image with no detectable EEA, indicating that there was little aminopeptidase enzyme activity in the soils that I sampled. In the colorimetric acid phosphatase assay, there was an increase in EEA with distance from a root at the fine resolution that I did not observe at coarse resolution. I did not expect this result given the visual correspondence between EEA and roots in this assay. However, the acid phosphatase assay developed an orange-colored background. Uneven background color and image misalignment are two methodological concerns that would be exacerbated at fine resolution compared to coarse resolution, given the wider range of EEA and smaller pixel size, respectively. Analysis of a subset of a very-fine-resolution image suggests that a negative relationship between EEA and root distance is observable in colorimetric

assays at high resolution if the background color is even and the zymograph and thresholded root mask are well-aligned.

Rhizosphere extent across stand types and enzyme classes

For the fluorometric assays, EEA declined with increasing distance from a root. Break point analysis predicted that the rhizosphere extent ranged from 0.26 to 7.5 cm, depending on the resolution of analysis. Direct sampling and isotopic labeling studies place the rhizosphere extent between 0.1 and 1.2 cm (De Neergaard & Magid, 2001, Dessureault-Rompré *et al.*, 2007, Falchini *et al.*, 2003, Sauer *et al.*, 2006, zu Schweinsberg-Mickan *et al.*, 2010), but another study using a similar method to the one used here recorded enhanced EEA up to 6 cm away from the root surface (Spohn & Kuzyakov, 2014). It is therefore possible that recent estimates of rhizosphere contributions to decomposition and nutrient mineralization based on an exudate diffusion distance of 2 mm are very conservative (Finzi *et al.*, 2015).

Effects of image analysis resolution

The resolution of the image analysis affected the spatial distribution of EEA, the break-point location, and the influence of artifacts and image alignment. As resolution increased, the maximum observable EEA increased because there was a larger sample size and less averaging of high EEA pixels with pixels of intermediate and low EEA. In addition, the distance of the break point to the root surface declined due to greater visibility of root morphology relative to staining of EEA (Figure 4.5). Generally, this

suggests that matching the scale of resolution to the scale of fine root architecture will increase the accuracy of both EEA and break point estimates.

At fine image resolution, the spatial error model predicted a mixture of positive and negative relationships between EEA and distance from a root. There were a surprising number of instances where the relationship between EEA and distance from a root was positive. This was more common for the colorimetric assays, AP and PR (Figure 4.8). For AP in particular, background staining developed from the substrate solution, a mix of α -naphthyl phosphate and Fast Red TR. Though care was taken to apply the substrate evenly, there was variation in the background coloring of the zymograms. At high resolution, this variation in background color may have introduced artifacts into the assessment of EEA using pixel brightness. This was somewhat accounted for by subtracting the background using a rolling ball algorithm, but with very unevenly stained backgrounds such as that in Figure 4.4a, there may have been some pixels with under- or over-estimated EEA.

Image misalignment was another error that was exacerbated at fine resolution. Images were scaled to identical size and overlaid automatically, but root images were corrected for pixel distortion and cropped manually, and no image-aligning algorithm was used. Any misalignment of images would be on the scale of < 1 mm to 5 mm, so coarse image resolution that averages over large root clusters may alleviate errors that are a result of misalignment.

I wanted to explore whether or not there was value in investing the additional computing time to analyze very-fine-resolution images in order to more accurately

represent fine root morphology. I selected a subset of the zymogram pictured in Figure 4.4a (Box 4.1) that appeared to have even background staining and be well aligned with the image of the root. In this subset, EEA declined steeply as distance from the root increased up to 2.6 mm (Figure 4.10). From 2.6 mm to 7 cm the relationship was relatively flat. This analysis is not replicated, but suggests that high resolution images can be used to estimate relationships between EEA and roots if methodological concerns are alleviated.

Fluorescent clustering of EEA in the center of the image may result from the diffusion of the substrate when wet. In colorimetric zymograms, there was more EEA at the surface of the soil than at depth, corresponding with high root abundance. In the fluorescent zymograms, however, there was comparatively less EEA at the soil surface, suggesting that as the zymograms are incubated in a vertical position, the fluorescent tag diffused downward in response to gravity. Zymograms were moistened before incubation, and the 4-methylumbelliferone tag is known to diffuse readily when wet (Spohn & Kuzyakov, 2013). Because the zymogram staining is diffuse, coarse-resolution image processing is sufficient to represent the correspondence between EEA and root distribution. Thus, fine resolution is only necessary when the zymogram staining also has fine spatial resolution, as in the colorimetric acid phosphatase assay.

Methodological considerations

This methodology can be improved with image-analysis techniques. I counted the number of black pixels in the root image to estimate the proportion of sample area covered by roots and found that red oak stands were more sparsely rooted than hemlock.

From a visual inspection of the root boxes, it is clear that red oak root boxes are heavily rooted, but that these roots are very fine and similar in color to the soil. In contrast, hemlock roots are thick and light-colored compared to the soil (Figure 4.1). As a result, a greater number of roots in the hemlock stand were successfully thresholded relative to the red oak stand. A different annotation method or an edge-detection algorithm may improve root detection in stands with roots that are similar in color to their background (Canny, 1986, Lobet *et al.*, 2011). Higher resolution images may also aid in detecting very fine roots that may be smaller than the pixel size.

Some patches of high EEA were unrelated to root activity. This method cannot yet annotate mycorrhizal hyphae or detect other possible microbial hotspots associated with invertebrate casts or litter that may not be near a root surface. Additionally, not all roots produce an active rhizosphere. Exudates are primarily released from growing root tips, and assuming an average root growth rate of $1 \mu\text{m s}^{-1}$ and a 30-minute half-life for exudates, then at 30 mm behind the growing root tip there will be $< 1\%$ of the original exudate remaining (Hirsch *et al.*, 2013). Finally, my thresholding function does not distinguish between suberized roots, dead roots, absorptive roots, or growing root tips, and therefore areas of high root proliferation with low EEA may reflect different demographic stages of the root. For this reason, coarse resolution averaging over thickly rooted areas may partially alleviate this issue. An alternative would be to manually annotate fine absorptive roots and root tips.

Conclusions

In order to scale up measurements of microbial activity (e.g., enzyme activity, microbial biomass) made in bulk and rhizosphere soils to an ecosystem scale estimate, some assumption of the volume of the rhizosphere is necessary. Finzi et al. (2015) used a numerical model to estimate the volume of the rhizosphere, and demonstrated that changing the assumption of the exudate diffusion distance can cause estimates of the proportion of soil that is in the rhizosphere to vary by > 20%.

Soil zymography provides the opportunity to generate statistical relationships between EEA and distance from a root, in order to determine the rhizosphere extent of a given soil. Zymograms are easy to prepare and deploy in the field, and allow for spatial analysis of multiple enzymes across heterogeneous soil surfaces. Many techniques in automatic annotation, background correction, and image alignment are well-developed and can be applied to this method (Amat *et al.*, 2008, Nobis & Hunziker, 2005, Ritchie *et al.*, 2007). The main methodological concerns for this method are evenness of background staining and image alignment for the colorimetric assay and diffusion of the tag in the fluorometric assay. Methodological improvements such as using agarose gel to keep soil particles from quenching the fluorescent tag are also promising (Spohn *et al.*, 2013). In this method, enzymes can diffuse through the gel to the zymogram, but soil particles do not contact the zymogram, resulting in high staining accuracy.

To determine the rhizosphere extent of enzymes that degrade a colorimetric substrate, I make the following recommendations:

- Use very fine image resolution (~0.13 mm)

- Use an image-aligning algorithm
- Annotate root tips and absorptive roots

To determine the rhizosphere extent of enzymes that degrade a fluorometric substrate, I make the following recommendations:

- Use coarse or fine image resolution (2 mm – 6 mm)
- Dry zymogram flat after substrate application and soil incubation to reduce vertical diffusion
- Prepare zymogram using agarose gel layer, following Spohn *et al.*, (2013)

I have provided a quantitative framework to analyze and estimate the rhizosphere extent from image data using a zymographic method. This analysis could be expanded to include uncertainty associated with the linear parameters estimated in both the spatial error regression and the break-point regression using Bayesian or Monte Carlo techniques. In addition, nesting images within stands, sites, and region may eventually allow for geographically specific estimates of rhizosphere extent interpolated between locations for which zymographic data has been collected. Given access to a rooted soil surface, preparation and incubation of zymograms is a simple and relatively inexpensive process. Once a quantitative framework for image analysis is adopted, determination of rhizosphere extent using zymograms will be much easier than cutting, extracting, and measuring enzyme activity from soil directly.

Table 4.1. Summary of spatial error model regression coefficients estimated at coarse resolution. Enzyme activity (EU ml⁻¹ or mM) is modeled as a function of distance from a root (mm) and soil depth (mm). ρ is the spatial error coefficient. AIC is the Akaike information criterion, a model-selection score that balances goodness-of-fit against the number of parameters. Regression coefficients, ρ , and AIC for each image were averaged to obtain one value for each stand and enzyme. AP = acid phosphatase, PR = aminopeptidase, BG = beta-glucosidase, NAG = N-acetyl-beta-D-glucosaminidase, F = white ash, Q = red oak, T = eastern hemlock.

Enzyme	Stand	Intercept	Distance	Depth	ρ	AIC
AP	F	2.45	-0.018	-0.13	0.92	2498
	Q	0.63	-0.029	-0.44	0.93	2821
	T	-1.70	-0.045	-0.45	0.93	2412
PR	F	1.71	-0.003	-0.04	0.85	3791
	Q	1.16	0.000	-0.02	0.80	3518
	T	1.98	0.005	-0.05	0.84	3786
BG	F	0.81	-0.006	-0.04	0.99	2096
	Q	0.96	-0.011	-0.08	1.00	2385
	T	1.20	-0.004	-0.05	0.99	2028
NAG	F	0.62	-0.004	-0.10	0.98	1596
	Q	1.60	-0.009	-0.08	0.98	1283
	T	2.84	-0.005	-0.16	1.00	2131

Table 4.2. Summary of spatial error model regression coefficients estimated at fine resolution. Enzyme activity (EU ml⁻¹ or mM) is modeled as a function of distance from a root (mm) and soil depth (mm). ρ is the spatial error coefficient. AIC is the Akaike information criterion, a model-selection score that balances goodness-of-fit against the number of parameters. Regression coefficients, ρ , and AIC for each image were averaged to obtain one value for each stand and enzyme. AP = acid phosphatase, PR = aminopeptidase, BG = beta-glucosidase, NAG = N-acetyl-beta-D-glucosaminidase, F = white ash, Q = red oak, T = eastern hemlock.

Enzyme	Stand	Intercept	Distance	Depth	ρ	AIC
AP	F	0.58	0.058	0.87	0.96	36234
	Q	0.30	0.060	0.85	0.96	39796
	T	1.69	0.029	0.01	0.96	33604
PR	F	-2.23	0.185	0.06	0.96	59046
	Q	-4.19	0.190	0.10	0.96	58653
	T	-2.19	0.209	0.08	0.95	61021
BG	F	-4.46	-0.010	0.05	1.00	24530
	Q	-5.63	-0.019	0.05	1.00	27673
	T	-5.46	-0.005	0.03	1.00	23748
NAG	F	-2.30	-0.004	-0.01	1.00	19855
	Q	-8.07	-0.006	0.04	1.00	16399
	T	-0.44	-0.005	-0.01	1.00	24662

Table 4.3. Tukey's HSD test on an ANOVA model of rooted area (cm²) per 20 × 20 cm panel as a function of stand. Different superscript letters denote significant differences at P < 0.05.

Stand	Rooted area (cm²)	
	6mm	2mm
White ash	13.9 ± 0.84 ^b	13.6 ± 1.0 ^b
Red oak	17.1 ± 1.1 ^b	14.9 ± 1.1 ^b
Eastern hemlock	26.6 ± 1.9 ^a	27.4 ± 1.7 ^a



Figure 4.1. Plexiglass root box designed and constructed for this study at Boston University. Roots can be accessed by lifting a hinged panel. The second hinged panel is partially visible in the lower right hand corner.

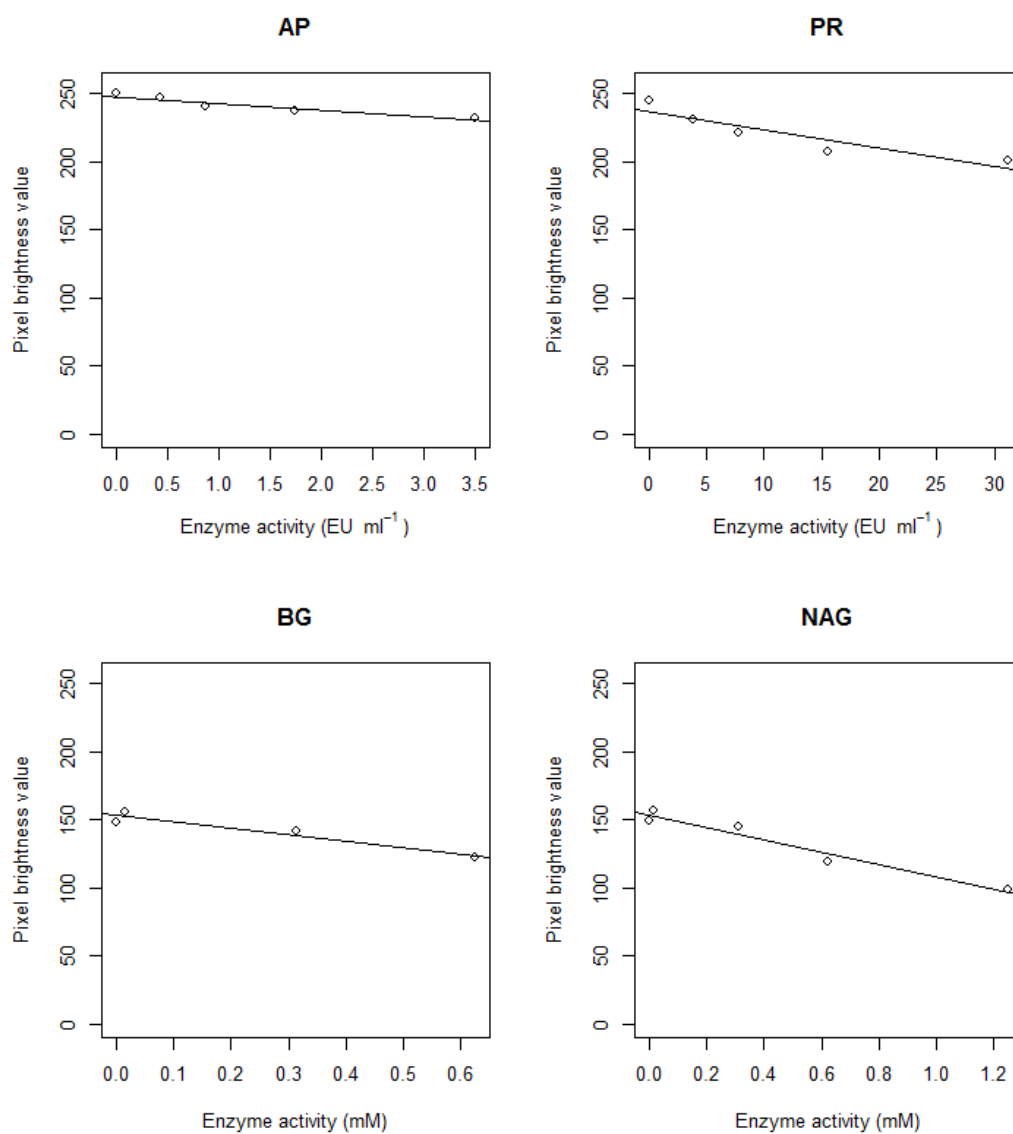


Figure 4.2. Linear relationship between enzyme activity and brightness values for the zymogram area, determined by staining the zymogram with a range of acid phosphatase, protease, or 4-MUB concentrations. AP = acid phosphatase, PR = aminopeptidase, BG = beta-glucosidase, NAG = N-acetyl-beta-D-glucosaminidase.

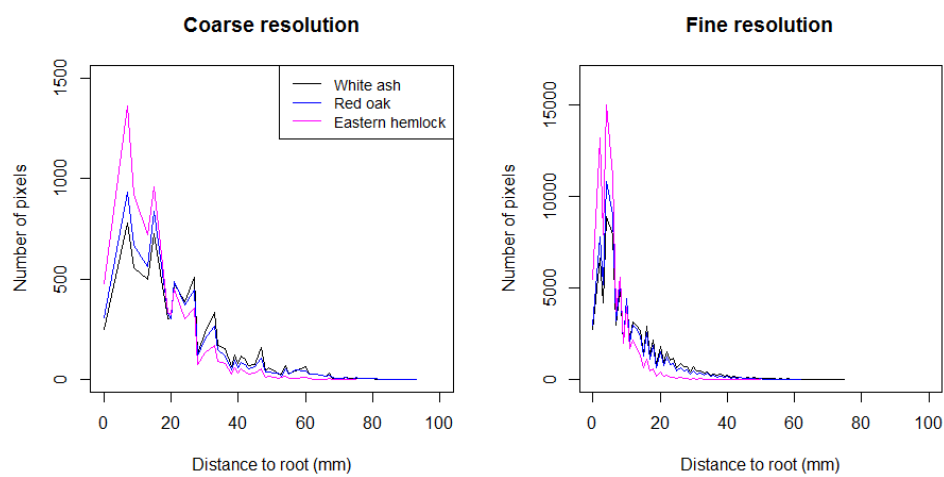


Figure 4.3. Sample size (number of pixels) in each 1 mm distance from root bin at coarse (6.7 mm) and fine (2 mm) image resolution.

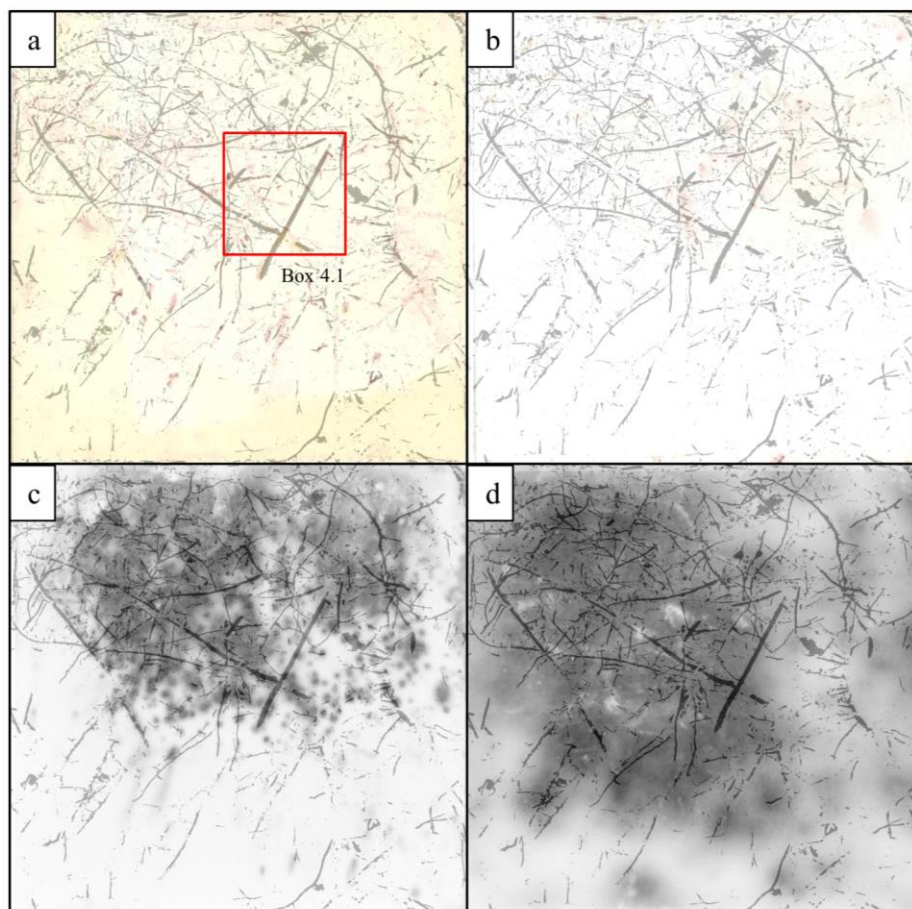


Figure 4.4. Zymograms measuring the activity of (a) acid phosphatase, (b) aminopeptidase, (c) beta-glucosidase, and (d) N-acetyl-beta-D-glucosaminidase on the same hemlock stand root box panel. Thresholded mask of roots is overlaid on each zymogram at 70% transparency. Box 4.1 is the image subset used in very-fine-resolution analysis.

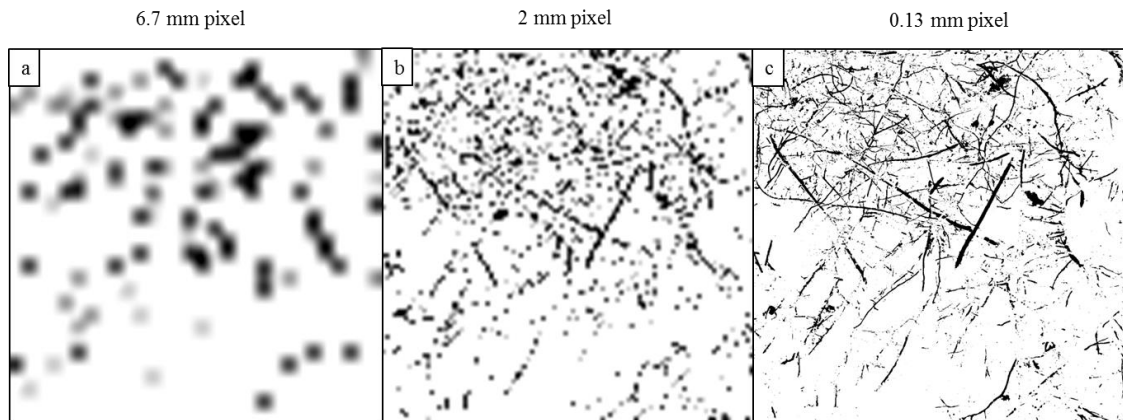


Figure 4.5. Level of detail visible across a range of spatial resolution. Length of the side of one pixel is, (a) 6.7 mm, (b) 2 mm, or (c) 0.13 mm (resolution of original 8-bit image).

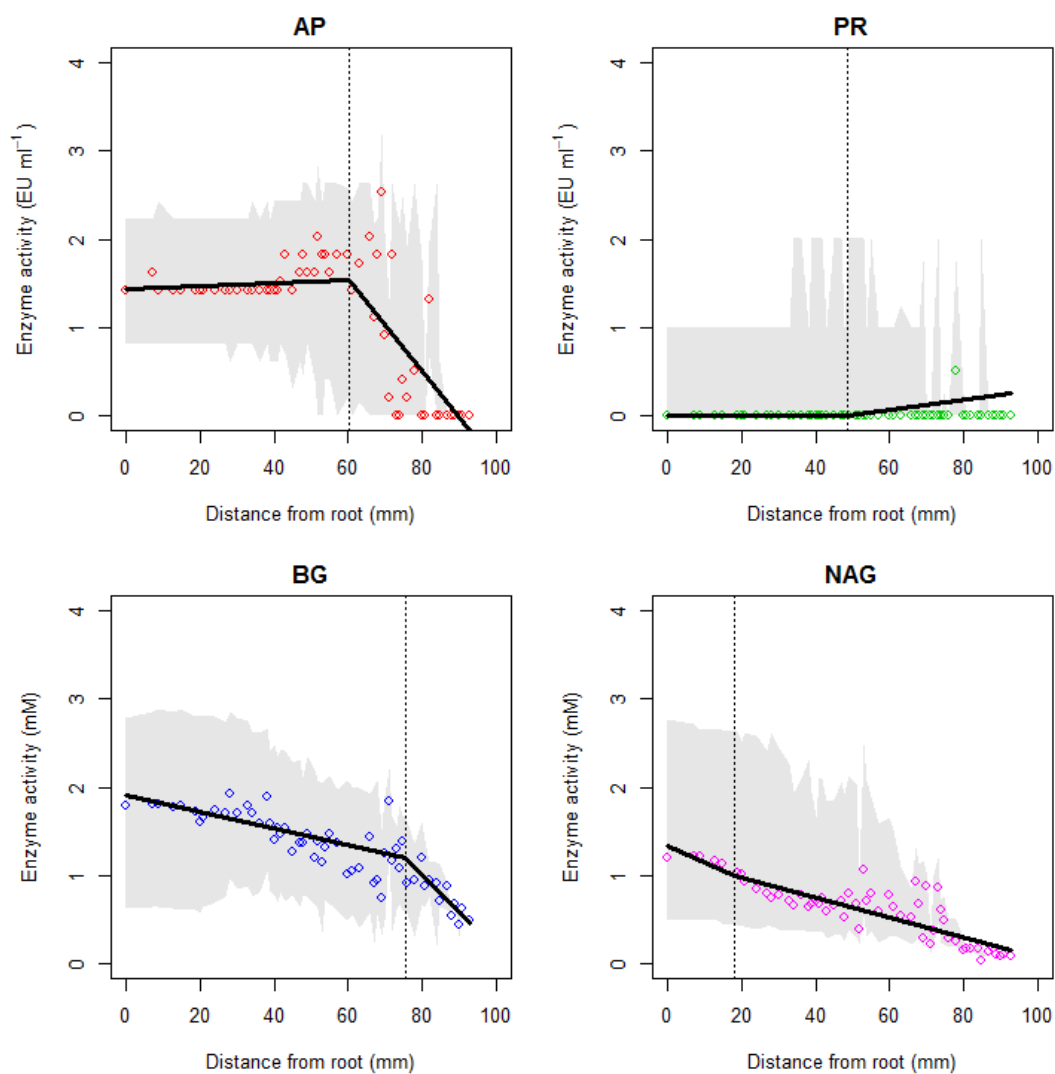


Figure 4.6. Enzyme activity (EU ml⁻¹ or mM) versus distance from root (mm) for four extracellular enzymes: acid phosphatase (AP), aminopeptidase (PR), beta-glucosidase (BG), and N-acetyl-beta-D-glucosaminidase (NAG) at coarse resolution. The broken solid line is the best-fit break-point regression line. The dotted vertical line indicates the location of the break point. The shaded gray area is the interquartile range of the data.

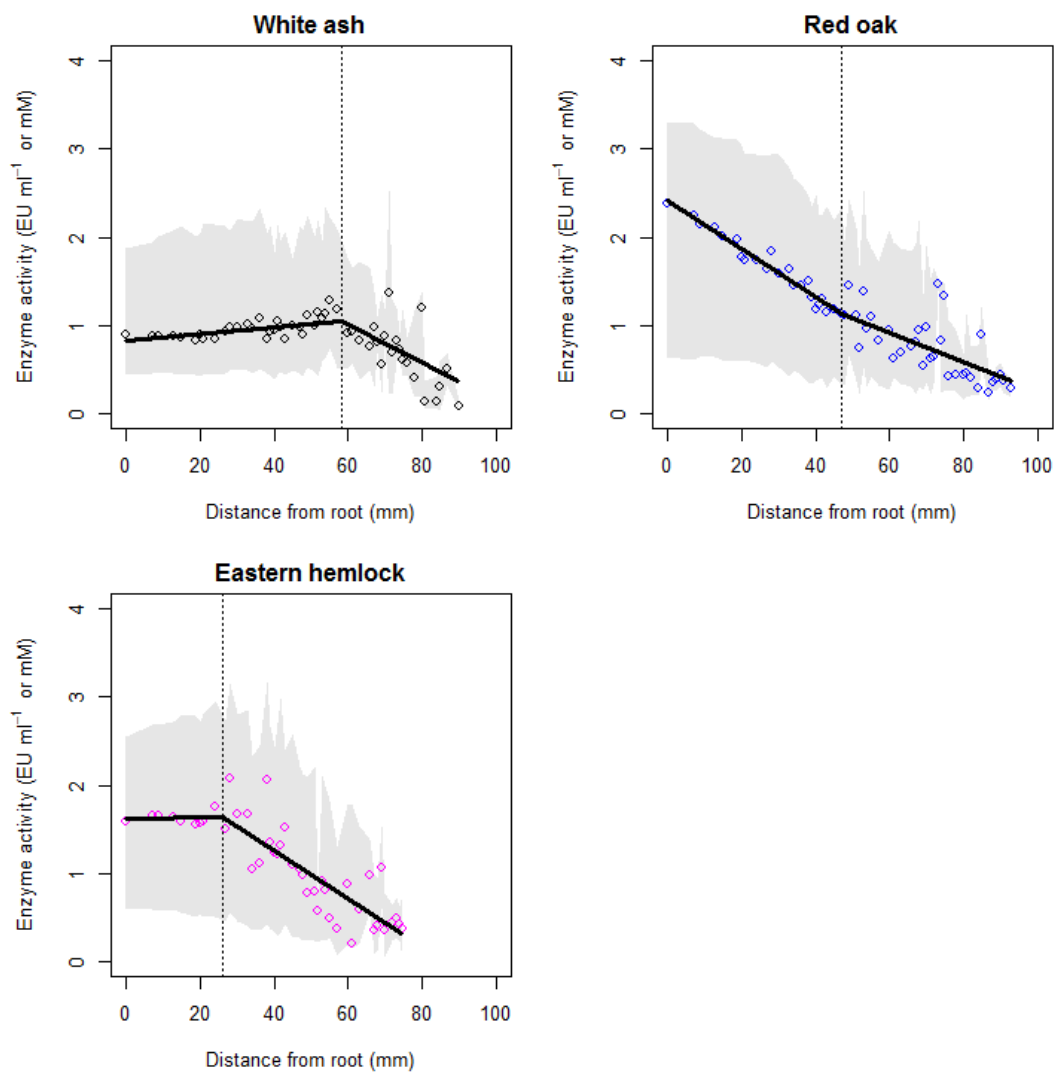


Figure 4.7. Enzyme activity (EU ml⁻¹ or mM) versus distance from root (mm) for white ash, red oak, and eastern hemlock stands at coarse resolution. The broken solid line is the best-fit break-point regression line. The dotted vertical line indicates the location of the break point. The shaded gray area is the interquartile range of the data.

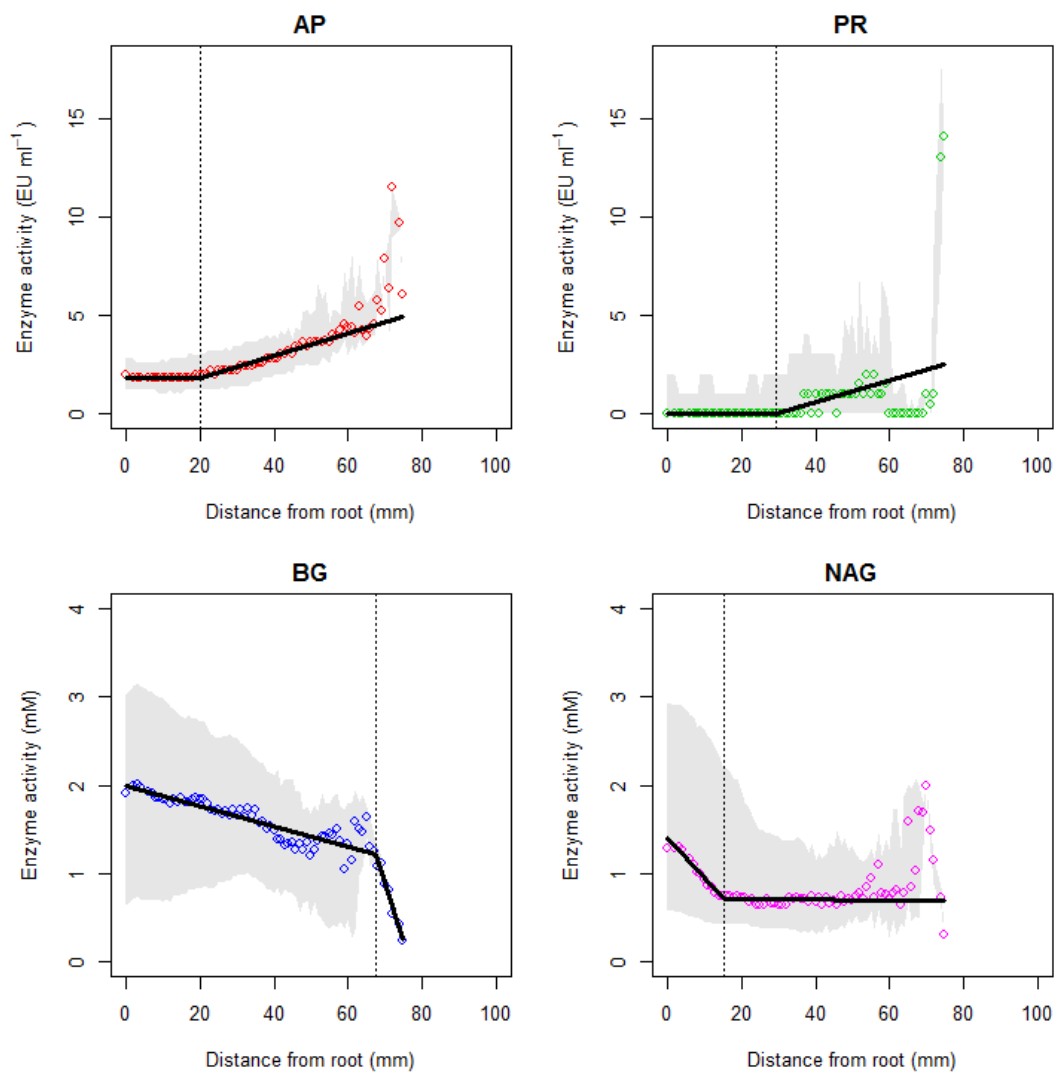


Figure 4.8. Enzyme activity (EU ml⁻¹ or mM) versus distance from root (mm) for four extracellular enzymes, acid phosphatase (AP), aminopeptidase (PR), beta-glucosidase (BG), and N-acetyl-beta-D-glucosaminidase (NAG) at fine resolution. The broken solid line is the best-fit break-point regression line. The dotted vertical line indicates the location of the break point. The shaded gray area is the interquartile range of the data.

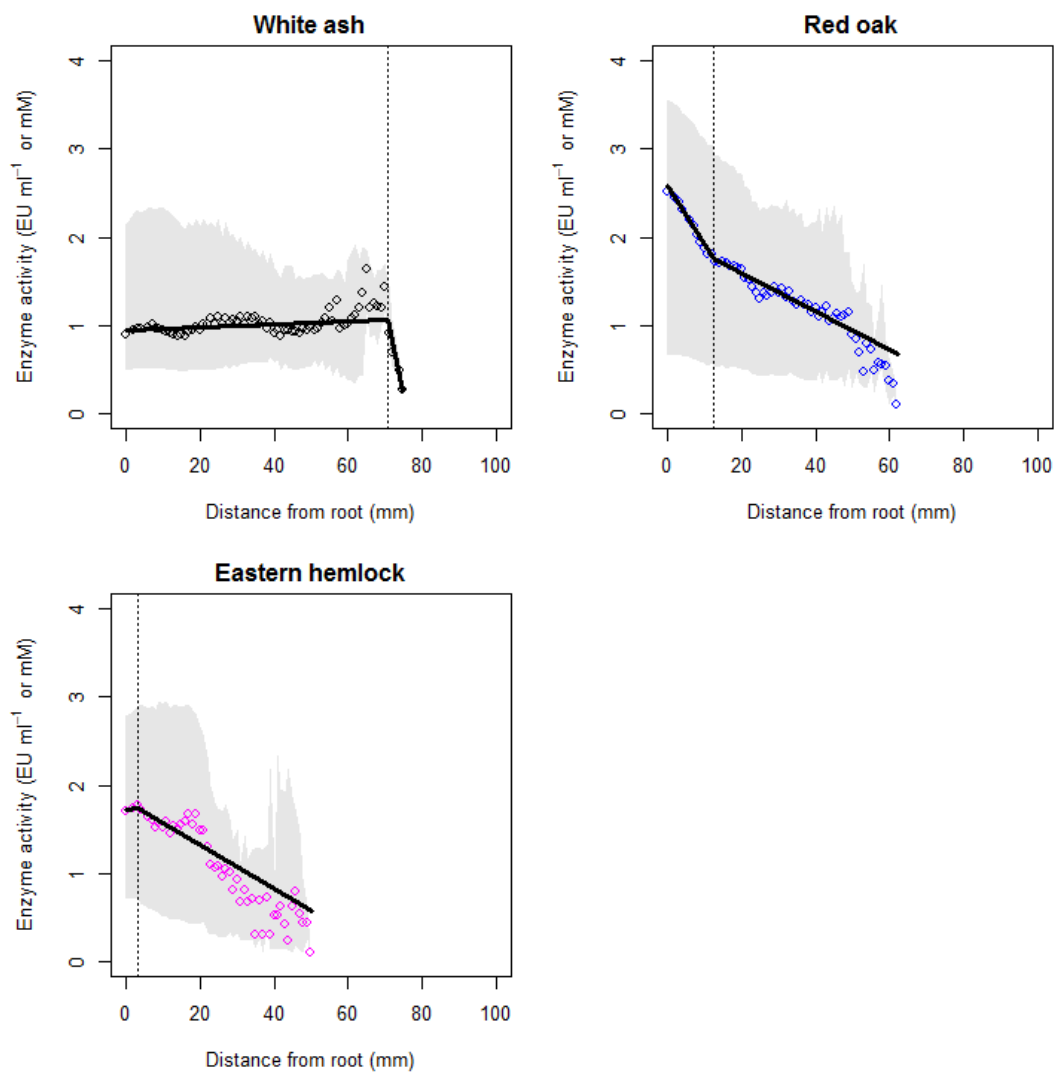


Figure 4.9. Enzyme activity (EU ml⁻¹ or mM) versus distance from root (mm) for white ash, red oak, and eastern hemlock stands at fine resolution. The broken solid line is the best-fit break-point regression line. The dotted vertical line indicates the location of the break point. The shaded gray area is the interquartile range of the data.

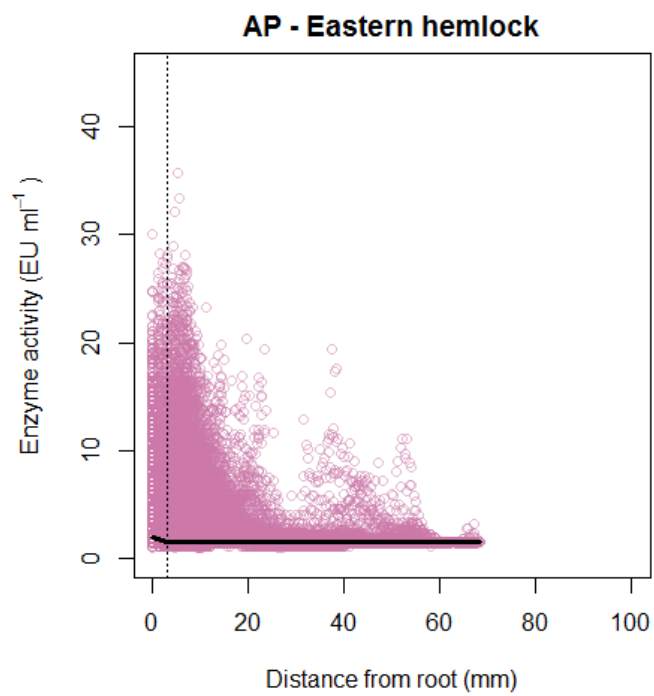


Figure 4.10. Enzyme activity (EU ml⁻¹) in a 400 × 400 pixel subsection of a high-resolution photo (1500 × 1500 pixels). Break point for this subsection is 2.6 mm.

**CHAPTER FIVE: A PARSIMONIOUS MODULAR APPROACH TO BUILDING
A MECHANISTIC BELOWGROUND C AND N MODEL**

Abstract

More carbon (C) is stored in soil than in the atmosphere and terrestrial vegetation combined, and microbial decomposition of soil organic matter (SOM) makes up the largest proportion of the flux of carbon dioxide from the soil to the atmosphere. As a result, microbial activity can have a large effect on the global C cycle. Microbial decomposition and uptake of dissolved substrate is sensitive to temperature and substrate supply, the latter of which can be limited by diffusion of substrate to microbial extracellular enzymes or by oxygen limitation. Many decomposition models use temperature and soil moisture in a linear decomposition coefficient, and few explicitly model the processes that limit substrate supply on the micro-site level. In order to build process-level representation of the effect of temperature and substrate supply on microbial physiology, I merged a model that uses temperature and substrate supply to predict depolymerization rate with a C and nitrogen (N) microbial physiology model.

I tested the performance of the combined model relative to each model alone using measurements of heterotrophic respiration in a mid-latitude forest located in central Massachusetts, USA. I then applied the combined model to theoretical concepts such as the response of microbial activity to varying ratios of C-to-N (C:N), and global change-inspired perturbations to mean annual temperature and soil moisture. The combined model predicted realistic C efflux during transient wet-up events, but over-predicted C efflux in constant high soil moisture conditions. Model predictions of SOM

decomposition in response to variable C:N inputs are consistent with the observation that wide C:N stands store more C than narrow C:N stands. The combined model reproduced realistic responses to temperature perturbation, and thus may be useful for investigating the interaction between substrate and temperature controls on soil C storage at regional and global scales.

Introduction

Soil is the largest terrestrial carbon (C) pool, and the flux of CO₂ from the soil to the atmosphere is dominated by microbial decomposition (Schlesinger & Bernhardt, 2013). Hence, the rate of C mineralized by soil micro-organisms affects the global C cycle. A number of biotic and abiotic factors control the amount of C that microbes release via decomposition. Soil microbes produce extracellular enzymes in order to depolymerize soil organic matter (SOM), but they can also utilize C and N substrates released by plant roots (Brzostek & Finzi, 2011, Frey *et al.*, 2013). Labile organic C and N exuded from plant roots can induce microbial population growth and nutrient limitation, which results in enhanced production of microbial extracellular enzymes that decompose SOM (Brzostek *et al.*, 2013, Kuzyakov, 2010).

The carbon-to-nitrogen (C:N) ratio of root exudates has been shown to affect depolymerization rates, with root inputs of C and N together stimulating decomposition more than additions of C alone (Drake *et al.*, 2013). Since litter and root inputs affect microbial activity, differences in the C:N of inputs owing to differences in species traits may affect the function of soil microbial communities. For example, a stand with acidic soils that supports ectomycorrhizal fungi such as eastern hemlock (*Tsuga canadensis*) has a wider litter and root C:N ratio as well as a higher fungal-to-bacterial (F:B) ratio relative to a stand such as white ash (*Fraxinus americana*), that has narrow litter C:N and a low F:B ratio (Finzi *et al.*, 1998, Strickland & Rousk, 2010).

Microbial activity is also temperature sensitive, with depolymerization of SOM and uptake of dissolved organic carbon (DOC) conforming to Arrhenius kinetics (Lloyd

& Taylor, 1994). However, soil temperature is only the dominant driver of microbial activity when substrate supply is not limiting. When substrate supply is limited by diffusion or oxygen (O₂) limitation, then decomposition conforms to Michaelis-Menten kinetics (Davidson & Janssens, 2006). Substrate and O₂ limitation have been demonstrated using field experiments measuring carbon dioxide (CO₂) efflux under different soil moisture conditions (Davidson *et al.*, 1998, McNicol & Silver, 2015). Physical separation between substrate and enzyme is cited as a mechanism by which SOM persists through time (Schmidt *et al.*, 2011).

Despite well-known effects of temperature and substrate supply on the activity of soil microbes, microbial processes have not been modeled explicitly in terrestrial biosphere models. In these models, decomposition rate is determined using a linear rate constant that may vary as a function of temperature or soil moisture (Bolker *et al.*, 1998, Jenkinson *et al.*, 1990). Indeed, none of the models in the Fifth Coupled Model Intercomparison Project (CMIP5), used by the Fifth Assessment Report of the Intergovernmental Panel on Climate Change (2013), have process-level representation of microbial physiology (Todd-Brown *et al.*, 2013). Where they have been included, the models suggest that process-level representation of microbial physiology influences soil C storage at the global scale (Hararuk *et al.*, 2014, Tang & Riley, 2015, Wieder *et al.*, 2013).

Linear rate constants do have the advantage of being computationally and mathematically tractable, and do not result in the oscillatory behavior that is commonly reported in models that incorporate non-linear processes such as Arrhenius and

Michaelis-Menten relationships (Hararuk *et al.*, 2014, Wieder *et al.*, 2014). Given the importance of microbial physiology to global C cycling, I believe that process-level representation is necessary, but the resulting model should be as parsimonious as possible and modular enough to easily exclude features that are not necessary to a particular user or for which data is not available at a particular site.

In order to build process-level representation of the effect of temperature and substrate supply on microbial physiology, I merged a model that uses temperature and substrate supply to predict depolymerization rate (Davidson *et al.*, 2012) with a C and N microbial physiology model (Finzi *et al.*, 2015). Merging two models involves a number of challenges including combining model equations, parameterization, and model assessment. To simplify the presentation of these processes I describe two overarching objectives here. My first objective is to test the performance of the combined model relative to each model alone using measurements of heterotrophic respiration in a mid-latitude forest located in central Massachusetts, USA. My second objective is to apply the combined model to theoretical concepts such as the response of microbial activity to varying ratios of C and N substrate additions, and global-change-inspired perturbations to mean annual temperature and soil moisture. To link these modeling activities to my prior research on belowground C allocation and rhizosphere processes, I hypothesize that forest stands characterized by a high C-to-N ratio [litter, root inputs, microbial biomass] will have lower C efflux rates, and store more soil C than narrow C:N stands (Averill *et al.*, 2014). My second hypothesis is that warming will increase C efflux, but that added

soil moisture will not increase microbial activity as a result of the cancellation of a positive effect on C supply and a negative effect on O₂ supply.

Methods

Model description

The DAMM-MCNIp model is a parsimonious belowground C and N model with core processes-level representation of microbial and exoenzymatic activity. This model was developed from the merger of the Dual-Arrhenius Michaelis Menten (DAMM) model of Davidson *et al.* (2012) with the Microbial Carbon and Nitrogen Physiology (MCNIp) model of Finzi *et al.* (2015). DAMM explicitly simulates the effects of temperature, soil moisture and substrate supply on the kinetics of soil organic matter (SOM) depolymerization. Outputs of the MCNIp model include microbial maintenance respiration, biomass production, exoenzyme production, and C and N uptake and mineralization.

Soil temperature and moisture inputs constrain the rate of unprotected SOM depolymerization and uptake of dissolved organic matter, including carbon and nitrogen (DOM) to the microbial biomass pool. Microbes depolymerize SOM and take up DOM according to Arrhenius and Michaelis-Menten kinetics. Further, SOM availability is limited by soil moisture according to DAMM principles of substrate diffusion, and DOM uptake is limited by soil moisture via O₂ availability. Microbes allocate C to maintenance respiration, enzyme production, growth, and overflow C and N mineralization. Enzyme production and growth are dependent on the C:N ratio of the DOM taken up, as well as the carbon use efficiency of microbial metabolism. Microbial biomass and enzymes turn

over at a constant rate, and this carbon is partitioned to SOM and DOM pools (Figure 5.1).

In DAMM-MCNiP, a series of differential equations determines the change in each pool size at each time step. The change in the soluble C and N pool is modeled as:

$$dDOC/dt = inputDOC + DEPOLY_C + DEATH * (1 - MIC_C to SOM_C) + (CNe/(1+CNe)) + ELOSS_C - UPT_C \quad [1]$$

$$dDON/dt = inputDON + DEPOLY_N + DEATH * (1 - MIC_N to SOM_N) + (1/CNe) + ELOSS_N - UPT_N \quad [2]$$

where $dDOM/dt$ is the change in the DOM pool size, $inputDOM$ is the root input [exudation, turnover], $DEPOLY$ is the depolymerization rate of SOM, $DEATH$ is microbial turnover, $MIC to SOM$ is the fraction of dead microbial biomass C or N returned to the SOM pool, CNe is the C:N ratio of exoenzymes, $ELOSS$ is the enzyme turnover rate, and UPT is the rate of DOM uptake by the microbial biomass pool.

Depolymerization rate is modeled as:

$$DEPOLY_C = Vmax_C * a * Enz * avail_SOC / (Km_C + avail_SOC) \quad [3]$$

$$DEPOLY_N = Vmax_N * (1-a) * Enz * avail_SON / (Km_N + avail_SON) \quad [4]$$

where $Vmax$ is the maximum reaction rate when the enzyme is saturated with substrate, a is the proportion of the enzyme pool acting on the SOC pool (i.e., $1-a$ is the proportion acting on the SON pool), Enz is the enzyme pool size, $avail_SOM$ is unprotected SOM, and Km is the half-saturation constant for depolymerization.

Unprotected SOM and $Vmax$ are modeled as:

$$avail_SOM = SOM * frac * Dliq * soilM^3 \quad [5]$$

$$Vmax_{C,N} = A_{C,N} * \exp(-Ea_{C,N} / RT) \quad [6]$$

where $frac$ is the fraction of unprotected SOM, using soluble substrate estimated from Magill *et al.* (2000), D_{liq} is the diffusion coefficient for unprotected SOM in liquid, $soilM$ is the volumetric water content, A is the pre-exponential constant for SOM depolymerization, E_a is the activation energy for SOM depolymerization, R is the universal gas constant, and T is temperature.

Microbial biomass is modeled as:

$$dMIC_C / dt = CNm * GROWTH - DEATH_C \quad [7]$$

$$dMIC_N / dt = GROWTH - DEATH_N \quad [8]$$

where MIC is the microbial biomass, CNm is the C:N ratio of microbial biomass, and $GROWTH$ is microbial biomass growth, and:

$$GROWTH = ((1-p) * UPT_C * CUE + Enz_C - CNe * EPROD) / CNm \quad [C \text{ limited}] \quad [9]$$

$$GROWTH = (1-q) * UPT_N * Enz_N - EPROD \quad [N \text{ limited}] \quad [10]$$

$$DEATH = r_{death} * Mi_{C_N} \quad [11]$$

where p and q are the proportion of assimilated C or N, respectively, allocated to enzyme production, CUE is carbon use efficiency, $EPROD$ is enzyme production, and r_{death} is the microbial turnover rate.

Microbial uptake is defined as:

$$UPT_{C_N} = Mi_{C_N} * Vmax_{upt_{C_N}} * DOC_N / (Km_{upt_{C_N}} + DOC_N) * O_2 / (Km_{O_2} + O_2) \quad [12]$$

where $Vmax_{upt}$ and Km_{upt} are the maximum reaction rate and half-saturation constants for uptake, respectively. O_2 is the oxygen concentration and Km_{O_2} is the half-saturation constant for O_2 as a substrate. $Vmax_{upt}$ and O_2 are determined by:

$$Vmax_{upt_{C_N}} = A_{upt_{C_N}} * \exp(-E_{a_{upt_{C_N}}} / RT) \quad [13]$$

$$O_2 = D_{gas} * O_{2airfrac} * [(porosity - soilM)^{4/3}] \quad [14]$$

$$porosity = 1 - BD/PD \quad [15]$$

where A_{upt} is the pre-exponential constant for DOC uptake, Ea_{upt} is the activation energy for DOC uptake, D_{gas} is the diffusion coefficient for O₂ in air, $O_{2airfrac}$ is the volume fraction of O₂ air, BD is bulk density and PD is particle density of the soil.

Enzyme production can be C or N limited depending on the stoichiometry of the DOM taken up:

$$EPROD = p * (CUE * UPT_C) / CNe \quad [C \text{ limited}] \quad [16]$$

$$EPROD = q * UPT_N \quad [N \text{ limited}] \quad [17]$$

C mineralization, overflow C, and N mineralization are modeled as:

$$CMIN = UPT_C * (1 - CUE) \quad [18]$$

$$NMIN = GROWTH_N - GROWTH \quad [19]$$

$$OverflowC = GROWTH_C - CNm * GROWTH \quad [20]$$

The enzyme pool is a balance between production and turnover, defined as a first order process:

$$dEnz/dt = EPROD - ELOSS \quad [21]$$

$$ELOSS = r_{enzloss} * Enz \quad [22]$$

where $r_{enzloss}$ is the enzyme turnover rate.

Lastly, the change in the SOM pool is modeled as:

$$dSOM_{C,N}/dt = Litter_{C,N} + DEATH * MIC_{C,N} to SOM_{C,N} - DEPOLY_{C,N} \quad [23]$$

where $Litter_{C,N}$ is the litter input to the SOC pool.

Inputs to the model include litter and root exudate C and N, temperature and soil moisture. Outputs used in this study are the rate of C mineralization (i.e., C efflux) and N mineralization. Litter (leaf, root) is partitioned to SOM and DOM pools at each timestep (h^{-1}). Root exudates enter the DOM pool only.

Model parameters were identical to original DAMM and MCNiP parameters, excepting the following: A_{uptC_N} , Ea_{uptC_N} , A_{C_N} , Ea_{C_N} , Km_{C_N} . I estimated A_{uptC_N} , Ea_{uptC_N} , A_{C_N} , and Ea_{C_N} from independent measurements of β -glucosidase activity from organic and mineral soil (Davidson *et al.*, 2012, Finzi *et al.*, 2015). Because I cannot experimentally distinguish between depolymerization kinetics and uptake kinetics, each pair of A and Ea values are identical. Km_{C_N} was estimated such that at standard temperature, 293 K (20°C), and the mean soil moisture value for this site, $0.229 \text{ cm}^3 \text{ H}_2\text{O cm}^{-3}$ soil, Km_{C_N} was equal to the initial available substrate SOM concentration (sensu Davidson *et al.*, 2012). In contrast to Allison *et al.* (2010) and MCNiP, I did not choose a Km larger than the available SOM pool. Microbes in MCNiP have access to the entire SOM pool, so without a Km value that is high relative to the SOM pool size, substrate will always be saturating. My parameterization allows for substrate to saturate a reaction site, for example, if substrate is temporarily mobilized during a wet-up event (Birch, 1958, Davidson *et al.*, 2014). Model parameters are found in Table 5.1.

Model parameters in MCNiP are based on Allison *et al.* (2010). One exception is the C:N of soil, taken from Schimel and Weintraub (2003). Default initial pool sizes were determined after model spin up for 2000 years using spin up parameters from Allison *et al.* (2010) for the C pool. The N pool was parameterized using the following principles,

SON = SOC/27.6 [C:N ratio of soil], DON = DOC/15 [mid-range of DOC:DON from Hopkinson *et al.* (1997) and Neff & Hooper (2002)], microbial biomass N = microbial biomass C/10 [C:N ratio of microbes]. For the default model, I assume that litter and root inputs have C:N of 27.6 (Table 5.2).

Model comparison

I compared model performance of the DAMM-MCNiP model against three other models, DAMM alone, MCNiP alone, and DAMM-MCP (without any mechanistic linkage between C and N cycling). DAMM parameters are from Davidson *et al.* (2012). MCNiP's enzyme kinetic parameters, A_{uptC_N} , $E_{\text{a}_{\text{uptC}_N}}$, A_{C_N} , $E_{\text{a}_{\text{C}_N}}$, $K_{\text{m}_{\text{C}_N}}$ and initial values were parameterized as in Finzi *et al.* (2015). DAMM-MCNiP and DAMM-MCP have identical parameter values (Table 5.1). In DAMM-MCP, N limitation is not possible because I removed the conditional statements that determine whether or not the system is N-limited. As a result, C dynamics control the model and N pools follow C pools according to stoichiometry. I ran DAMM and MCNiP for one year. I ran DAMM-MCNiP and DAMM-MCP for 200 years to achieve stable efflux values.

To test model performance, I used measurements of soil temperature, moisture, and C efflux from a trenching experiment at Harvard Forest, MA. A 5 x 5 m trench was dug to 1 m depth in November 2008 in a mixed hardwood stand on the Prospect Hill tract of Harvard Forest. Automated measurements of C efflux were collected from April through October 2009. I used C efflux from trenched plots as an estimate of heterotrophic respiration. This dataset is described in greater detail in Davidson *et al.* (2012).

Linear regression was used to fit the output predicted by each model with C efflux measurements from trenching, and to fit model-predicted N mineralization with soil moisture measurements. I computed the correlation coefficient (Pearson's ρ) between model-predicted C efflux and temperature or soil moisture. All analyses were conducted in R Statistical Software (R Development Core Team, 2013).

Root input measurements

Root C inputs were measured in three stands at Harvard Forest, white ash (*Fraxinus americana*), red oak (*Quercus rubra*), and eastern hemlock (*Tsuga canadensis*). Root exudates were collected from six root systems per stand in June and August of 2012, and April, May, July and October of 2013 following the method of Phillips *et al.* (2008, 2011). Root turnover was measured April–December 2012, March–November 2013, and April–November 2014 in ten minirhizotron tubes per stand using a BTC-100x high magnification minirhizotron camera system (Bartz Technology Company, Carpinteria, CA). I averaged across the three stands and across replicate samples to determine the base rate of root input, $120 \text{ g C m}^{-2} \text{ yr}^{-1}$, which was comprised of an exudation ($102 \text{ g C m}^{-2} \text{ yr}^{-1}$) and root turnover ($18 \text{ g C m}^{-2} \text{ yr}^{-1}$) flux component. I assume that exudation occurs primarily during the growing season and follows a unimodal Gaussian distribution with a standard deviation of 42 days. I used this root input rate and phenology for the following simulations that manipulate C:N, temperature, and soil moisture.

Model simulation of microbial physiology response to C:N ratio

I conducted model simulations of DAMM-MCNIp that test the importance of stand-level differences in C:N on microbial physiology. C and N mineralization was simulated in two theoretical forests differing in their litter, root input, and microbial biomass C:N, based on ranges reported in literature for an arbuscular-mycorrhizal hardwood stand where decomposition is dominated by bacteria (herein Narrow C:N), and an ectomycorrhizal conifer stand where decomposition is dominated by fungi (herein Wide C:N; Table 5.3). In order to compare the effects of varying input and microbial C:N, I conducted three tests. First, I ran the model using either high or low values of litter and root input C:N. Second, I ran the model using high or low values of microbial biomass C:N. Finally, I varied both input and biomass C:N (Table 5.3).

To determine the effect of root input C:N on depolymerization and microbial efficiency, I varied root input C:N between 1 and 100 and recorded the SOC pool size at different quantities of root input and root input C:N. I used the ratio of depolymerization rate to microbial biomass as a measure of microbial efficiency.

Model simulations of global change

In order to estimate the effect of global change on annual C and N efflux, I perturbed the temperature and soil moisture inputs for the last year of each model run of DAMM-MCNIp. First, I increased and decreased the temperature at each time point by 5°C. Second, using ambient temperature forcing, I increased and decreased soil moisture at each time point by 50%. I calculated the absolute difference between each temperature

and soil moisture treatment relative to ambient, and cumulatively summed the C or N efflux over the year.

Results

Model comparison

From a visual inspection of the model output, DAMM captures the seasonality of measured C efflux well, though it slightly over-predicts C efflux during mid-summer (DOY 220-250), and under-predicts efflux during large precipitation events (e.g., DOY 170, 240; Figure 5.2a). The RMSE of the correlation between DAMM and measured C efflux is 31.7 ($\beta = 0.85$, $F_{1,2903} = 3102$, $P < 0.001$, $R^2_{\text{adj}} = 0.52$; Figure 5.3a). MCNiP has an RMSE of 7.6 with little change in amplitude between summer and winter efflux (Figure 5.2b). The slope (β) of the relationship between MCNiP and measured efflux is lower than 1 ($\beta = 0.20$, $F_{1,2965} = 2998$, $P < 0.001$, $R^2_{\text{adj}} = 0.50$; Figure 5.3b). The RMSE of DAMM-MC NiP is 26.7, and is lower than that of DAMM. The slope of the relationship between predicted and measured efflux for DAMM-MC NiP is lower than 1, but higher than MC NiP ($\beta = 0.59$, $F_{1,2965} = 2156$, $P < 0.001$, $R^2_{\text{adj}} = 0.42$; Figure 5.3c). DAMM-MCP lacks any linkage to the N cycle, and has an RMSE of 25.9 ($\beta = 0.57$, $F_{1,2965} = 2096$, $P < 0.001$, $R^2_{\text{adj}} = 0.41$; Figure 5.3d).

DAMM-MC NiP model residuals indicate that DAMM-MC NiP slightly over-predicts C efflux across the range of soil moisture values and under-predicts some C efflux values between 0.3 and 0.5 $\text{cm}^3 \text{H}_2\text{O cm}^{-3}$ soil (Figure 5.4a). DAMM alone over-predicts C efflux at low and high soil moisture values and under-predicts C efflux between 0.3 and 0.5 $\text{cm}^3 \text{H}_2\text{O cm}^{-3}$ soil (Figure 5.4b). At soil moisture values $> 0.68 \text{ cm}^3$

$\text{H}_2\text{O cm}^{-3}$ soil, DAMM cannot solve for a C efflux value, because soil pores are completely filled with water. In DAMM-MCNIp, however, I implemented a drainage subroutine that allows water to exit soil pores, alleviating the mathematical impossibility of having more water in the soil than available pore space.

DAMM is more strongly correlated with temperature ($\rho = 0.90$) than soil moisture ($\rho = 0.15$). DAMM-MCNIp is correlated with temperature ($\rho = 0.69$) and soil moisture ($\rho = 0.33$). In DAMM-MCNIp, the seasonal pattern of temperature and soil moisture is similar to the pattern of depolymerization rate, C uptake rate, C mineralization rate and the size of DOC pool (Figure 5.5a,b,e,f,g,j). The phenology of the SOC pool is opposite that of the microbial biomass and enzyme C pools, such that SOC is most depleted (i.e., DOY 250) when the microbial biomass pool reaches its annual peak (Figure 5.5i,k,l). N mineralization is not confined to the growing season and has a significant negative relationship with soil moisture ($F_{1,4559} = 925$, $P < 0.001$, $R^2_{\text{adj}} = 0.17$; Figure 5.5b,d). Overflow C is the release of excess C from microbes after allocation to maintenance respiration, enzyme production, and biomass growth. Overflow C is an intermittent flux that only occurs when all available N is immobilized (i.e., when N mineralization is low or absent; Figure 5.5h; Figure 5.6).

Model simulation of microbial physiology response to C:N

The theoretical Narrow C:N stand had higher C and N mineralization rates compared to the Wide C:N stand, by $12 \text{ g C m}^{-2} \text{ yr}^{-1}$ and $0.9 \text{ g N m}^{-2} \text{ yr}^{-1}$, respectively. When input C:N was changed from default settings but microbial biomass C:N was held constant, the Narrow C:N stand mineralized $27 \text{ g C m}^{-2} \text{ yr}^{-1}$ and $1.4 \text{ g N m}^{-2} \text{ yr}^{-1}$ more than

the Wide C:N stand (Figure 5.7a,d). In contrast, the Wide C:N stand had higher C and N mineralization by $12 \text{ g C m}^{-2} \text{ yr}^{-1}$ and $0.9 \text{ g N m}^{-2} \text{ yr}^{-1}$, respectively, when only microbial biomass C:N was changed from default settings (Figure 5.7b,e). As a result, the difference in C and N mineralization between the Wide and Narrow C:N stands was small when both input and microbial biomass C:N were varied (Figure 5.7c,f; Table 5.3).

SOC depolymerization increased with the magnitude of root input to the DOC pool, depleting the SOC pool. This effect appeared to exhibit asymptotic behavior at high values of exudate inputs. Low root input C:N resulted in more depolymerization than high input C:N (Figure 5.8a). At low C:N, there was an increase in microbial efficiency with root inputs (Figure 5.8b, red line). At high C:N, SOC was depleted as a result of an increase in microbial biomass (Figure 5.8c).

Model simulations of global change

A 5°C warming of seasonal temperature inputs increased C efflux by $119 \text{ g C m}^{-2} \text{ yr}^{-1}$. An equivalent decrease in ambient temperature caused C efflux to fall by $71 \text{ g C m}^{-2} \text{ yr}^{-1}$ (Table 5.4; Figure 5.9a). N mineralization increased by $0.37 \text{ g N m}^{-2} \text{ yr}^{-1}$ with warming and decreased $0.32 \text{ g N m}^{-2} \text{ yr}^{-1}$ with cooling (Figure 5.9b).

A 50% increase in seasonal soil moisture caused a large increase in C ($220 \text{ g C m}^{-2} \text{ yr}^{-1}$) efflux and a smaller increase in N mineralization ($0.9 \text{ g C m}^{-2} \text{ yr}^{-1}$), while a 50% decrease in soil moisture decreased C efflux by $156 \text{ g C m}^{-2} \text{ yr}^{-1}$ and N mineralization by $0.21 \text{ g N m}^{-2} \text{ yr}^{-1}$ (Figure 5.9c,d). There were also large changes in the seasonal pattern of N mineralization, with more variation in the wet treatment compared to the dry treatment (Figure 5.9d). The absolute difference in C efflux in the warming and added soil moisture

treatments were greater than the reduced temperature and soil moisture treatments, but the effect of each treatment was similar for N mineralization (Figure 5.10). Cumulative sums of mineralization measured over the growing season demonstrate that temperature and soil moisture treatments had a larger effect on annual C efflux than on N mineralization (Figure 5.11). In addition, N mineralization in the dry treatment exceeded both ambient and wet treatments for large portions of the year (Figure 5.10d, 5.11d).

Discussion

As currently parameterized, DAMM-MCNIp predicts realistic C efflux during transient wet-up events (Figure 5.4a), an area where many present-day models struggle to represent the increase in C efflux with soil moisture (Ise & Moorcroft, 2006, Rodrigo *et al.*, 1997). However, DAMM-MCNIp over-predicts C efflux in constant high soil moisture conditions. DAMM-MCNIp produces realistic responses to temperature perturbation, and thus may be useful for investigating the interaction between substrate and temperature controls on microbial activity. Consistent with hypothesis 1, model predictions of SOM decomposition in response to variable C:N inputs show that N-rich root exudates increase the decomposition rate of SOM and that wide C:N stands store more C than narrow C:N stands (Averill *et al.*, 2014).

Model comparison

DAMM alone captures the seasonality of C efflux. The slope of the C efflux predicted by DAMM plotted against measured C efflux is the closest to 1 of the four models. However, DAMM parameters were fit to these data using parameter optimization, and therefore it is not surprising that model bias is low. The RMSE of

DAMM, however, is highest of the four models. In contrast, MCNiP alone has the lowest RMSE of the four models, but does not capture the observed seasonal pattern of C efflux, with the slope between observed and predicted efflux equal to 0.2. This indicates that while MCNiP has high precision, alone it has low predictive accuracy. In contrast to DAMM, MCNiP is currently parameterized from literature values as a theoretical model, and has not been previously fit to data (Allison *et al.*, 2010, Schimel & Weintraub, 2003). That it performs as well as it does is notable.

Together, DAMM and MCNiP capture the seasonal cycle of soil C efflux. Though the RMSE of DAMM-MCNiP is much higher than that of MCNiP, DAMM-MCNiP has the ability to predict realistic seasonal patterns in response to fluctuations in temperature and soil moisture. That is, the slope of the predicted compared to observed efflux is closer to 1 for DAMM-MCNiP compared to MCNiP.

The correlation coefficients between C efflux predicted by DAMM and temperature ($\rho = 0.90$) or soil moisture ($\rho = 0.15$) indicate that DAMM alone is more sensitive to temperature than to soil moisture. DAMM-MCNiP is relatively more sensitive to soil moisture ($\rho = 0.33$) than is DAMM. As a result, DAMM-MCNiP successfully predicts the large increase in C efflux after wet-up events, which DAMM alone cannot recreate.

The major benefit of DAMM-MCNiP in comparison to DAMM and MCNiP alone is the process-level representation of microbial physiology coupled with the ability to represent substrate availability at the micro-site scale. Another benefit is the coupling of the C and N cycle, which allows for investigation into nutrient limitation and priming

effects. Although, DAMM-MCP is decoupled from the N cycle, model performance is similar to DAMM-MCNiP [slightly lower RMSE and slope], though the lack of a N cycle limits its utility. The fact that it does perform as well as DAMM-MCNiP suggests the need to assess both models against other datasets. The stoichiometric coupling in DAMM-MCNiP may also benefit from data-model assimilation using Harvard Forest datasets, modifications to the model's core structure, or both.

From a visual inspection of the model inputs, pools and fluxes, it is clear that temperature and soil moisture together determine the rate of depolymerization, which then constrains the DOC pool, C uptake, and C efflux (Figure 5.5e,f,g). N mineralization occurs throughout the growing season, and is negatively correlated with soil moisture. Overflow C occurs when the system is N-limited, and as a result overflow C and N mineralization are nearly mutually exclusive (Figure 5.6). This is an important model diagnostic which demonstrates that the coupling of C and N in the model is working properly.

Model simulation of microbial physiology response to C:N

When I narrowed the C:N ratio of root inputs and microbial biomass, I observed a small increase in the amounts of C and N mineralized, supporting my first hypothesis that stands with narrow C:N will have higher C efflux rates (Figure 5.7). This response to low C:N is consistent with my understanding of priming based on MCNiP (Finzi *et al.*, 2015) and related models (Drake *et al.*, 2013), where adding N increased C efflux and SOM decomposition (Figure 5.8a).

The mechanism by which more SOM is decomposed with added exudates at root C:N > 3 is an increase in microbial biomass rather than an increase in microbial efficiency (Figure 5.8b,c). This understanding of priming is not necessarily counter to findings that suggest that low N inputs stimulate foraging for N by inducing N limitation (Craine *et al.*, 2007). Adding more N to the system supports a larger microbial biomass, but these microbes can still be N limited, since the C:N of litter and root inputs is still higher than the C:N of microbial biomass (Table 5.3).

When only microbial biomass C:N was varied, the wide C:N stand predicted a slightly higher C efflux than the narrow C:N stand, because microbial biomass with high C:N is more closely matched to the C:N of litter and root inputs. Varying input and microbial biomass C:N together does not change the overall C efflux by a large amount, consistent with idea that microbial activity is limited by the stoichiometry of its substrate (Sinsabaugh *et al.*, 2009).

Model simulations of global change

Warming seasonal temperatures by 5°C increased C efflux by about 55%, supporting the first part of the second hypothesis that warming increases heterotrophic respiration. C efflux increased ~50% from cold to ambient treatments, suggesting that the temperature response to 5°C warming is consistent regardless of the starting temperature. A 50 – 55% increase in heterotrophic respiration with warming was greater than the observed increase in total soil CO₂ efflux in response to 5°C warming in two studies at the Harvard Forest by 11 and 27% (Contosta, 2011, Melillo *et al.*, 2002). Soil warming in the field usually dries the soil along with heating, which may account for the smaller

increase in C efflux observed in the field. In fact, when I simultaneously warmed the soil by 5°C and decreased soil moisture by 10%, which corresponds to the amount of drying observed by Contosta *et al.* (2011) in the soil organic horizon, I predicted an increase in C efflux increase of only 17% over ambient conditions (Figure 5.12).

Warming and cooling treatments had similar effects on N mineralization (Figure 5.10b), with a slightly positive effect of warming, but many instances over the growing season where N mineralization decreased with additional warming. At the seasonal time-scale, N mineralization was not very sensitive to temperature with perhaps marginally more N mineralization during the growing season, so it is not surprising that at the annual time-scale, an increase in temperature also had a small effect on N mineralization.

In contrast to the second part of hypothesis 2, soil moisture manipulations had a larger effect on C efflux than did either warming or cooling. I hypothesized that a 50% increase in soil moisture would have a relatively small positive effect, because the increase in diffusive transport of substrates would be moderated by O₂ limitation. However, I found that O₂ limitation had a small effect relative to diffusion because C efflux was strongly stimulated in the 1.5x soil moisture treatment and strongly limited in the 0.5x soil moisture treatment. Suseela *et al.* (2012) found that heterotrophic respiration was reduced in a mesic suburban old-field site when volumetric soil moisture was outside of a 15-26% window. Davidson *et al.* (1998) found high soil respiration at similar volumetric soil moisture values. The mean volumetric soil moisture for the dry and wet treatments in the simulation was outside of this window (15% and 41%, respectively), suggesting that DAMM-MCNiP may overestimate C efflux at high soil moisture values.

Soil moisture manipulations had a large impact on N mineralization. At low soil moisture, N mineralization had a lower coefficient of variation ($CV = 0.41$) over the growing season than it had at ambient ($CV = 0.96$) or added soil moisture ($CV = 1.1$; Figure 5.9d). During dry conditions there is little substrate available for depolymerization and microbial uptake. Because substrate supply is low throughout the growing season, this limits the rate N mineralization. Conversely, when substrate is plentiful during wet conditions, N mineralization is widely variable depending upon whether microbial growth is C or N limited. Since the wet treatment resulted in a large pool of available SOC, I expected that N mineralization would decrease because microbial growth becomes N limited. This was not the case, however, because there were many time periods throughout the simulation when microbial growth was C limited (Figure 5.10d). This suggests that the model may be operating under greater C limitation than expected.

Summary

The DAMM-MCNIp model is a parsimonious model that simulates decomposition and C and N mineralization using process-level representation of microbial physiology and stoichiometry. It is one of the first microbial physiology models that can represent the C and N cycle together with plant substrate supply, making DAMM-MCNIp a candidate for linkage with terrestrial biosphere models that allocate a fraction of fixed C belowground at each time-step. The model inputs are similar to CENTURY (i.e., soil temperature, moisture, C and N), but rather than combining temperature and soil moisture effects into a linear decomposition factor, DAMM-MCNIp

explicitly models the processes by which temperature and moisture affect substrate availability and enzyme kinetics (Bolker *et al.*, 1998).

DAMM-MCNI_P requires parameter estimation and sensitivity analyses beyond those performed here (i.e., by varying C:N, soil temperature and soil moisture) in order to reproduce measured C efflux without bias. Future work will focus on parameterizing DAMM-MCNI_P using Bayesian data assimilation, first at the Harvard Forest in Petersham, MA and then at other sites. I will nest parameter value estimates and their associated uncertainty at each site using a hierarchical framework that can then estimate broader regional-scale parameters. A broadly parameterized microbial physiology model such as DAMM-MCNI_P may improve terrestrial biosphere model predictions of SOC pools under global change.

Table 5.1. DAMM-MCNiP default model parameter values.

Parameter	Units	Default Value	Description
rootDOC	mg cm ⁻³	input	Root exudates
T	K	input	temperature in Kelvin
θ	cm ³ H ₂ O cm ⁻³ soil	input	volumetric water content
BD	g cm ⁻³	0.8	bulk density
PD	g cm ⁻³	2.52	particle density
O_{2airfrac}	L O ₂ / L air	0.209	volume fraction of O ₂ air
frac	g C cm ⁻³ / g C cm ⁻³	0.000414	fraction of unprotected SOM, using soluble substrate estimated from Magill et al., 2000
D_{liq}	-	3.17	diffusion coefficient for unprotected SOM and DOM in liquid
D_{gas}	-	1.67	diffusion coefficient for O ₂ in air
K_{mO₂}	cm ³ O ₂ cm ⁻³ air	0.121	Michaelis constant for O ₂
R	kJ K ⁻¹ mol ⁻¹	0.0083145	universal gas constant
endTime	h	2000000	number of hours simulated in model run
p	-	0.5	proportion of assimilated C allocated to enzyme production
q	-	0.5	proportion of assimilated N allocated to enzyme production
a	-	0.5	proportion of enzyme pool acting on SOC pool (1-a = proportion acting on SON pool)
initSOC	mg cm ⁻³	144.5986	initial SOC pool
initSON	mg cm ⁻³	5.4413	initial SON pool
initDOC	mg cm ⁻³	0.00091631	initial DOC pool
initDON	mg cm ⁻³	0.00049421	initial DON pool
initBiomassC	mg cm ⁻³	1.1957	initial microbial biomass C
initBiomassN	mg cm ⁻³	0.1196	initial microbial biomass N
Litter_{C_N}	mg cm ⁻³ hr ⁻¹	0.0005	litter input to SOC pool
LitterCN	mg cm ⁻³ hr ⁻¹	27.6	C:N of litter input to SOC pool
initEnz	mg cm ⁻³	0.0381	initial enzyme pool
inputDOC	mg cm ⁻³ hr ⁻¹	0.0005	root input to DOC pool
inputDOCN	mg cm ⁻³ hr ⁻¹	27.6	C:N of litter input to DOC pool
r_{death}	hr ⁻¹	0.00015	microbial turnover rate
r_{EnzLoss}	hr ⁻¹	0.001	enzyme turnover rate
MIC_{C_N}toSOC_{C_N}	mg mg ⁻¹	0.5	fraction of dead microbial biomass

Parameter	Units	Default Value	Description
A_{C_N}	mg SOM cm ⁻³ (mg Enz cm ⁻³) ⁻¹ h ⁻¹	1.0815*10 ¹¹	Pre-exponential constant for SOM depolymerization
A_{uptC_N}	mg DOC cm ⁻³ (mg biomass cm ⁻³) ⁻¹ h ⁻¹	1.0815*10 ¹¹	Pre-exponential constant for DOC uptake
Km_{C_N}	mg cm ⁻³	0.0025	Half-saturation constant for SOM depolymerization
Km_{uptC_N}	mg cm ⁻³	0.3	Half-saturation constant for DOC uptake
CUE	mg mg ⁻¹	0.31	Carbon use efficiency
Ea_{C_N}	kJ mol ⁻¹	61.77	Activation energy for SOM depolymerization
Ea_{uptC_N}	kJ mol ⁻¹	61.77	Activation energy for DOC uptake
CN_s	-	27.6	C:N of soil
CN_l	-	27.6	C:N of litter
CN_m	-	10	C:N of microbial biomass
CN_e	-	3	C:N of enzymes
CN_{ex}	-	27.6	C:N of root inputs

Table 5.2. Initial pool sizes (Spin Up) and the resulting default initial pool sizes (Default) after 2000 years of spin-up.

Parameter	Abbreviation	Units	Spin Up	Default
SOC pool	initSOC	mg cm ⁻³	100	144.5986
SON pool	initSON	mg cm ⁻³	3.6232	5.4413
DOC pool	initDOC	mg cm ⁻³	0.5	0.00091631
DON pool	initDON	mg cm ⁻³	0.0333	0.00049421
microbial biomass C	initBiomassC	mg cm ⁻³	0.5	1.1957
microbial biomass N	initBiomassN	mg cm ⁻³	0.05	0.1196
enzyme pool	initEnz	mg cm ⁻³	0.01	0.0325

Table 5.3. Parameter values for the C:N of litter, root inputs, and microbial biomass for two theoretical stands.

	Narrow C:N	Wide C:N	Reference
Litter input	50	100	Finzi <i>et al.</i> 2001
Root input	10	100	Drake <i>et al.</i> 2013, Finzi <i>et al.</i> 2015
Microbial biomass	6	12	Wallenstein <i>et al.</i> 2006, Bengtson <i>et al.</i> 2012

Table 5.4. Annual C and N mineralization predicted by DAMM-MCNP in four simulations that manipulate either temperature or soil moisture. Here θ refers to volumetric soil moisture.

	Ambient	+5°C	-5°C	1.5x θ	0.5x θ
C mineralization (g C m ⁻² yr ⁻¹)	217	337	146	437	61
N mineralization (g N m ⁻² yr ⁻¹)	2.9	3.2	2.5	3.7	2.6

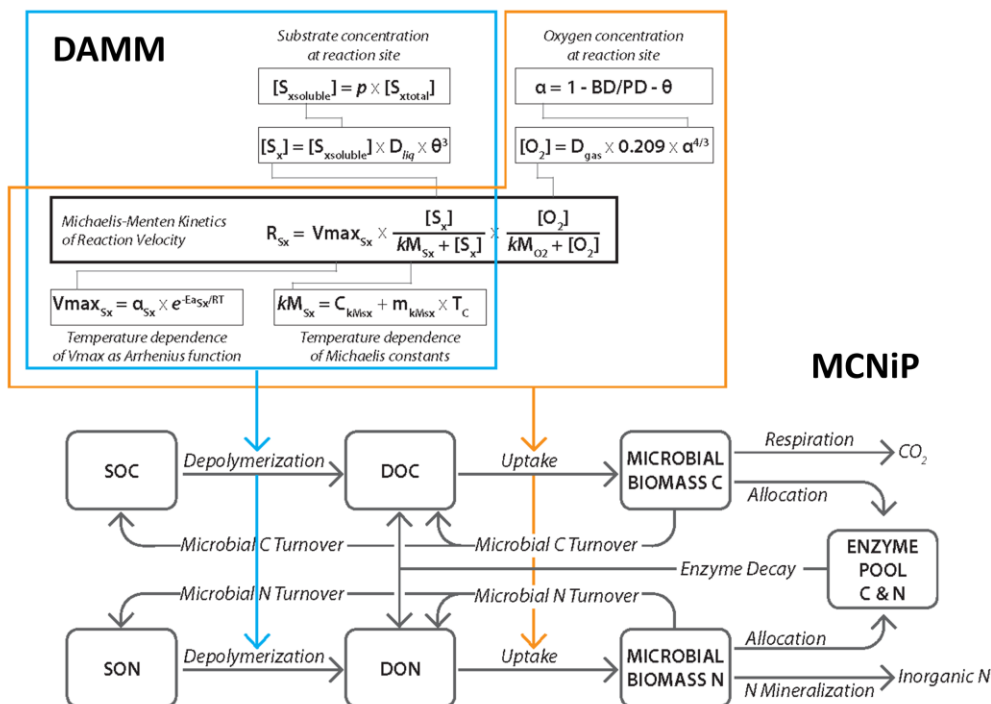


Figure 5.1. Conceptual figure of the merger of DAMM (blue and orange boxes) and MCNiP (box and arrow diagram). SOM depolymerization occurs using Arrhenius and Michaelis-Menten kinetics, substrate diffusion, and a temperature-dependent Vmax (blue box). I held Km constant for the model runs in this study, but a linear temperature-sensitivity relationship can be applied to it if desired. DOC uptake is controlled by DAMM kinetics as well as O_2 concentration at the reaction site (orange box; see Table 5.1 for DAMM equation parameter definitions). MCNiP has four pools: SOM, DOM, Microbial biomass, and Enzymes. Litter and root inputs enter the SOM and DOM pools, respectively, and outputs are CO_2 as a product of respiration and inorganic N as a product of N mineralization.

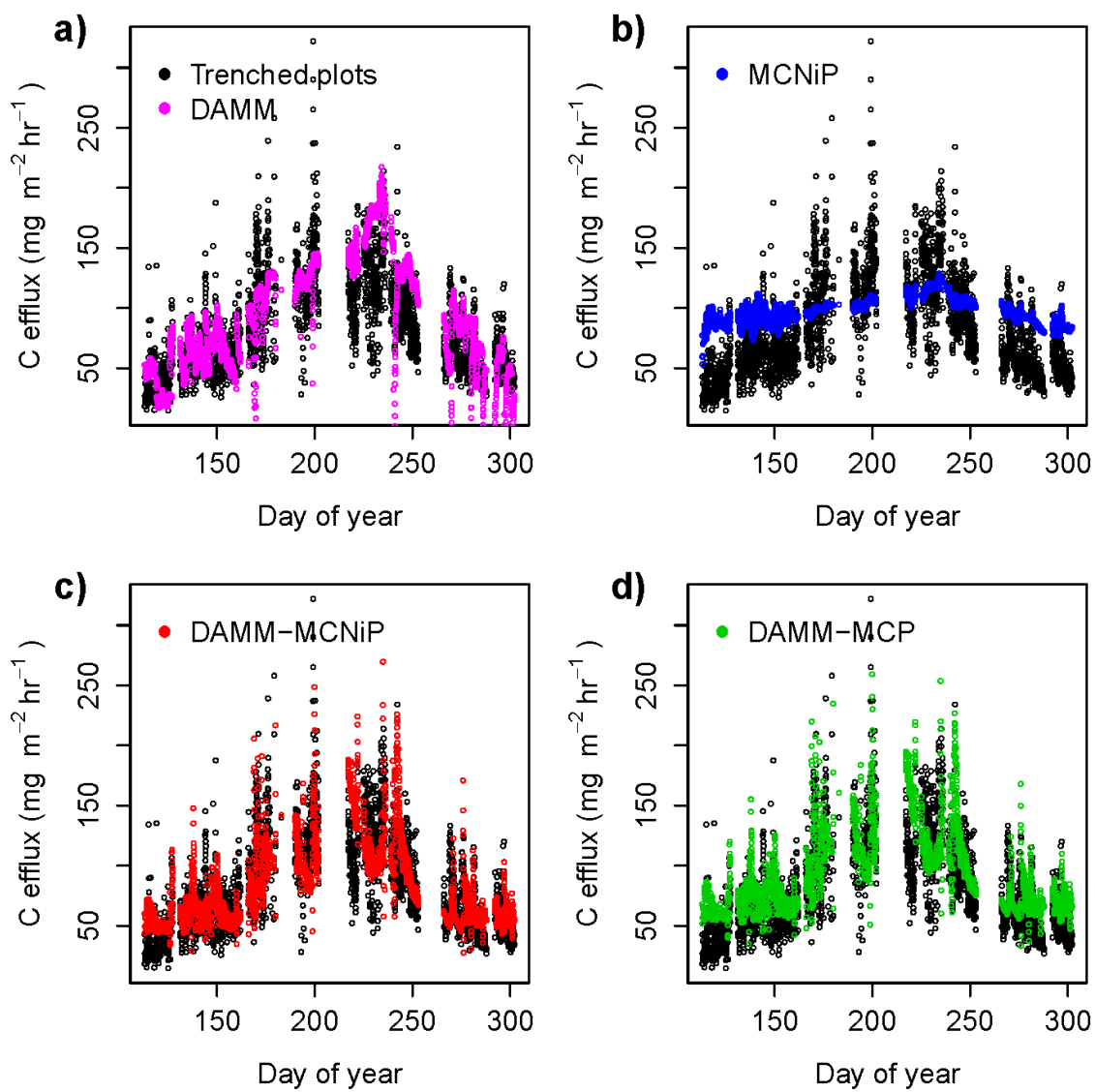


Figure 5.2. Model inter-comparison of (a) DAMM (pink), (b) MCNiP (blue), (c) DAMM-MCNiP (red), and (d) DAMM-MCP (green) overlaid on soil C efflux measurements from trenched plots in Harvard Forest, MA.

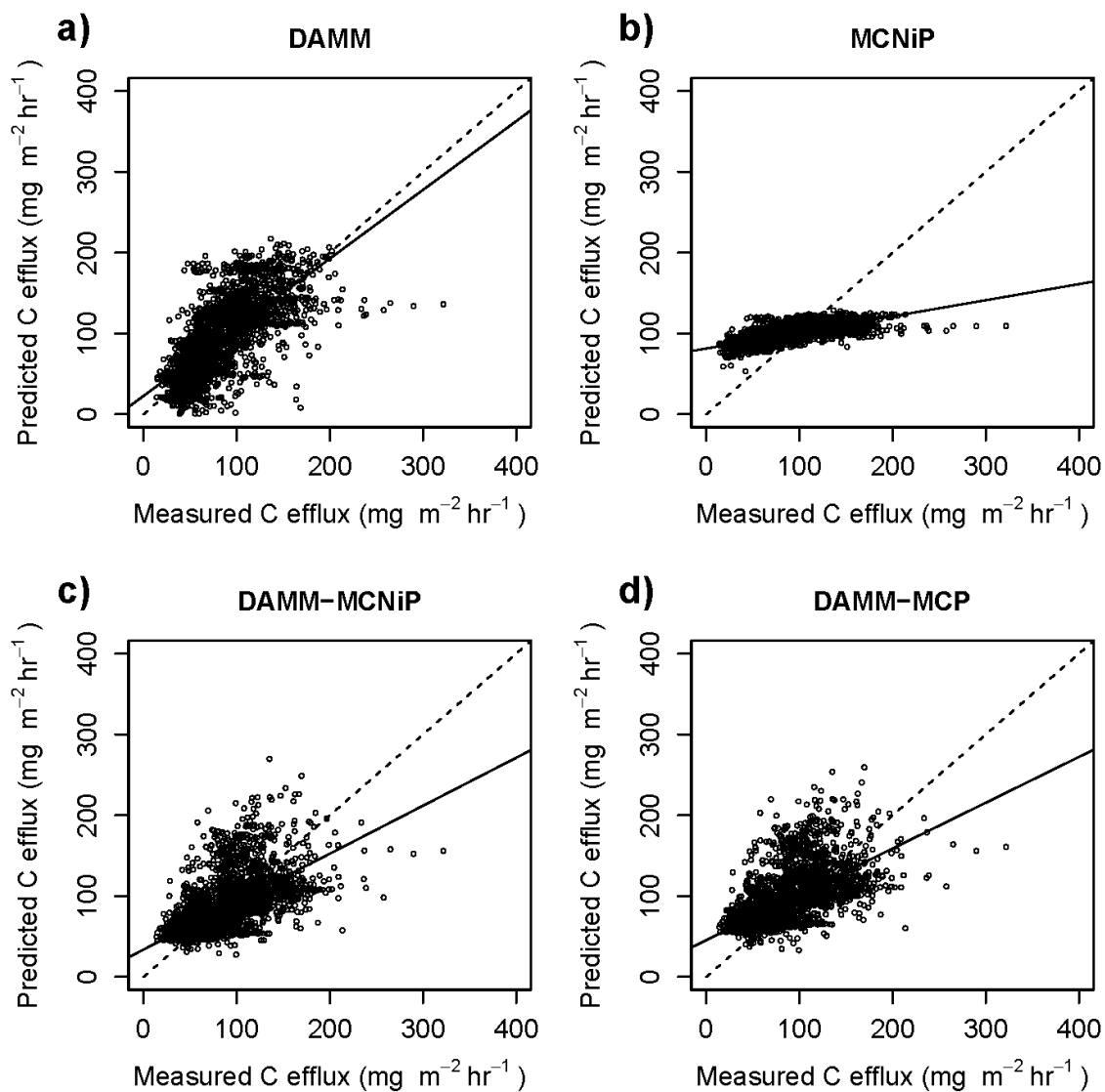


Figure 5.3. Relationship between predicted and measured C efflux for (a) DAMM, (b) MCNiP, (c) DAMM-MCniP, and (d) DAMM-MCP. The solid line is the regression fit, and the dotted line is the 1:1 line.

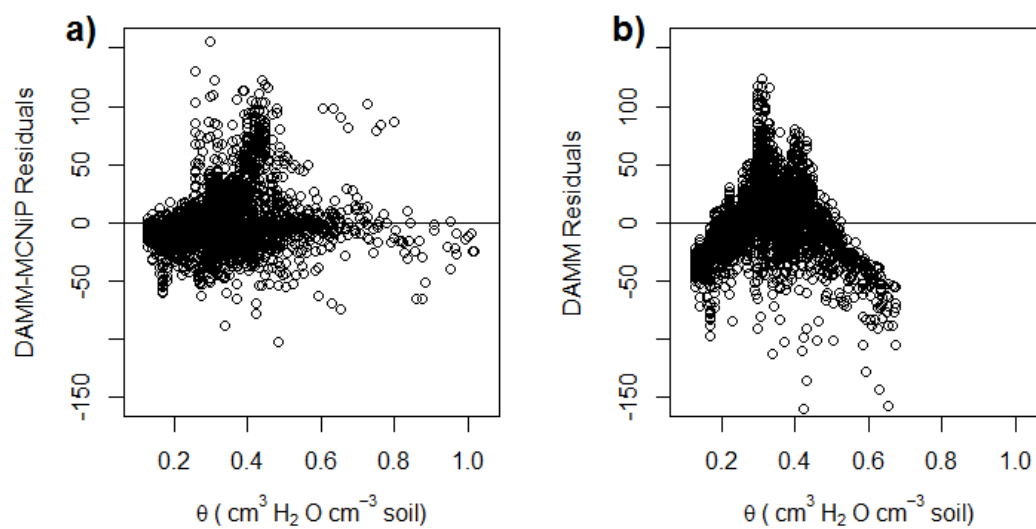


Figure 5.4. (a) DAMM-MCNiP and (b) DAMM model residuals plotted as a function of soil moisture (θ).

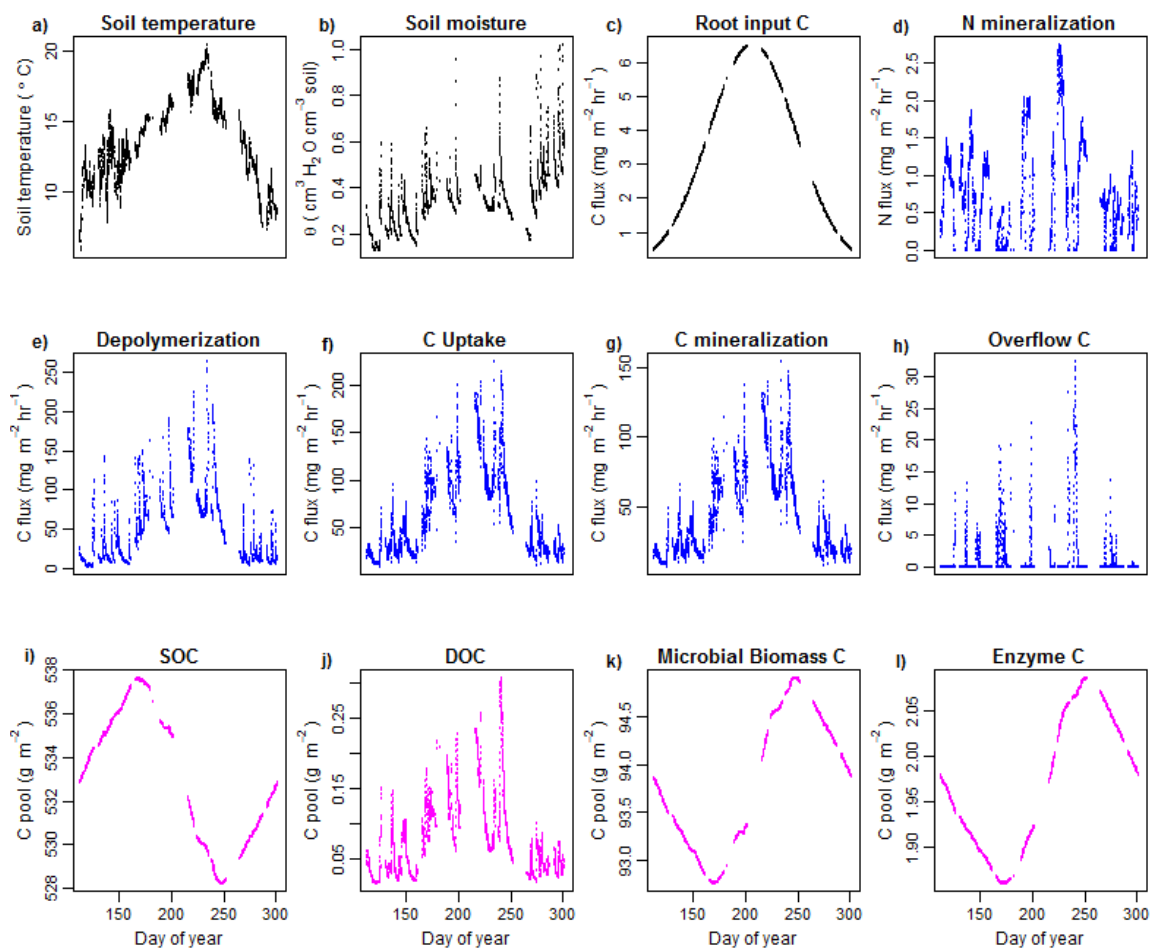


Figure 5.5. DAMM-MCNiP model inputs (black), fluxes (blue) and pools (pink).

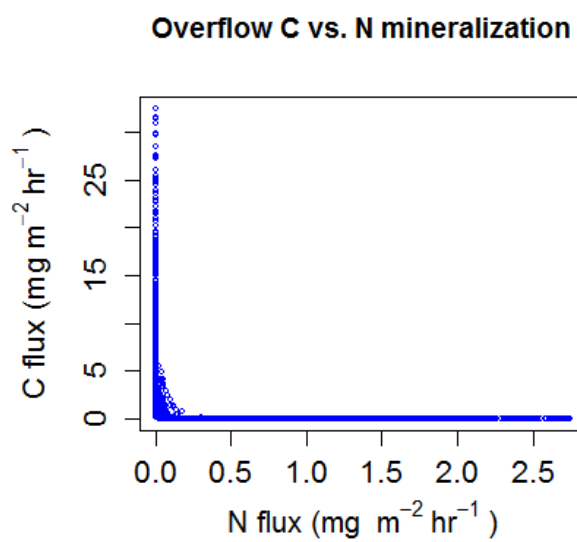


Figure 5.6. Plot of overflow C as a function of N mineralization.

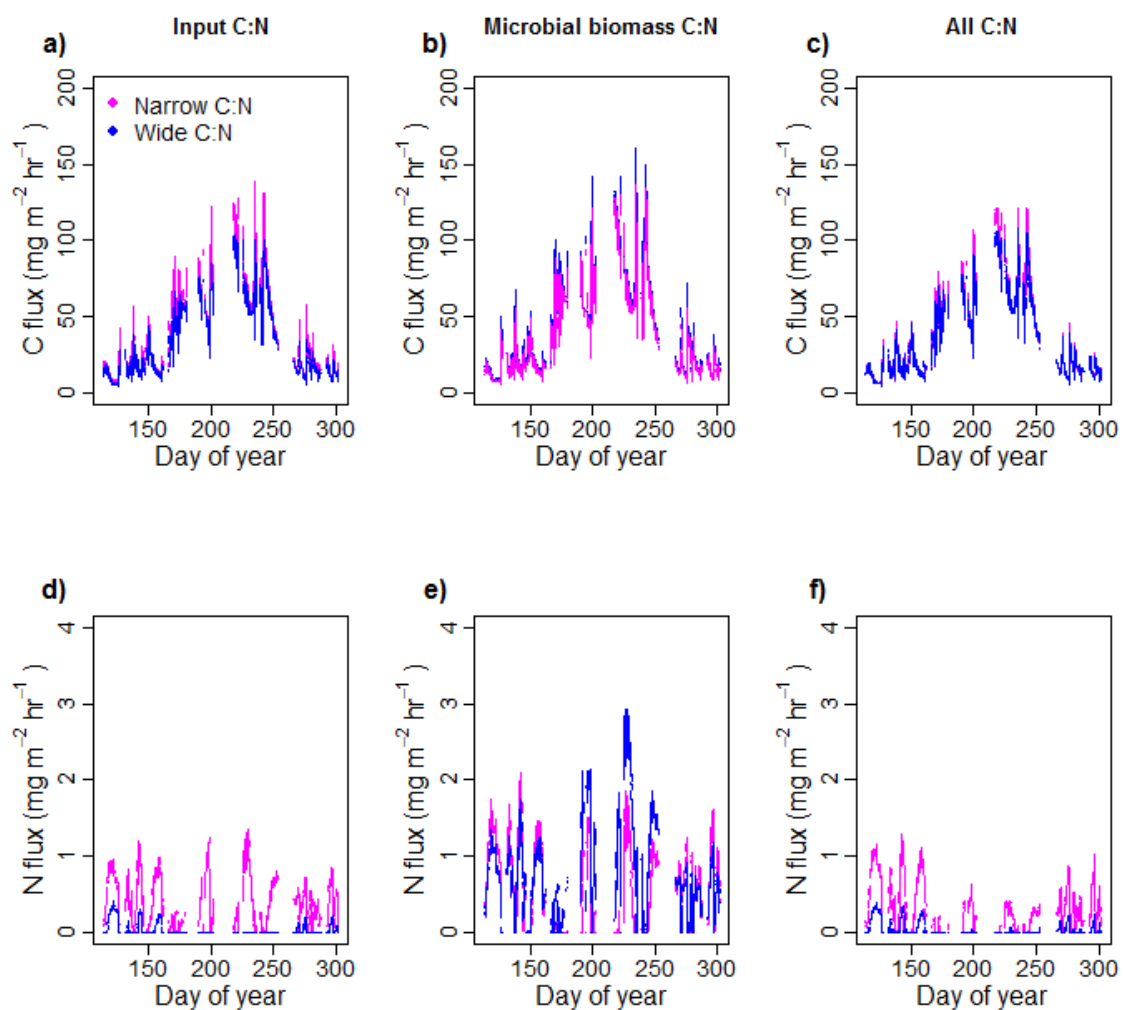


Figure 5.7. Annual C and N mineralization in stands with narrow (pink) or wide (blue) C:N using parameters defined in Table 5.3. (a) C and (d) N mineralization when only input C:N was varied between stands and microbial biomass was held at the default value. (b) C and (e) N mineralization when only microbial biomass C:N was varied and inputs were held at their default value. (c) C and (f) N mineralization when both input C:N and microbial biomass C:N were varied between stands.

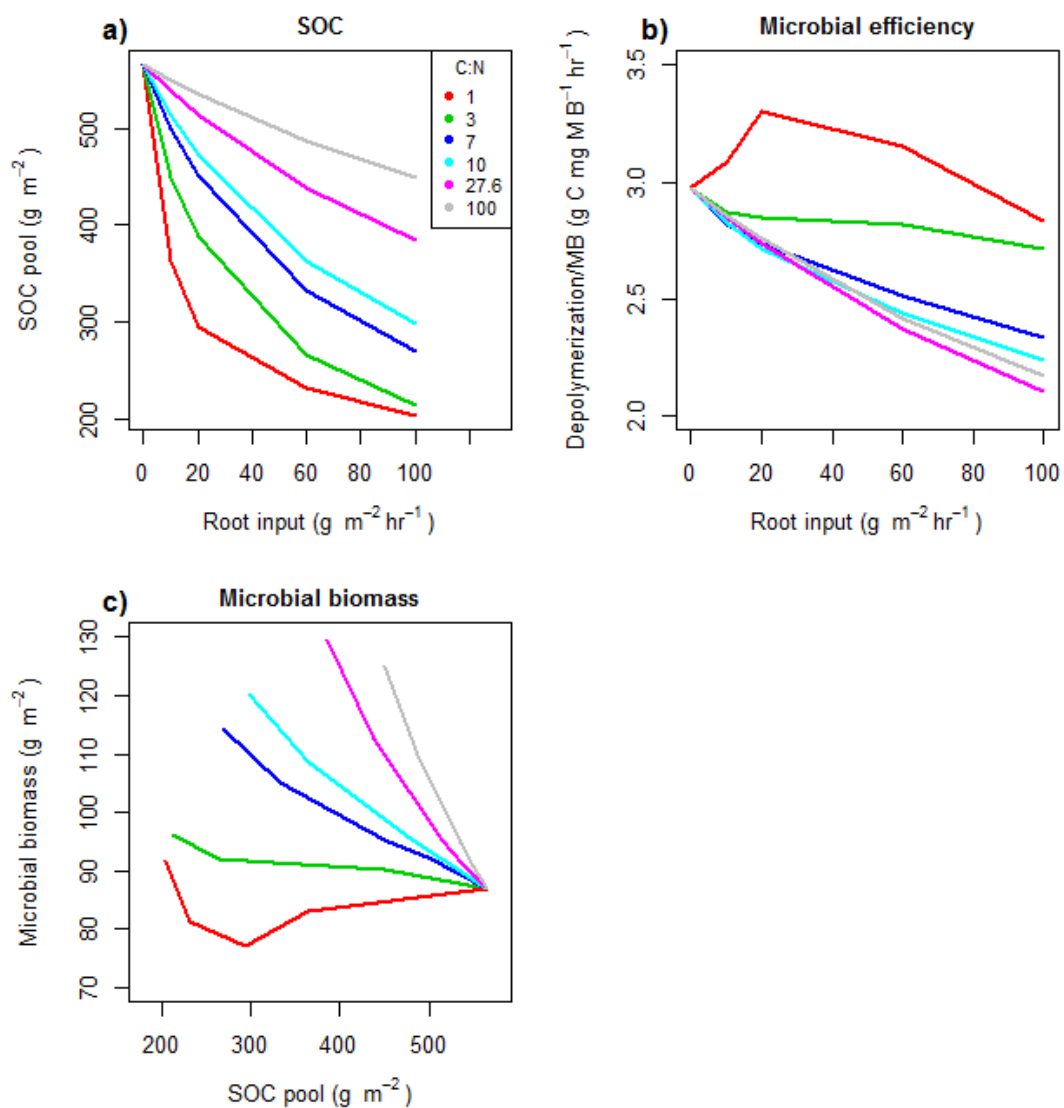


Figure 5.8. (a) SOC as a function of root inputs. (b) Microbial efficiency (depolymerization per unit microbial biomass) as a function of root inputs. (c) Microbial biomass as a function of the SOC pool. In panels a-c, root input C:N varies between 1 and 100 (colored lines).

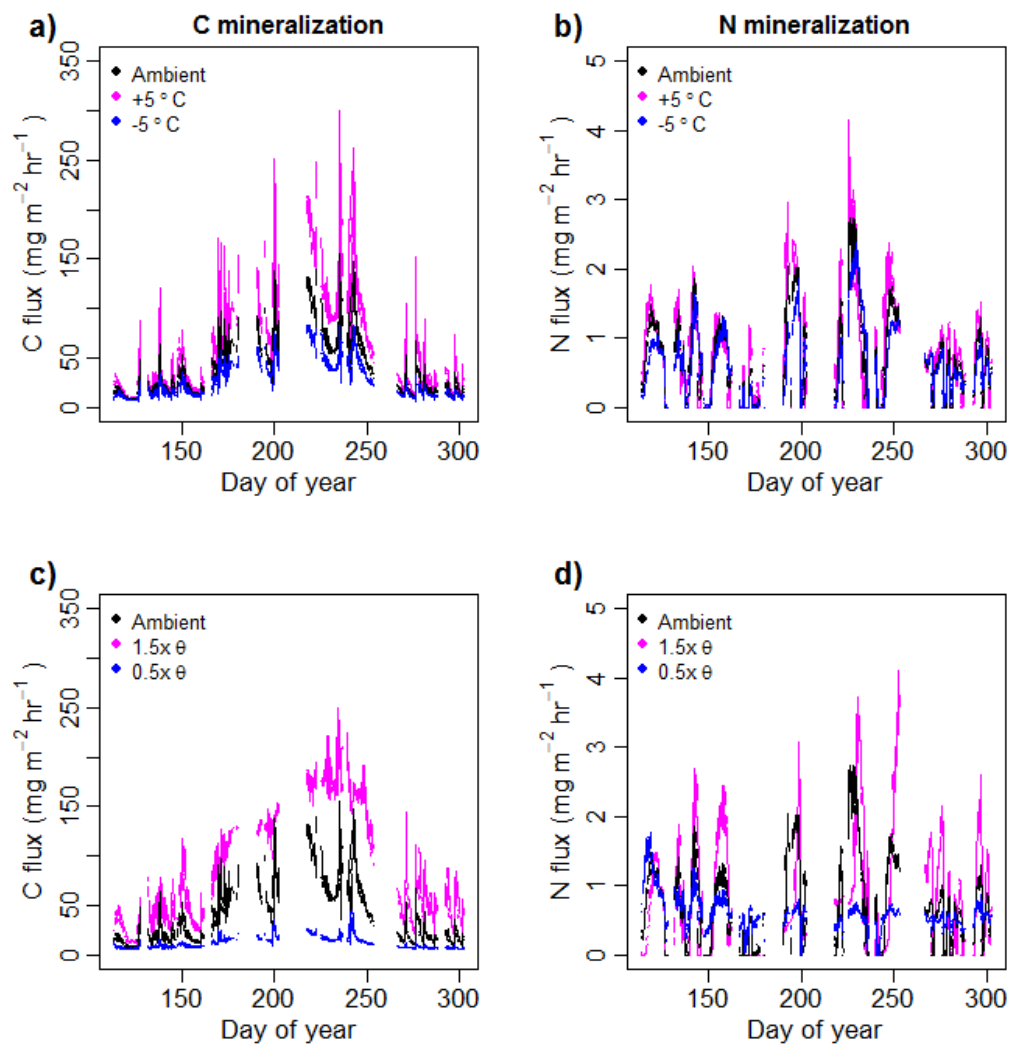


Figure 5.9. Effect of 5°C warming (pink) and 5°C cooling (blue) on (a) C and (b) N mineralization. Effect of 1.5x soil moisture (pink) and 0.5x soil moisture (blue) on (c) C and (d) N mineralization. Black lines indicate C or N mineralization at ambient temperature and soil moisture conditions.

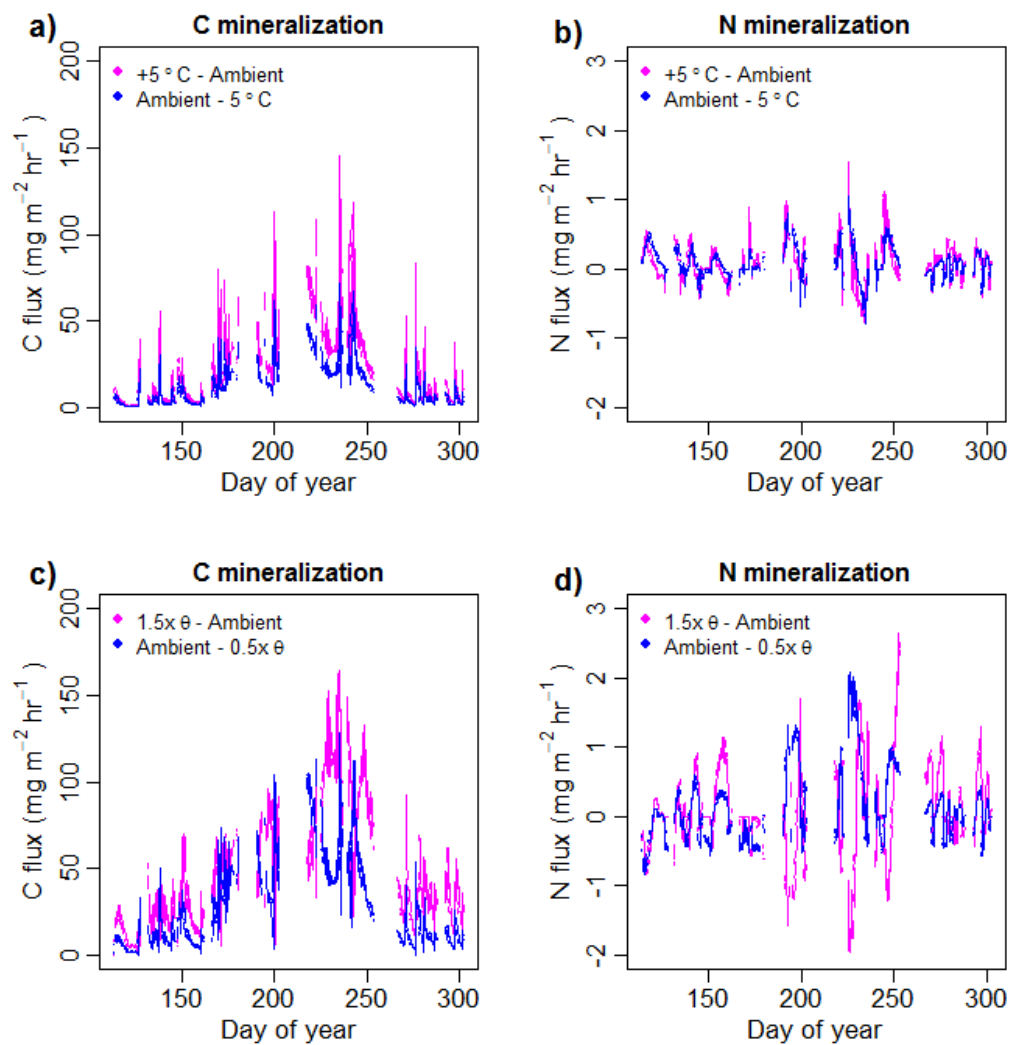


Figure 5.10. Absolute difference in (a) C and (b) N mineralization between ambient and 5°C of warming (pink) or cooling (blue). Absolute difference in (c) C and (d) N mineralization between ambient and 1.5x (pink) or 0.5x soil moisture (θ ; blue).

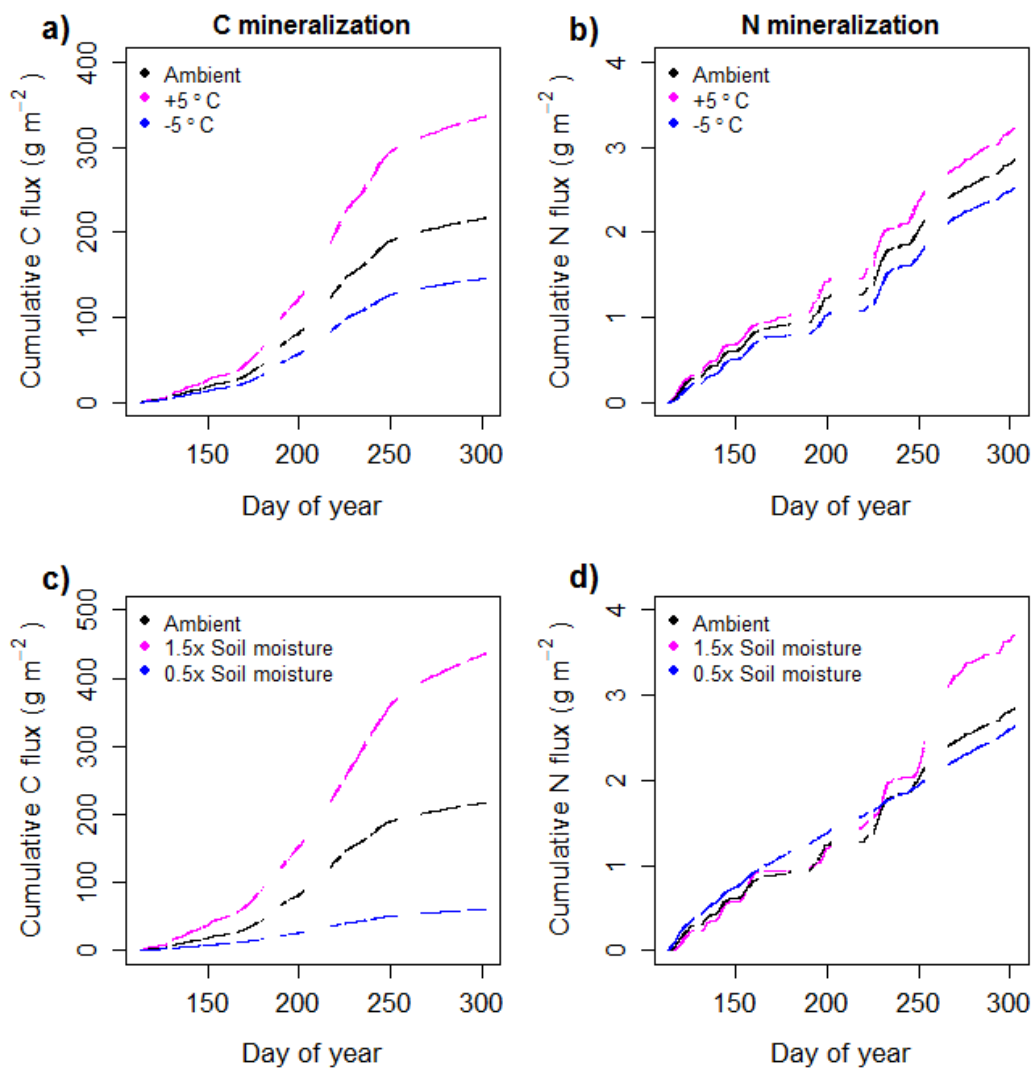


Figure 5.11. Cumulative sums of (a) C and (b) N mineralization rates under 5°C warming (pink) and cooling (blue). Cumulative sums of (c) C and (d) N mineralization rates with 1.5x soil moisture (pink) and 0.5x soil moisture (blue). Black lines indicate cumulative sums of C or N mineralization at ambient temperature and soil moisture conditions.

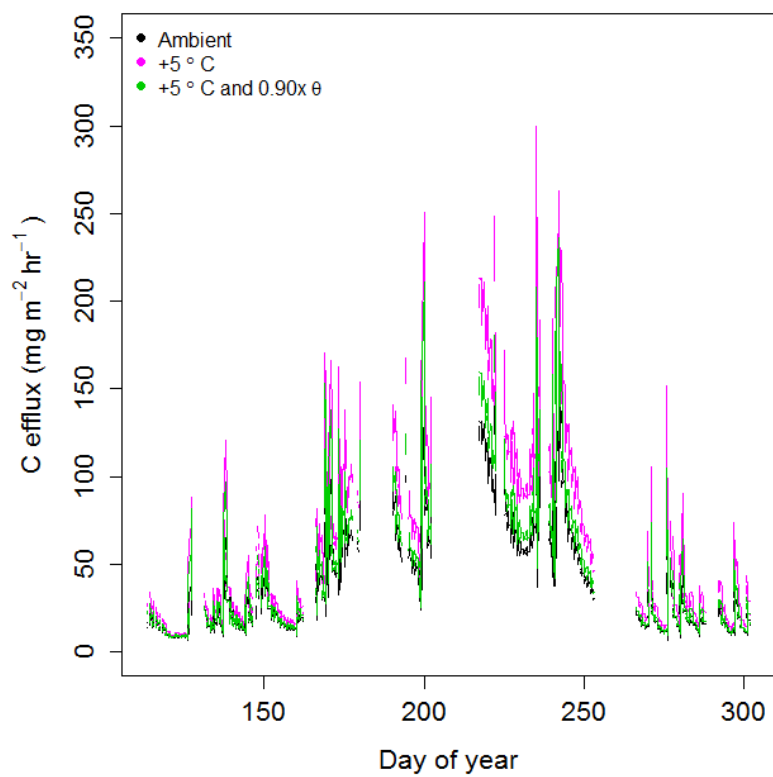


Figure 5.12. C mineralization under ambient temperature and soil moisture (θ ; black line), 5°C warming with no change in soil moisture (pink line), and 5°C warming with a 10% decrease in soil moisture (0.90x; green line).

CHAPTER SIX: CONCLUSION

The research in this dissertation followed C from aboveground allocation through roots to soil microbes at seasonal and inter-annual timescales. I used data compilation, field studies, and computer simulation to study global, plot-level, and micro-site spatial scales, respectively. One overarching objective of this work was to scale up measurements of local or micro-site processes to make ecosystem scale inferences. This was accomplished using plot averaging in the field study in Chapter 3, and using computer simulation to scale micro-site microbial activity to recreate plot-level phenomena (i.e., heterotrophic respiration) in Chapter 5. I explored a new method for quantifying rhizosphere extent in Chapter 4, which could then be used to scale up microbial activity in models that represent the distribution of roots in soil and root-derived substrate supply (Finzi *et al.*, 2015).

A second overarching theme was the effect of substrate supply on plant and microbial activity, such as the temporal coupling between photosynthesis and root growth or respiration, or the exudation of labile C to support microbial growth and soil organic matter (SOM) decomposition. My primary focus on C cycling was motivated by the fundamental role of C in organizing biological systems, as well as its role as a potent greenhouse gas that is altering the Earth's climate, with largely negative impacts on ecosystem services (Field & Van Aalst, 2014).

Phenology and C allocation

In both a meta-analysis across multiple biomes and field studies in a mid-latitude temperate forest, I found a difference in the phenology of evergreen compared to

deciduous trees. Deciduous root growth occurred earlier in the growing season relative to evergreen trees. Moreover, the timing of maximum root production in deciduous trees was more synchronous with measurements of aboveground phenology than that of evergreen trees. If this difference in phenology is consistent among the many species that are represented in each growth form, then there are implications for the ecosystem models that currently assume all phenology is synchronous (Medvigy *et al.*, 2009, Oleson *et al.*, 2010, Woodward & Lomas, 2004). Based on the findings of Chapters 2 and 3, this assumption of synchronicity is accurate for the temperate broadleaf deciduous plant functional type (PFT). However, a more accurate representation of the temperate needleleaf evergreen PFT is a lagged allocation of C belowground to roots.

It is difficult to determine one set of parameters for the all of species represented in a PFT because of the diversity of plant trait values among different species. As a result of this limitation, recent proposals are focusing on replacing PFTs altogether with species-specific or phylogenetically hierarchical plant traits that may vary as a function of temperature, soil moisture, clay content, or other widely available correlates of plant function (Wullschleger *et al.*, 2014). Though existing plant trait databases are very sparse (Kattge *et al.*, 2011), advances in matrix imputation may be able to use phylogenetic relationships to fill in missing plant traits with traits of closely-related taxa (Swenson, 2014). My data are immediately applicable as part of a plant trait database. Chapter 2 meta-analysis data have already been submitted to TRY, a global plant trait database initiated in 2007 (Kattge *et al.*, 2011).

Temperate deciduous trees have high growing season photosynthetic rates relative to temperate conifers (Hadley *et al.*, 2008), resulting in similarly high rates of belowground C allocation. I found that red oak (*Quercus rubra*) stands allocated ~250 g m⁻² more C belowground than eastern hemlock (*Tsuga canadensis*) during the growing season. This discrepancy is driven by the difference in root production between stands. This observation suggests that long-term increases in C uptake and biomass noted in red oak trees at the Harvard Forest are facilitated by root production to meet nutrient demand (Keenan *et al.*, 2012, Urbanski *et al.*, 2007).

In red oak, increasing root production was a confirmation of high stand productivity, but in eastern hemlock, decreasing root production suggested a stand-level decline. The year-over-year decline in root production is coincident with the arrival of the hemlock woolly adelgid in 2012, its spread throughout Harvard Forest in subsequent years, and visible signs of crown thinning and HWA-induced tree mortality recorded by 2014. From these data, I conclude that disease-related declines in productivity are manifested belowground. Notably, live roots sampled from the hemlock stand had similar nonstructural carbohydrate, exudation, and respiration measurements to the other stands. Both the tight coupling of above and belowground phenology in red oak and the rapidity of disease-related decline in hemlock suggest that newly fixed C is important to root growth and longevity.

There is still little known about the phenology of roots. The National Ecological Observatory Network (NEON), founded in 2006 to collect standardized observational data across the United States, is building soil arrays that include minirhizotron cameras

permanently mounted in tubes installed into their terrestrial sites (Pennisi, 2010). These cameras can rotate and move vertically on a track in order to take photos and wirelessly transmit data back to a field station (Roberti *et al.*, 2014). This will be the first large-scale implementation of this technology, and will also create the need to improve automated root detection, as the number of root images proposed cannot be annotated manually (Vamerali *et al.*, 1999, Zeng *et al.*, 2008). I am optimistic that NEON's national implementation of minirhizotron cameras as well as ancillary soil and environmental measurements will produce data that greatly improve estimates of root production and its environmental drivers.

Modeling the micro-site at global scales

I developed a model that represents the effect of temperature and substrate supply on microbial activity by merging the Dual Arrhenius Michaelis-Menten model of Davidson *et al.* (2012) with the Microbial Carbon and Nitrogen Physiology Model of Finzi *et al.* (2015). The combined model, DAMM-MCNIp, reproduced measured rates of heterotrophic respiration over the growing season, and performed particularly well compared to each model alone when confronted with wet-up events. I show that the stoichiometry of root exudates influences both the amount and the mechanism by which priming occurs.

In order to scale up DAMM-MCNIp's rhizosphere and bulk soil model outputs to an ecosystem flux, I had to make an assumption about the rhizosphere volume. Currently, DAMM-MCNIp is parameterized for 1 cm³ of soil that is assumed to be exactly 20% rhizosphere, determined using a modeling exercise based on the assumption that exudates

diffuse 2 mm away from the root surface (Finzi *et al.*, 2015). I developed a quantitative framework for estimating the spatial extent of the rhizosphere using image analysis of 2-D zymographs that may be able to improve estimates of the exudate diffusion distance.

An alternative to using a single value for the rhizosphere volume in models is to explicitly represent fluid transport of root exudates. I am preparing a depth-resolved version of DAMM-MCNIp that can include vertical or lateral transport of root exudates that are dissolved into the DOC pool, as well as declining root inputs with depth based on the depth distribution of root biomass (Finzi *et al.*, 2015). Given adequate data on the enzyme activity of bulk versus rhizosphere soil, it may also be possible to use a future version of DAMM-MCNIp to estimate an effective rhizosphere distance by fitting it as a parameter to measurable outputs such as C and N mineralization.

The main contribution of DAMM-MCNIp is that it explicitly represents the processes that control the availability of SOM. However, SOM availability is also determined by the chemical composition of the soil, which influences aggregate formation, adsorption, and desorption of organic matter to minerals (Conant *et al.*, 2011, Grandy & Neff, 2008). DAMM-MCNIp does not currently represent physical or chemical protection of SOM dynamically. Rather, DAMM-MCNIp considers a fixed fraction of SOM at each time step to be “unprotected”. This unprotected SOM is available for microbial depolymerization if it can diffuse to an extracellular enzyme. While DAMM-MCNIp can reproduce C efflux after a wet-up event by accurately representing the large amount of available C released by wet-up (Parton *et al.*, 2012), it

over-predicts C efflux in constant high soil moisture conditions. DAMM-MCNIp's representation of soil moisture dynamics may improve with parameter optimization, but it is also possible that there is a temperature control on SOM protection that is not currently represented.

Some microbial physiology models have also started to incorporate some representation of sorption to soil minerals (Tang & Riley, 2015, White *et al.*, 2014). One microbial physiology model that has an intriguing simplification of SOM protection is MIMICS, which omits soil moisture but calculates the half-saturation constant of depolymerization as a function of soil clay content. This approximation of SOM "protection" simulates changes in SOM pools better than DAYCENT, a model lacking microbial physiology (Wieder *et al.*, 2014).

There are a large number of decomposition models, many of which have some representation of microbial physiology (Allison *et al.*, 2010, Drake *et al.*, 2013, Moorhead *et al.*, 2012, Schimel & Weintraub, 2003, Tang & Riley, 2015). Though DAMM-MCNIp is the only microbial physiology model to include representation of temperature, substrate supply, C and N cycling, it may not necessarily have the most predictive power. In order to determine which models perform well when confronted with new data, there needs to be a framework for model testing and comparison. In CMIP5, the predicted pools or fluxes of different process-models are plotted together and a moving average of these models is considered the most likely scenario (Ahlström *et al.*, 2012). If parameter uncertainty can be propagated through to outputs, then it is possible

to compare model outputs to each other and also identify which parameters require more data constraints. This type of error propagation could be done in a Bayesian framework (Tang & Zhuang, 2009) or in a computationally simpler Monte Carlo framework (Keenan *et al.*, 2013).

Summary

The research presented in this dissertation focuses on the seasonality and partitioning of belowground C allocation to roots and soil microbes. I found that above and belowground phenology are often asynchronous, and that root growth drives the phenology of belowground C allocation. Root growth and respiration are positively correlated with temperature, and C allocation to root production in a deciduous mid-latitude forest is tightly coupled with photosynthesis. Continued burning of fossil fuels will increase the temperature and CO₂ concentration in the atmosphere, resulting in an increase in belowground C allocation (Drake *et al.*, 2011). Root allocation and elevated temperature both stimulate soil microbial activity, and ultimately, the flux of CO₂ into the atmosphere via heterotrophic respiration. This cycle constitutes a positive feedback to climate change, one that may be mitigated by C sequestration in plant biomass, acclimation of microbial metabolism, or depletion of substrate supply (Frey *et al.*, 2013, Norby *et al.*, 2005).

DAMM-MCNIp is one of the first microbial physiology models that can represent the C and N cycle together with plant substrate supply, making it a candidate for linkage with terrestrial biosphere models that are used to estimate feedbacks between plants, microbes, soil and the atmosphere. Though I have only tested DAMM-MCNIp against

one data set thus far, others have demonstrated that including microbial processes in C cycle models substantially improves predictions of the spatial distribution of SOC (Hararuk *et al.*, 2014). Inclusion of these processes can change the prediction of future SOC pool size by > 300 Pg C (Tang & Riley, 2015, Wieder *et al.*, 2013), indicating that plant–microbe–soil feedbacks are critical to the global C cycle.

LITERATURE CITED

- Abramoff RZ, Finzi AC (2015) Are above- and below-ground phenology in sync? *New Phytologist*, **205**, 1054-1061.
- Aerts R, De Caluwe H, Konings H (1992) Seasonal allocation of biomass and nitrogen in four *Carex* species from mesotrophic and eutrophic fens as affected by nitrogen supply. *Journal of Ecology*, 653-664.
- Ahlström A, Schurgers G, Arneth A, Smith B (2012) Robustness and uncertainty in terrestrial ecosystem carbon response to CMIP5 climate change projections. *Environmental Research Letters*, **7**, 044008.
- Allison SD, Wallenstein MD, Bradford MA (2010) Soil-carbon response to warming dependent on microbial physiology. *Nature Geoscience*, **3**, 336-340.
- Amat F, Moussavi F, Comolli LR, Elidan G, Downing KH, Horowitz M (2008) Markov random field based automatic image alignment for electron tomography. *Journal of structural biology*, **161**, 260-275.
- Aono Y, Kazui K (2008) Phenological data series of cherry tree flowering in Kyoto, Japan, and its application to reconstruction of springtime temperatures since the 9th century. *International Journal of Climatology*, **28**, 905-914.
- Arrhenius S, Sandström JW (1903) *Lehrbuch der kosmischen Physik*, S. Hirzel.
- Averill C (2014) Divergence in plant and microbial allocation strategies explains continental patterns in microbial allocation and biogeochemical fluxes. *Ecology Letters*, **17**, 1202-1210.

- Averill C, Turner BL, Finzi AC (2014) Mycorrhiza-mediated competition between plants and decomposers drives soil carbon storage. *Nature*, **505**, 543-545.
- Bai S, Li J, He Z *et al.* (2013) GeoChip-based analysis of the functional gene diversity and metabolic potential of soil microbial communities of mangroves. *Applied microbiology and biotechnology*, **97**, 7035-7048.
- Barker Plotkin A (2010) Litterfall in Hemlock Removal Experiment at Harvard Forest since 2005. Harvard Forest Data Archive. HF161.
- Barney CW (1951) Effects of soil temperature and light intensity on root growth of loblolly pine seedlings. *Plant Physiology*, **26**, 146.
- Bassow S, Bazzaz F (1997) Intra-and inter-specific variation in canopy photosynthesis in a mixed deciduous forest. *Oecologia*, **109**, 507-515.
- Bates D, Maechler M, Bolker B, Walker S (2014) lme4: Linear mixed-effects models using Eigen and S4. *R package version*, 1.1-5.
- Bengtson P, Barker J, Grayston SJ (2012) Evidence of a strong coupling between root exudation, C and N availability, and stimulated SOM decomposition caused by rhizosphere priming effects. *Ecology and evolution*, **2**, 1843-1852.
- Bevington KB, Castle WS (1985) Annual root growth pattern of young citrus trees in relation to shoot growth, soil temperature, and soil water content. *Journal of the American Society for Horticultural Science*, **110**, 840-845.
- Birch H (1958) The effect of soil drying on humus decomposition and nitrogen availability. *Plant and Soil*, **10**, 9-31.
- Bivand R, Altman M, Anselin L *et al.* (2014) Package ‘spdep’.

- Boldingh H, Smith G, Klages K (2000) Seasonal concentrations of non-structural carbohydrates of five Actinidia species in fruit, leaf and fine root tissue. *Annals of botany*, **85**, 469-476.
- Bolker BM, Pacala SW, Parton Jr WJ (1998) Linear analysis of soil decomposition: insights from the century model. *Ecological Applications*, **8**, 425-439.
- Bonomelli C, Bonilla C, Acuña E, Artacho P (2012) Seasonal pattern of root growth in relation to shoot phenology and soil temperature in sweet cherry trees (*Prunus avium*): A preliminary study in central Chile. *Ciencia e Investigación Agraria*, **39**, 127-136.
- Bosac C, Gardner S, Taylor G, Wilkins D (1995) Elevated CO₂ and hybrid poplar: a detailed investigation of root and shoot growth and physiology of *Populus euramericana*, 'Primo'. *Forest Ecology and Management*, **74**, 103-116.
- Bowden R, Mcclaugherty C, Sipe T (2009) Soil Properties in CRUI Land Use Project at Harvard Forest 1995-1998. Harvard Forest Data Archive. HF143.
- Bradford MA, Davies CA, Frey SD *et al.* (2008) Thermal adaptation of soil microbial respiration to elevated temperature. *Ecology Letters*, **11**, 1316-1327.
- Broschat TK (1998) Root and shoot growth patterns in four palm species and their relationships with air and soil temperatures. *HortScience*, **33**, 995-998.
- Brown D, Upchurch D (1987) Minirhizotrons: a summary of methods and instruments in current use. *Minirhizotron observation tubes: methods and applications for measuring rhizosphere dynamics*, 15-30.

- Brzostek ER (2012) *Proteolytic enzyme activity in soils: Interactive effects of soil temperature and moisture, substrate availability, and mycorrhizal fungi*, Boston University.
- Brzostek ER, Finzi AC (2011) Substrate supply, fine roots, and temperature control proteolytic enzyme activity in temperate forest soils. *Ecology*, **92**, 892-902.
- Brzostek ER, Finzi AC (2012) Seasonal variation in the temperature sensitivity of proteolytic enzyme activity in temperate forest soils. *Journal of Geophysical Research*, **117**, G01018.
- Brzostek ER, Greco A, Drake JE, Finzi AC (2013) Root carbon inputs to the rhizosphere stimulate extracellular enzyme activity and increase nitrogen availability in temperate forest soils. *Biogeochemistry*, **115**, 65-76.
- Burke MK, Raynal DJ (1994) Fine-Root Growth Phenology, Production, and Turnover in a Northern Hardwood Forest Ecosystem. *Plant and Soil*, **162**, 135-146.
- Burke MK, Raynal DJ, Mitchell MJ (1992) Soil nitrogen availability influences seasonal carbon allocation patterns in sugar maple (*Acer saccharum*). *Canadian Journal of Forest Research*, **22**, 447-456.
- Burton A, Pregitzer K, Ruess R, Hendrick R, Allen M (2002) Root respiration in North American forests: effects of nitrogen concentration and temperature across biomes. *Oecologia*, **131**, 559-568.
- Burton AJ, Jarvey JC, Jarvi MP, Zak DR, Pregitzer KS (2012) Chronic N deposition alters root respiration-tissue N relationship in northern hardwood forests. *Global Change Biology*, **18**, 258-266.

- Burton AJ, Melillo JM, Frey SD (2008) Adjustment of Forest Ecosystem Root Respiration as Temperature Warms. *Journal of Integrative Plant Biology*, **50**, 1467-1483.
- Burton AJ, Pregitzer KS (2003) Field measurements of root respiration indicate little to no seasonal temperature acclimation for sugar maple and red pine. *Tree Physiology*, **23**, 273-280.
- Canny J (1986) A computational approach to edge detection. *Pattern Analysis and Machine Intelligence, IEEE Transactions on*, 679-698.
- Cardon ZG, Czaja AD, Funk JL, Vitt PL (2002) Periodic carbon flushing to roots of *Quercus rubra* saplings affects soil respiration and rhizosphere microbial biomass. *Oecologia*, **133**, 626-626.
- Chamberlin TC (1899) An attempt to frame a working hypothesis of the cause of glacial periods on an atmospheric basis. *The Journal of Geology*, **7**, 545-584.
- Chen XY, Eamus D, Hutley LB (2004) Seasonal patterns of fine-root productivity and turnover in a tropical savanna of northern Australia. *Journal of Tropical Ecology*, **20**, 221-224.
- Chow PS, Landhausser SM (2004) A method for routine measurements of total sugar and starch content in woody plant tissues. *Tree Physiology*, **24**, 1129-1136.
- Ciais P, Sabine C, Bala G *et al.* (2014) Carbon and other biogeochemical cycles. In: *Climate Change 2013: The Physical Science Basis. Contribution of Working Group I to the Fifth Assessment Report of the Intergovernmental Panel on Climate Change*. pp 465-570. Cambridge University Press.

- Clemmensen K, Bahr A, Ovaskainen O *et al.* (2013) Roots and associated fungi drive long-term carbon sequestration in boreal forest. *Science*, **339**, 1615-1618.
- Comas LH, Eissenstat DM (2009) Patterns in root trait variation among 25 co-existing North American forest species. *New Phytologist*, **182**, 919-928.
- Conant RT, Ryan MG, Ågren GI *et al.* (2011) Temperature and soil organic matter decomposition rates—synthesis of current knowledge and a way forward. *Global Change Biology*, **17**, 3392-3404.
- Contosta AR, Frey, S.D, Cooper, A.B. (2011) Seasonal dynamics of soil respiration and N mineralization in chronically warmed and fertilized soils. *Ecosphere*, **2**.
- Côté B, Hendershot WH, Fyles JW, Roy AG, Bradley R, Biron PM, Courchesne F (1998) The phenology of fine root growth in a maple-dominated ecosystem: relationships with some soil properties. *Plant and Soil*, **201**, 59-69.
- Craine JM, Dybzinski R (2013) Mechanisms of plant competition for nutrients, water and light. *Functional Ecology*, **27**, 833-840.
- Craine JM, Fierer N, Mclauchlan KK (2010) Widespread coupling between the rate and temperature sensitivity of organic matter decay. *Nature Geoscience*, **3**, 854-857.
- Craine JM, Morrow C, Fierer N (2007) Microbial nitrogen limitation increases decomposition. *Ecology*, **88**, 2105-2113.
- Curtis PS, Zak DR, Pregitzer KS, Teeri JA (1995) Above-and belowground response of *Populus grandidentata* to elevated atmospheric CO₂ and soil N availability. In: *Belowground Responses to Rising Atmospheric CO₂: Implications for Plants, Soil Biota, and Ecosystem Processes*. pp 45-51. Springer.

- Darrah P (1991a) Measuring the diffusion coefficient of rhizosphere exudates in soil. I. The diffusion of non-sorbing compounds. *Journal of soil science*, **42**, 413-420.
- Darrah P (1991b) Measuring the diffusion coefficients of rhizosphere exudates in soil. II. The diffusion of sorbing compounds. *Journal of soil science*, **42**, 421-434.
- Davidson E, Belk E, Boone RD (1998) Soil water content and temperature as independent or confounded factors controlling soil respiration in a temperate mixed hardwood forest. *Global Change Biology*, **4**, 217-227.
- Davidson E, Savage K, Verchot L, Navarro R (2002) Minimizing artifacts and biases in chamber-based measurements of soil respiration. *Agricultural and Forest Meteorology*, **113**, 21-37.
- Davidson EA, Holbrook NM (2009) Is Temporal Variation of Soil Respiration Linked to the Phenology of Photosynthesis? *Phenology of Ecosystem Processes*, 187-199.
- Davidson EA, Janssens IA (2006) Temperature sensitivity of soil carbon decomposition and feedbacks to climate change. *Nature*, **440**, 165-173.
- Davidson EA, Janssens IA, Luo Y (2006) On the variability of respiration in terrestrial ecosystems: moving beyond Q₁₀. *Global Change Biology*, **12**, 154-164.
- Davidson EA, Samanta S, Caramori SS, Savage K (2012) The Dual Arrhenius and Michaelis–Menten kinetics model for decomposition of soil organic matter at hourly to seasonal time scales. *Global Change Biology*, **18**, 371-384.
- Davidson EA, Savage KE, Finzi AC (2014) A big-microsite framework for soil carbon modeling. *Global Change Biology*, **20**, 3610-3620.

- De Neergaard A, Magid J (2001) Influence of the rhizosphere on microbial biomass and recently formed organic matter. *European journal of soil science*, **52**, 377-384.
- Deans J (1979) Fluctuations of the soil environment and fine root growth in a young Sitka spruce plantation. *Plant and Soil*, **52**, 195-208.
- Desrochers A, Landhäusser SM, Lieffers VJ (2002) Coarse and fine root respiration in aspen (*Populus tremuloides*). *Tree Physiology*, **22**, 725-732.
- Dessureault-Rompré J, Nowack B, Schulin R, Luster J (2007) Spatial and temporal variation in organic acid anion exudation and nutrient anion uptake in the rhizosphere of *Lupinus albus* L. *Plant and Soil*, **301**, 123-134.
- Dohleman FG, Heaton EA, Arundale RA, Long SP (2012) Seasonal dynamics of above- and below-ground biomass and nitrogen partitioning in *Miscanthus* × *giganteus* and *Panicum virgatum* across three growing seasons. *GCB Bioenergy*, **4**, 534-544.
- Domagalska MA, Leyser O (2011) Signal integration in the control of shoot branching. *Nature Reviews Molecular Cell Biology*, **12**, 211-221.
- Dong S, Brooks D, Jones MD, Grayston SJ (2007) A method for linking in situ activities of hydrolytic enzymes to associated organisms in forest soils. *Soil Biology and Biochemistry*, **39**, 2414-2419.
- Dornbush ME, Raich JW (2006) Soil temperature, not aboveground plant productivity, best predicts intra-annual variations of soil respiration in central Iowa grasslands. *Ecosystems*, **9**, 909-920.

- Drake J, Darby B, Giasson M-A, Kramer M, Phillips R, Finzi A (2013) Stoichiometry constrains microbial response to root exudation-insights from a model and a field experiment in a temperate forest. *Biogeosciences*, **10**, 821-838.
- Drake J, Oishi A, Giasson M-A, Oren R, Johnsen K, Finzi A (2012) Trenching reduces soil heterotrophic activity in a loblolly pine (*Pinus taeda*) forest exposed to elevated atmospheric CO₂ and N fertilization. *Agricultural and Forest Meteorology*, **165**, 43-52.
- Drake JE, Gallet-Budynek A, Hofmockel KS *et al.* (2011) Increases in the flux of carbon belowground stimulate nitrogen uptake and sustain the long-term enhancement of forest productivity under elevated CO₂. *Ecology Letters*, **14**, 349-357.
- Drew A, Ledig FT (1980) Episodic growth and relative shoot: root balance in loblolly pine seedlings. *Annals of botany*, **45**, 143-148.
- Drew AP, Ledig FT (1981) Seasonal patterns of CO₂ exchange in the shoot and root of loblolly pine seedlings. *Botanical Gazette*, 200-205.
- Dušek J, Květ J (2006) Seasonal dynamics of dry weight, growth rate and root/shoot ratio in different aged seedlings of *Salix caprea*. *Biologia*, **61**, 441-447.
- Dybzinski R, Farrior C, Wolf A, Reich PB, Pacala SW (2011) Evolutionarily Stable Strategy Carbon Allocation to Foliage, Wood, and Fine Roots in Trees Competing for Light and Nitrogen: An Analytically Tractable, Individual-Based Model and Quantitative Comparisons to Data. *American Naturalist*, **177**, 153-166.

- Ellison AM, Kendrick J, Classen A, Ribbons R (2015) Changes in canopy structure and ant assemblages affect soil ecosystem variables as a foundation species declines. *Ecosphere*, **6**.
- Fahey T, Siccama T, Driscoll C *et al.* (2005) The biogeochemistry of carbon at Hubbard Brook. *Biogeochemistry*, **75**, 109-176.
- Fahey TJ, Yavitt JB, Sherman RE, Groffman PM, Wang G (2013) Partitioning of belowground C in young sugar maple forest. *Plant and Soil*, **367**, 379-389.
- Falchini L, Naumova N, Kuikman P, Bloem J, Nannipieri P (2003) CO₂ evolution and denaturing gradient gel electrophoresis profiles of bacterial communities in soil following addition of low molecular weight substrates to simulate root exudation. *Soil Biology and Biochemistry*, **35**, 775-782.
- Farrar J, Jones D (2008) The control of carbon acquisition by roots. *New Phytologist*, **147**, 43-53.
- Field C, Van Aalst M (2014) *Climate change 2014: impacts, adaptation, and vulnerability*, IPCC.
- Finzi AC, Abramoff RZ, Spiller KS, Brzostek ER, Darby BA, Kramer MA, Phillips RP (2015) Rhizosphere processes are quantitatively important components of terrestrial carbon and nutrient cycles. *Global Change Biology*.
- Finzi AC, Allen AS, Delucia EH, Ellsworth DS, Schlesinger WH (2001) Forest litter production, chemistry, and decomposition following two years of free-air CO₂ enrichment. *Ecology*, **82**, 470-484.

- Finzi AC, Canham CD, Van Breemen N (1998a) Canopy tree-soil interactions within temperate forests: species effects on pH and cations. *Ecological Applications*, **8**, 447-454.
- Finzi AC, Van Breemen N, Canham CD (1998b) Canopy tree-soil interactions within temperate forests: species effects on soil carbon and nitrogen. *Ecological Applications*, **8**, 440-446.
- Fitter A, Graves J, Self G, Brown T, Bogie D, Taylor K (1998) Root production, turnover and respiration under two grassland types along an altitudinal gradient: influence of temperature and solar radiation. *Oecologia*, **114**, 20-30.
- Fitter A, Self G, Brown T, Bogie D, Graves J, Benham D, Ineson P (1999) Root production and turnover in an upland grassland subjected to artificial soil warming respond to radiation flux and nutrients, not temperature. *Oecologia*, **120**, 575-581.
- Foster D, Swanson F, Aber J, Burke I, Brokaw N, Tilman D, Knapp A (2003) The importance of land-use legacies to ecology and conservation. *Bioscience*, **53**, 77-88.
- Frey S, Ollinger S (1999) Chronic Nitrogen Amendment Experiment at Harvard Forest since 1988. Harvard Forest Data Archive. HF008.
- Frey S, Ollinger S, Nadelhoffer K *et al.* (2014) Chronic nitrogen additions suppress decomposition and sequester soil carbon in temperate forests. *Biogeochemistry*, **121**, 305-316.

- Frey SD, Lee J, Melillo JM, Six J (2013) The temperature response of soil microbial efficiency and its feedback to climate. *Nature Climate Change*, **3**, 395-398.
- Fukuzawa K, Shibata H, Takagi K, Satoh F, Koike T, Sasa K (2013) Temporal variation in fine-root biomass, production and mortality in a cool temperate forest covered with dense understory vegetation in northern Japan. *Forest Ecology and Management*, **310**, 700-710.
- Gaudinski JB, Trumbore SE, Davidson EA, Zheng S (2000) Soil carbon cycling in a temperate forest: radiocarbon-based estimates of residence times, sequestration rates and partitioning of fluxes. *Biogeochemistry*, **51**, 33-69.
- Giardina CP, Ryan MG (2002) Total belowground carbon allocation in a fast-growing Eucalyptus plantation estimated using a carbon balance approach. *Ecosystems*, **5**, 487-499.
- Giasson M-A, Ellison AM, Bowden R *et al.* (2013) Soil respiration in a northeastern US temperate forest: a 22-year synthesis. *Ecosphere*, **4**, art140.
- Goulden ML, Munger JW, Fan SM, Daube BC, Wofsy SC (1996) Measurements of carbon sequestration by long-term eddy covariance: Methods and a critical evaluation of accuracy. *Global Change Biology*, **2**, 169-182.
- Grandy AS, Neff JC (2008) Molecular C dynamics downstream: the biochemical decomposition sequence and its impact on soil organic matter structure and function. *Science of the Total Environment*, **404**, 297-307.
- Graves WR, Joly RJ, Dana MN (1991) Water use and growth of honey locust and tree-of-heaven at high root-zone temperature. *HortScience*, **26**, 1309-1312.

- Green IJ, Dawson LA, Proctor J, Duff EI, Elston DA (2005) Fine root dynamics in a tropical rain forest is influenced by rainfall. *Plant and Soil*, **276**, 23-32.
- Grier CC, Vogt KA, Keyes MR, Edmonds RL (1981) Biomass distribution and above- and below-ground production in young and mature *Abies amabilis* zone ecosystems of the Washington Cascades. *Canadian Journal of Forest Research*, **11**, 155-167.
- Guo DL, Li H, Mitchell RJ, Han WX, Hendricks JJ, Fahey TJ, Hendrick RL (2008) Fine root heterogeneity by branch order: exploring the discrepancy in root turnover estimates between minirhizotron and carbon isotopic methods. *New Phytologist*, **177**, 443-456.
- Hadley J (2009) Litterfall at Harvard Forest HEM and LPH Towers since 2002. Harvard Forest Data Archive: HF151.
- Hadley JL, Kuzeja PS, Daley MJ, Phillips NG, Mulcahy T, Singh S (2008) Water use and carbon exchange of red oak- and eastern hemlock-dominated forests in the northeastern USA: implications for ecosystem-level effects of hemlock woolly adelgid. *Tree Physiology*, **28**, 615-627.
- Hararuk O, Smith MJ, Luo Y (2014) Microbial models with data-driven parameters predict stronger soil carbon responses to climate change. *Global Change Biology*.
- Harcombe WR, Riehl WJ, Dukovski I *et al.* (2014) Metabolic resource allocation in individual microbes determines ecosystem interactions and spatial dynamics. *Cell reports*, **7**, 1104-1115.

- Harris JR, Bassuk NL, Zobel RW, Whitlow TH (1995) Root and shoot growth periodicity of green ash, scarlet oak, turkish hazelnut, and tree lilac. *Journal of the American Society for Horticultural Science*, **120**, 211-216.
- Hartley IP, Heinemeyer A, Ineson P (2007) Effects of three years of soil warming and shading on the rate of soil respiration: substrate availability and not thermal acclimation mediates observed response. *Global Change Biology*, **13**, 1761-1770.
- Helmisaari H-S, Makkonen K, Kellomäki S, Valtonen E, Mälkönen E (2002) Below-and above-ground biomass, production and nitrogen use in Scots pine stands in eastern Finland. *Forest Ecology and Management*, **165**, 317-326.
- Hendrick RL, Pregitzer KS (1996) Applications of minirhizotrons to understand root function in forests and other natural ecosystems. *Plant and Soil*, **185**, 293-304.
- Hester AJ, Millard P, Baillie GJ, Wendler R (2004) How does timing of browsing affect above-and below-ground growth of *Betula pendula*, *Pinus sylvestris* and *Sorbus aucuparia*? *Oikos*, **105**, 536-550.
- Hirsch PR, Miller AJ, Dennis PG (2013) Do root exudates exert more influence on rhizosphere bacterial community structure than other rhizodeposits. *Molecular microbial ecology of the rhizosphere*. Wiley, Hoboken, **1**, 229-242.
- Hobbie EA (2006) Carbon allocation to ectomycorrhizal fungi correlates with belowground allocation in culture studies. *Ecology*, **87**, 563-569.
- Hogberg P, Hogberg MN, Gottlicher SG *et al.* (2008) High temporal resolution tracing of photosynthate carbon from the tree canopy to forest soil microorganisms. *New Phytologist*, **177**, 220-228.

- Högberg P, Nordgren A, Buchmann N *et al.* (2001) Large-scale forest girdling shows that current photosynthesis drives soil respiration. *Nature*, **411**, 789-792.
- Hutrya LR, Munger JW, Saleska SR *et al.* (2007) Seasonal controls on the exchange of carbon and water in an Amazonian rain forest. *Journal of Geophysical Research-Biogeosciences*, **112**.
- Iivonen S, Rikala R, Vapaavuori E (2001) Seasonal root growth of Scots pine seedlings in relation to shoot phenology, carbohydrate status, and nutrient supply. *Canadian Journal of Forest Research-Revue Canadienne De Recherche Forestiere*, **31**, 1569-1578.
- Ise T, Moorcroft PR (2006) The global-scale temperature and moisture dependencies of soil organic carbon decomposition: an analysis using a mechanistic decomposition model. *Biogeochemistry*, **80**, 217-231.
- Jackson RB, Mooney HA, Schulze ED (1997) A global budget for fine root biomass, surface area, and nutrient contents. *Proceedings of the National Academy of Sciences of the United States of America*, **94**, 7362-7366.
- Jenkinson D, Andrew S, Lynch J, Goss M, Tinker P (1990) The turnover of organic carbon and nitrogen in soil [and discussion]. *Philosophical Transactions of the Royal Society B: Biological Sciences*, **329**, 361-368.
- Johnsen K, Maier C, Sanchez F, Anderson P, Butnor J, Waring R, Linder S (2006) Physiological girdling of pine trees via phloem chilling: proof of concept. *Plant, cell & environment*, **30**, 128-134.

- Jones DL (1998) Organic acids in the rhizosphere—a critical review. *Plant and Soil*, **205**, 25-44.
- Joslin JD, Wolfe MH, Hanson PJ (2001) Factors controlling the timing of root elongation intensity in a mature upland oak stand. *Plant and Soil*, **228**, 201-212.
- Kaakinen S, Jolkkonen A, Iivonen S, Vapaavuori E (2004) Growth, allocation and tissue chemistry of *Picea abies* seedlings affected by nutrient supply during the second growing season. *Tree Physiology*, **24**, 707-719.
- Kattge J, Diaz S, Lavorel S *et al.* (2011) TRY—a global database of plant traits. *Global Change Biology*, **17**, 2905-2935.
- Kaur J, Percival D, Hainstock LJ, Prive J-P (2012) Seasonal growth dynamics and carbon allocation of the wild blueberry plant (*Vaccinium angustifolium* Ait.). *Canadian Journal of Plant Science*, **92**, 1145-1154.
- Keel SG, Siegwolf RTW, Korner C (2006) Canopy CO₂ enrichment permits tracing the fate of recently assimilated carbon in a mature deciduous forest. *New Phytologist*, **172**, 319-329.
- Keenan TF, Davidson E, Moffat AM, Munger W, Richardson AD (2012) Using model-data fusion to interpret past trends, and quantify uncertainties in future projections, of terrestrial ecosystem carbon cycling. *Global Change Biology*, **18**, 2555-2569.
- Keenan TF, Davidson EA, Munger JW, Richardson AD (2013) Rate my data: quantifying the value of ecological data for the development of models of the terrestrial carbon cycle. *Ecological Applications*, **23**, 273-286.

- Keenan TF, Gray J, Friedl MA *et al.* (2014) Net carbon uptake has increased through warming-induced changes in temperate forest phenology. *Nature Climate Change*, **4**, 598-604.
- Keller M (2010) NEON Scientific Data Products Catalog. In: *NEON Doc. #: NEON.MGMT.DPS.005003.REQ.*
- Keyes MR, Grier CC (1981) Above-and below-ground net production in 40-year-old Douglas-fir stands on low and high productivity sites. *Canadian Journal of Forest Research*, **11**, 599-605.
- Kho LK, Malhi Y, Tan SKS (2013) Annual budget and seasonal variation of aboveground and belowground net primary productivity in a lowland dipterocarp forest in Borneo. *Journal of Geophysical Research: Biogeosciences*, **118**, 1282-1296.
- Koch K (1996) Carbohydrate-modulated gene expression in plants. *Annual review of plant biology*, **47**, 509-540.
- Kourtev PS, Ehrenfeld JG, Häggblom M (2002) Exotic plant species alter the microbial community structure and function in the soil. *Ecology*, **83**, 3152-3166.
- Kuzyakov Y (2010) Priming effects: Interactions between living and dead organic matter. *Soil Biology & Biochemistry*, **42**, 1363-1371.
- Kuzyakov Y, Raskatov A, Kaupenjohann M (2003) Turnover and distribution of root exudates of *Zea mays*. *Plant and Soil*, **254**, 317-327.

- Lahti M, Aphalo P, Finér L, Ryyppö A, Lehto T, Mannerkoski H (2005) Effects of soil temperature on shoot and root growth and nutrient uptake of 5-year-old Norway spruce seedlings. *Tree Physiology*, **25**, 115-122.
- Lambers H, Chapin FS, Pons TL (2008) *Plant physiological ecology*, New York, Springer.
- Landi L, Valori F, Ascher J, Renella G, Falchini L, Nannipieri P (2006) Root exudate effects on the bacterial communities, CO₂ evolution, nitrogen transformations and ATP content of rhizosphere and bulk soils. *Soil Biology and Biochemistry*, **38**, 509-516.
- Lemos PC (2013) Variations in carbon fluxes lead to resilience of carbon storage in New England forests affected by the hemlock woolly adelgid at a centennial time scale. Boston University.
- Li R, Volenec J, Joern B, Cunningham S (1996) Seasonal changes in nonstructural carbohydrates, protein, and macronutrients in roots of alfalfa, red clover, sweetclover, and birdsfoot trefoil. *Crop Science*, **36**, 617-623.
- Litton CM, Raich JW, Ryan MG (2007) Carbon allocation in forest ecosystems. *Global Change Biology*, **13**, 2089-2109.
- Lloyd J, Taylor J (1994) On the temperature dependence of soil respiration. *Functional Ecology*, 315-323.
- Lobet G, Pagès L, Draye X (2011) A novel image-analysis toolbox enabling quantitative analysis of root system architecture. *Plant Physiology*, **157**, 29-39.

- Loescher WH, Mccamant T, Keller JD (1990) Carbohydrate reserves, translocation, and storage in woody plant roots. *HortScience*, **25**, 274-281.
- López B, Sabaté S, Gracia C (2001) Annual and seasonal changes in fine root biomass of a *Quercus ilex* L. forest. *Plant and Soil*, **230**, 125-134.
- Lopushinsky W, Max T (1990) Effect of soil temperature on root and shoot growth and on budburst timing in conifer seedling transplants. *New Forests*, **4**, 107-124.
- Lyford WH (1980) *Development of the root system of northern red oak (Quercus rubra L.)*, Harvard University, Harvard Forest.
- Lyford WH, Wilson BF (1964) *Development of the root system of Acer Rubrum L.*, Harvard University, Harvard Forest.
- Lynch DJ, Matamala R, Iversen CM, Norby RJ, Gonzalez-Meler MA (2013) Stored carbon partly fuels fine-root respiration but is not used for production of new fine roots. *New Phytologist*, **199**, 420-430.
- Macduff J, Wild A, Hopper M, Dhanoa M (1986) Effects of temperature on parameters of root growth relevant to nutrient uptake: measurements on oilseed rape and barley grown in flowing nutrient solution. *Plant and Soil*, **94**, 321-332.
- Magill AH, Aber JD, Berntson GM, Mcdowell WH, Nadelhoffer KJ, Melillo JM, Steudler P (2000) Long-term nitrogen additions and nitrogen saturation in two temperate forests. *Ecosystems*, **3**, 238-253.
- Majdi H, Andersson P (2005) Fine root production and turnover in a Norway spruce stand in northern Sweden: effects of nitrogen and water manipulation. *Ecosystems*, **8**, 191-199.

- Margary ID (1926) The Marsham phenological record in Norfolk, 1736–1925, and some others. *Quarterly Journal of the Royal Meteorological Society*, **52**, 27-54.
- Marhan S, Scheu S (2005) Effects of sand and litter availability on organic matter decomposition in soil and in casts of *Lumbricus terrestris* L. *Geoderma*, **128**, 155-166.
- Marler TE, Willis LE (1996) Root and Stem Growth Patterns of Young Mauritius' Lychee Trees. *HortScience*, **31**, 815-818.
- Mccormack ML, Adams TS, Smithwick EaH, Eissenstat DM (2014) Variability in root production, phenology, and turnover rate among 12 temperate tree species. *Ecology*, **95**, 2224-2235.
- Menicol G, Silver WL (2015) Non-linear response of carbon dioxide and methane emissions to oxygen availability in a drained histosol. *Biogeochemistry*, **123**, 299-306.
- Medvigy D, Wofsy SC, Munger JW, Hollinger DY, Moorcroft PR (2009) Mechanistic scaling of ecosystem function and dynamics in space and time: Ecosystem Demography model version 2. *Journal of Geophysical Research-Biogeosciences*, **114**.
- Melillo J, Steudler P, Aber J *et al.* (2002) Soil warming and carbon-cycle feedbacks to the climate system. *Science*, **298**, 2173-2176.
- Melillo JM, Butler S, Johnson J *et al.* (2011) Soil warming, carbon–nitrogen interactions, and forest carbon budgets. *Proceedings of the National Academy of Sciences*, **108**, 9508-9512.

- Melillo JM, Richmond T, Yohe GW (2014) Climate change impacts in the United States: the third national climate assessment. *US Global change research program*, **841**.
- Mickelbart MV, Robinson PW, Witney G, Arpaia ML (2012) 'Hass' avocado tree growth on four rootstocks in California. II. Shoot and root growth. *Scientia Horticulturae*, **143**, 205-210.
- Miller-Rushing AJ, Primack RB (2008) Global warming and flowering times in Thoreau's Concord: a community perspective. *Ecology*, **89**, 332-341.
- Misson L, Gershenson A, Tang J, McKay M, Cheng W, Goldstein A (2006) Influences of canopy photosynthesis and summer rain pulses on root dynamics and soil respiration in a young ponderosa pine forest. *Tree Physiology*, **26**, 833-844.
- Moorhead DL, Lashermes G, Sinsabaugh RL (2012) A theoretical model of C-and N-acquiring exoenzyme activities, which balances microbial demands during decomposition. *Soil Biology and Biochemistry*, **53**, 133-141.
- Muggeo VM (2008) Segmented: an R package to fit regression models with broken-line relationships. *R news*, **8**, 20-25.
- Munger JW, Wofsy S (1999) Biomass Inventories at Harvard Forest EMS Tower since 1993. Harvard Forest Data Archive. HF069.
- Nadelhoffer K, Boone R, Bowden R (1999) DIRT Litter Manipulation Experiment at Harvard Forest since 1990. Harvard Forest Data Archive: HF007.
- Nobis M, Hunziker U (2005) Automatic thresholding for hemispherical canopy-photographs based on edge detection. *Agricultural and Forest Meteorology*, **128**, 243-250.

- Noguchi K, Nagakura J, Konôpka B, Sakata T, Kaneko S, Takahashi M (2013) Fine-root dynamics in sugi (*Cryptomeria japonica*) under manipulated soil nitrogen conditions. *Plant and Soil*, **364**, 159-169.
- Norby RJ, Delucia EH, Gielen B *et al.* (2005) Forest response to elevated CO₂ is conserved across a broad range of productivity. *Proceedings of the National Academy of Sciences of the United States of America*, **102**, 18052-18056.
- Nordgren A, Ottosson Löfvenius M, Högberg M, Mellander PE, Högberg P (2003) Tree root and soil heterotrophic respiration as revealed by girdling of boreal Scots pine forest: extending observations beyond the first year. *Plant, cell & environment*, **26**, 1287-1296.
- Nuruzzaman M, Lambers H, Bolland MD, Veneklaas EJ (2006) Distribution of carboxylates and acid phosphatase and depletion of different phosphorus fractions in the rhizosphere of a cereal and three grain legumes. *Plant and Soil*, **281**, 109-120.
- Oades J (1989) An introduction to organic matter in mineral soils. *Minerals in soil environments*, 89-159.
- Oleson KW, Lawrence DM, Gordon B *et al.* (2010) Technical description of version 4.0 of the Community Land Model (CLM).
- Ornl-Daac (2013) FLUXNET. In: *Oak Ridge National Laboratory Distributed Active Archive Center (ORNL-DAAC)*. Oak Ridge, Tennessee, U.S.A.
- Orwig D, Foster D (2009) Community and Ecosystem Impacts in Hemlock Removal Experiment at Harvard Forest since 2003. Harvard Forest Data Archive. HF054.

- Ostonen I, Lõhmus K, Pajuste K (2005) Fine root biomass, production and its proportion of NPP in a fertile middle-aged Norway spruce forest: comparison of soil core and ingrowth core methods. *Forest Ecology and Management*, **212**, 264-277.
- Palacio S, Montserrat-Marti G (2007) Above and belowground phenology of four Mediterranean sub-shrubs. Preliminary results on root-shoot competition. *Journal of Arid Environments*, **68**, 522-533.
- Palmroth S, Oren R, McCarthy HR *et al.* (2006) Aboveground sink strength in forests controls the allocation of carbon below ground and its CO₂-induced enhancement. *Proceedings of the National Academy of Sciences*, **103**, 19362-19367.
- Papathodorou EM, Pantis JD, Stamou GP (1998) The effect of grazing on phenology and biomass allocation in *Quercus coccifera* (L.). *Acta Oecologica*, **19**, 339-347.
- Parton W, Morgan J, Smith D *et al.* (2012) Impact of precipitation dynamics on net ecosystem productivity. *Global Change Biology*, **18**, 915-927.
- Patrick J (1997) Phloem unloading: sieve element unloading and post-sieve element transport. *Annual review of plant biology*, **48**, 191-222.
- Pennisi E (2010) A groundbreaking observatory to monitor the environment. *Science*, **328**, 418-420.
- Persson H (1980) Fine-root production, mortality and decomposition in forest ecosystems. *Vegetatio*, **41**, 101-109.
- Phillips DA, Fox TC, King MD, Bhuvaneshwari T, Teuber LR (2004) Microbial products trigger amino acid exudation from plant roots. *Plant Physiology*, **136**, 2887-2894.

- Phillips RP, ERLITZ Y, BIER R, BERNHARDT ES (2008) New approach for capturing soluble root exudates in forest soils. *Functional Ecology*, **22**, 990-999.
- Phillips RP, FAHEY TJ (2006) Tree species and mycorrhizal associations influence the magnitude of rhizosphere effects. *Ecology*, **87**, 1302-1313.
- Phillips RP, FINZI AC, BERNHARDT ES (2011) Enhanced root exudation induces microbial feedbacks to N cycling in a pine forest under long-term CO₂ fumigation. *Ecology Letters*, **14**, 187-194.
- Phillips RP, MEIER IC, BERNHARDT ES, GRANDY AS, WICKINGS K, FINZI AC (2012) Roots and fungi accelerate carbon and nitrogen cycling in forests exposed to elevated CO₂. *Ecology Letters*, **15**, 1042-1049.
- Piao S, CIAIS P, FRIEDLINGSTEIN P *et al.* (2008) Net carbon dioxide losses of northern ecosystems in response to autumn warming. *Nature*, **451**, 49-52.
- Ploetz RC, RAMOS JL, PARRADO JL, LOVATT C (1992) Shoot and root growth phenology of grafted avocado. In: *Proc. Second World Avocado Congress. University of California, Riverside, USA*. pp 215-220.
- Pregitzer KS, KING JA, BURTON AJ, BROWN SE (2000) Responses of tree fine roots to temperature. *New Phytologist*, **147**, 105-115.
- Pregitzer KS, LASKOWSKI MJ, BURTON AJ, LESSARD VC, ZAK DR (1998) Variation in sugar maple root respiration with root diameter and soil depth. *Tree Physiology*, **18**, 665-670.

- Pritchard SG, Strand AE, McCormack ML *et al.* (2008) Fine root dynamics in a loblolly pine forest are influenced by free-air-CO₂-enrichment: a six-year-minirhizotron study. *Global Change Biology*, **14**, 588-602.
- Psarras G, Merwin IA, Lakso AN, Ray JA (2000) Root Growth Phenology, Root Longevity, and Rhizosphere Respiration of Field Grown Mutsu' Apple Trees on Malling 9 Rootstock. *Journal of the American Society for Horticultural Science*, **125**, 596-602.
- R Development Core Team (2013) R: A language and environment for statistical computing., Vienna, Austria, R Foundation for Statistical Computing.
- Rasband W (1997) 2012 ImageJ US National Institutes of Health Bethesda, Maryland, USA <http://imagej.nih.gov/ij/> [accessed on 12 January 2013].
- Raynaud X (2010) Soil properties are key determinants for the development of exudate gradients in a rhizosphere simulation model. *Soil Biology and Biochemistry*, **42**, 210-219.
- Reich P (1999) World Biomes Map. In: *Soil climate map*. Washington D.C., USDA-NRCS, Soil Science Division, World Soil Resources.
- Reich P, Walters M, Tjoelker M, Vanderklein D, Buschena C (2002) Photosynthesis and respiration rates depend on leaf and root morphology and nitrogen concentration in nine boreal tree species differing in relative growth rate. *Functional Ecology*, **12**, 395-405.
- Reich PB, Teskey RO, Johnson PS, Hinckley TM (1980) Periodic root and shoot growth in oak. *Forest Science*, **26**, 590-598.

- Repo T, Lehto T, Finér L (2008) Delayed soil thawing affects root and shoot functioning and growth in Scots pine. *Tree Physiology*, **28**, 1583-1591.
- Restrepo-Coupe N, Da Rocha HR, Hutryra LR *et al.* (2013) What drives the seasonality of photosynthesis across the Amazon basin? A cross-site analysis of eddy flux tower measurements from the Brasil flux network. *Agricultural and Forest Meteorology*, **182**, 128-144.
- Revelle R, Suess HE (1957) Carbon dioxide exchange between atmosphere and ocean and the question of an increase of atmospheric CO₂ during the past decades. *Tellus*, **9**, 18-27.
- Richardson AD, Carbone MS, Keenan TF *et al.* (2013) Seasonal dynamics and age of stemwood nonstructural carbohydrates in temperate forest trees. *New Phytologist*, **197**, 850-861.
- Richardson AD, Hollinger DY, Dail DB, Lee JT, Munger JW, O'keefe J (2009) Influence of spring phenology on seasonal and annual carbon balance in two contrasting New England forests. *Tree Physiology*, **29**, 321-331.
- Ritchie ME, Silver J, Oshlack A, Holmes M, Diyagama D, Holloway A, Smyth GK (2007) A comparison of background correction methods for two-colour microarrays. *Bioinformatics*, **23**, 2700-2707.
- Roberti JA, Sanclements MD, Loescher HW, Ayres E (2014) Traceable Calibration, Performance Metrics, and Uncertainty Estimates of Minirhizotron Digital Imagery for Fine-Root Measurements. *PLoS One*, **9**, e112362.

- Rodrigo A, Recous S, Neel C, Mary B (1997) Modelling temperature and moisture effects on C–N transformations in soils: comparison of nine models. *Ecological Modelling*, **102**, 325-339.
- Rufty TW, Raper CD, Jackson WA (1981) Nitrogen assimilation, root growth and whole plant responses of soybean to root temperature, and to carbon dioxide and light in the aerial environment. *New Phytologist*, **88**, 607-619.
- Rytter R-M (2001) Biomass production and allocation, including fine-root turnover, and annual N uptake in lysimeter-grown basket willows. *Forest Ecology and Management*, **140**, 177-192.
- Sauer D, Kuzyakov Y, Stahr K (2006) Short Communication Spatial distribution of root exudates of five plant species as assessed by ¹⁴C labeling. *J. Plant Nutr. Soil Sci*, **169**, 360-362.
- Savage K, Davidson E, Tang J (2013) Diel patterns of autotrophic and heterotrophic respiration among phenological stages. *Global Change Biology*.
- Scagel CF, Bi G, Fuchigami LH, Regan RP (2007) Seasonal variation in growth, nitrogen uptake and allocation by container-grown evergreen and deciduous rhododendron cultivars. *HortScience*, **42**, 1440-1449.
- Scheu S (1987) The role of substrate feeding earthworms (Lumbricidae) for bioturbation in a beechwood soil. *Oecologia*, **72**, 192-196.
- Schimel JP, Weintraub MN (2003) The implications of exoenzyme activity on microbial carbon and nitrogen limitation in soil: a theoretical model. *Soil Biology and Biochemistry*, **35**, 549-563.

- Schlesinger WH, Bernhardt ES (2013) *Biogeochemistry: an analysis of global change*, Academic press.
- Schmidt MW, Torn MS, Abiven S *et al.* (2011) Persistence of soil organic matter as an ecosystem property. *Nature*, **478**, 49-56.
- Sharp R (2002) Interaction with ethylene: changing views on the role of abscisic acid in root and shoot growth responses to water stress. *Plant, cell & environment*, **25**, 211-222.
- Sinsabaugh RL, Hill BH, Shah JJF (2009) Ecoenzymatic stoichiometry of microbial organic nutrient acquisition in soil and sediment. *Nature*, **462**, 795-798.
- Sinsabaugh RL, Shah JJF, Findlay SG, Kuehn KA, Moorhead DL (2014) Scaling microbial biomass, metabolism and resource supply. *Biogeochemistry*, 1-16.
- Skjemstad JO, Clarke P, Taylor J, Oades J, McClure SG (1996) The chemistry and nature of protected carbon in soil. *Soil Research*, **34**, 251-271.
- Sloan JL, Jacobs DF (2008) Carbon translocation patterns associated with new root proliferation during episodic growth of transplanted *Quercus rubra* seedlings. *Tree Physiology*, **28**, 1121-1126.
- Smith B, Wårlind D, Arneth A, Hickler T, Leadley P, Siltberg J, Zaehle S (2013) Implications of incorporating N cycling and N limitations on primary production in an individual-based dynamic vegetation model. *Biogeosciences Discussions*, **10**, 18613-18685.

- Spohn M, Carminati A, Kuzyakov Y (2013) Soil zymography—a novel in situ method for mapping distribution of enzyme activity in soil. *Soil Biology and Biochemistry*, **58**, 275-280.
- Spohn M, Kuzyakov Y (2013) Distribution of microbial-and root-derived phosphatase activities in the rhizosphere depending on P availability and C allocation—coupling soil zymography with ^{14}C imaging. *Soil Biology and Biochemistry*, **67**, 106-113.
- Spohn M, Kuzyakov Y (2014) Spatial and temporal dynamics of hotspots of enzyme activity in soil as affected by living and dead roots—a soil zymography analysis. *Plant and Soil*, **379**, 67-77.
- Steinaker DF, Wilson SD (2008) Phenology of fine roots and leaves in forest and grassland. *Journal of Ecology*, **96**, 1222-1229.
- Steinaker DF, Wilson SD, Peltzer DA (2010) Asynchronicity in root and shoot phenology in grasses and woody plants. *Global Change Biology*, **16**, 2241-2251.
- Sternberg SR (1983) Biomedical Image Processing. *Computer*, **16**, 22-34.
- Stocker T, Qin D, Plattner G *et al.* (2013) IPCC, 2013: Climate Change 2013: The Physical Science Basis. Contribution of Working Group I to the Fifth Assessment Report of the Intergovernmental Panel on Climate Change.
- Strickland MS, Rousk J (2010) Considering fungal: bacterial dominance in soils—methods, controls, and ecosystem implications. *Soil Biology and Biochemistry*, **42**, 1385-1395.

- Suseela V, Conant RT, Wallenstein MD, Dukes JS (2012) Effects of soil moisture on the temperature sensitivity of heterotrophic respiration vary seasonally in an old-field climate change experiment. *Global Change Biology*, **18**, 336-348.
- Swenson NG (2014) Phylogenetic imputation of plant functional trait databases. *Ecography*, **37**, 105-110.
- Tang J, Riley WJ (2015) Weaker soil carbon-climate feedbacks resulting from microbial and abiotic interactions. *Nature Climate Change*, **5**, 56-60.
- Tang J, Zhuang Q (2009) A global sensitivity analysis and Bayesian inference framework for improving the parameter estimation and prediction of a process-based Terrestrial Ecosystem Model. *Journal of Geophysical Research: Atmospheres (1984–2012)*, **114**.
- Taylor BN, Beidler KV, Cooper ER, Strand AE, Pritchard SG (2013) Sampling volume in root studies: the pitfalls of under-sampling exposed using accumulation curves. *Ecology Letters*, **16**, 862-869.
- Taylor BN, Beidler KV, Strand AE, Pritchard SG (2014) Improved scaling of minirhizotron data using an empirically-derived depth of field and correcting for the underestimation of root diameters. *Plant and Soil*, **374**, 941-948.
- Teskey RO, Hinckley TM (1981) Influence of Temperature and Water Potential on Root-Growth of White Oak. *Physiologia Plantarum*, **52**, 363-369.
- Tingey DT, Johnson MG, Phillips DL, Johnson DW, Ball JT (1996) Effects of elevated CO₂ and nitrogen on the synchrony of shoot and root growth in ponderosa pine. *Tree Physiology*, **16**, 905-914.

- Todd-Brown K, Randerson J, Post W, Hoffman F, Tarnocai C, Schuur E, Allison S (2013) Causes of variation in soil carbon simulations from CMIP5 Earth system models and comparison with observations. *Biogeosciences*, **10**, 1717-1736.
- Trumbore S, Da Costa ES, Nepstad DC *et al.* (2006) Dynamics of fine root carbon in Amazonian tropical ecosystems and the contribution of roots to soil respiration. *Global Change Biology*, **12**, 217-229.
- Tryon PR, Chapin Iii FS (1983) Temperature control over root growth and root biomass in taiga forest trees. *Canadian Journal of Forest Research*, **13**, 827-833.
- Tscherko D, Hammesfahr U, Marx M-C, Kandeler E (2004) Shifts in rhizosphere microbial communities and enzyme activity of *Poa alpina* across an alpine chronosequence. *Soil Biology and Biochemistry*, **36**, 1685-1698.
- Urbanski S, Barford C, Wofsy S *et al.* (2007) Factors controlling CO₂ exchange on timescales from hourly to decadal at Harvard Forest. *Journal of Geophysical Research-Biogeosciences*, **112**.
- Vamerali T, Ganis A, Bona S, Mosca G (1999) An approach to minirhizotron root image analysis. *Plant and Soil*, **217**, 183-193.
- Vapaavuori E, Iivonen S, Rikala R (2001) Seasonal root growth of Scots pine seedlings in relation to shoot phenology, carbohydrate status, and nutrient supply. *Canadian Journal of Forest Research-Revue Canadienne De Recherche Forestiere*, **31**, 1569-1578.

- Vapaavuori E, Rikala R, Ryyppö A (1992) Effects of root temperature on growth and photosynthesis in conifer seedlings during shoot elongation. *Tree Physiology*, **10**, 217-230.
- Vendettuoli JF, Orwig DA, Krumins JA, Waterhouse MD, Preisser EL (2015) Hemlock woolly adelgid alters fine root bacterial abundance and mycorrhizal associations in eastern hemlock. *Forest Ecology and Management*, **339**, 112-116.
- Vogt KA, Grier CC, Gower ST, Sprugel DG, Vogt DJ (1986) Overestimation of net root production: a real or imaginary problem? *Ecology*, 577-579.
- Wallenstein MD, McNulty S, Fernandez IJ, Boggs J, Schlesinger WH (2006) Nitrogen fertilization decreases forest soil fungal and bacterial biomass in three long-term experiments. *Forest Ecology and Management*, **222**, 459-468.
- White C, Kemanian A, Kaye J (2014) Implications of carbon saturation model structures for simulated nitrogen mineralization dynamics. *Biogeosciences*, **11**, 6725-6738.
- Whittaker RH (1970) *Communities and ecosystems*, New York, Macmillan.
- Wieder W, Grandy A, Kallenbach C, Bonan G (2014) Integrating microbial physiology and physiochemical principles in soils with the Microbial-Mineral Carbon Stabilization (MIMICS) model. *Biogeosciences Discussions*, **11**, 1147-1185.
- Wieder WR, Bonan GB, Allison SD (2013) Global soil carbon projections are improved by modelling microbial processes. *Nature Climate Change*, **3**, 909-912.
- Wilcox CS, Ferguson JW, Fernandez GC, Nowak RS (2004) Fine root growth dynamics of four Mojave Desert shrubs as related to soil moisture and microsite. *Journal of Arid Environments*, **56**, 129-148.

- Willaume M, Pagès L (2006) How periodic growth pattern and source/sink relations affect root growth in oak tree seedlings. *Journal of Experimental Botany*, **57**, 815-826.
- World Weather Information Service (2013). World Meteorological Organization.
- Wofsy SC, Goulden ML, Munger JW *et al.* (1993) Net exchange of CO₂ in a midlatitude forest. *Science*, **260**, 1314-1317.
- Woodward F, Lomas M (2004) Vegetation dynamics—simulating responses to climatic change. *Biological reviews*, **79**, 643-670.
- Wright AN, Warren SL, Blazich FA, Blum U (2004) Root and Shoot Growth Periodicity of *Kalmia latifolia* Sarah' and *Ilex crenata* Compacta'. *HortScience*, **39**, 243-247.
- Wu C, Chen JM, Black TA *et al.* (2013) Interannual variability of net ecosystem productivity in forests is explained by carbon flux phenology in autumn. *Global Ecology and Biogeography*, **22**, 994-1006.
- Wu C, Munger JW, Niu Z, Kuang D (2010) Comparison of multiple models for estimating gross primary production using MODIS and eddy covariance data in Harvard Forest. *Remote Sensing of Environment*, **114**, 2925-2939.
- Wullschleger SD, Epstein HE, Box EO *et al.* (2014) Plant functional types in Earth system models: past experiences and future directions for application of dynamic vegetation models in high-latitude ecosystems. *Annals of botany*, mcu077.
- Yamashita M, Imamura H (2007) Shoot and Root Growth and Lysigenous Aerenchyma Formation in Rosetted and Stem-extensional Plants of *Eustoma grandiflorum* (Raf.) Shinn. *園芸学会雑誌*, **76**, 54-59.

- Yavitt JB, Wright SJ (2001) Drought and irrigation effects on fine root dynamics in a tropical moist forest, Panama. *Biotropica*, **33**, 421-434.
- Zasada JC, Tappeiner Iii JC, Maxwell BD, Radwan M (1994) Seasonal changes in shoot and root production and in carbohydrate content of salmonberry (*Rubus spectabilis*) rhizome segments from the central Oregon Coast Ranges. *Canadian Journal of Forest Research*, **24**, 272-277.
- Zeng G, Birchfield ST, Wells CE (2008) Automatic discrimination of fine roots in minirhizotron images. *New Phytologist*, **177**, 549-557.
- Zhu B, Gutknecht JL, Herman DJ, Keck DC, Firestone MK, Cheng W (2014) Rhizosphere priming effects on soil carbon and nitrogen mineralization. *Soil Biology and Biochemistry*, **76**, 183-192.
- Zu Schweinsberg-Mickan MS, Joergensen RG, Müller T (2010) Fate of ¹³C- and ¹⁵N-labelled rhizodeposition of *Lolium perenne* as function of the distance to the root surface. *Soil Biology and Biochemistry*, **42**, 910-918.

CURRICULUM VITAE

Rose Z. Abramoff

Address: 7414 Herschel Ave Apt 305, La Jolla, CA 92037
 Permanent email: rose.abramoff@gmail.com
 Phone number: (858) 531-1076
 Website: blogs.bu.edu/rza

EDUCATION

Boston University **May 2015**

Ph.D. Biology

- Certificate in Terrestrial Biogeoscience
- Advisor: Professor Adrien Finzi

Amherst College

May 2009

B.A. Biology, Theater and Dance

- Advisors: David Ratner, Wendy Woodson

RESEARCH EXPERIENCE

Finzi Lab, Boston University

March 2011-May 2015

Dissertation Research

- Literature review: Are root and shoot phenology in sync?
- The seasonality of C allocation to roots in a mid-latitude forest: Measurements of root growth, mortality and nonstructural carbohydrate content, respiration, and exudation on seasonal timescales; study system is three common northeastern temperate tree species, red oak (*Quercus rubra*), white ash (*Fraxinus americana*), and eastern hemlock (*Tsuga canadensis*)
- Where does the rhizosphere end? Measurements of spatially resolved *in situ* enzyme activity using zymograms incubated in root boxes: Image analysis is used to determine the spatial extent of enzyme activity and their proximity to roots
- Effects of soil warming and N addition on belowground phenology: Temperature and nitrogen manipulation experiment to determine the effect of warming and N fertilization on root mass, growth, mortality, mycorrhizal colonization, and emergence of soil fauna
- DAMM-MCNiP-RRM model fusion: Modular integration of three models that estimate 1) temperature, soil moisture and substrate supply effects on SOM depolymerization, 2) microbial physiology with C and N cycling, 3) rhizosphere and bulk soil spatial distribution and depth scaling

Elsevier **Jan 2010- June 2011**
 Editorial Assistant for Biological Conservation

- Invited appropriate candidates to review submitted manuscripts
- Addressed reviewer and author questions via e-mail on behalf of the journal

Amherst College Biology Department **Summer 2007**
 Independent Undergraduate Research

- Detected GFP (green fluorescent protein) fluorescence in *Dictyostelium discoideum* to determine localization of DG17 gene in the cell
- Transformed a synthetic gene into *Dictyostelium discoideum*
- Trained in use of fluorescent microscopy, confocal microscopy, Western blot, and flow cytometry

Amherst College Chemistry Department **January 2007 – Feb. 2007**
 Laboratory Assistant

- Synthesized organic chemicals, specifically a novel PTP (protein tyrosine phosphatase) inhibitor
- Trained in use of ^{13}C -NMR (nuclear magnetic resonance) spectroscopy

National Center for Microscopy and Imaging Research **Summer 2003, 2006**
 Laboratory Assistant

- Traced regions of interest in the hippocampus of the mouse brain, using xvoxtrace and imod tracing programs
- Created 3-d medium spiny dendrite model
- Performed in situ hybridization on hippocampal, cerebellar, and forebrain sections of mouse brain
- Trained in use of in situ hybridization, immunocytochemistry, cryostat operation

TEACHING EXPERIENCE

Pomona College **May 2013- May 2014**
 Undergraduate thesis advisor

- Served as thesis advisor and first reader for Johanna Recalde's senior honors thesis in root-mycorrhizal interactions
- Helped Johanna develop and execute an independent research project to fulfill honors thesis requirements

Harvard Forest REU Program **May 2013-August 2013, June 2012- August 2012**
 Mentor

- Mentored a total of three students for 11 weeks

- Helped students develop and execute an independent research project

Boston University **Sep 2012-Present, Sep 2010- May 2011**
Teaching Fellow

- Led two laboratory classes per week supervising a total of 42 undergraduate students
- Organized and presented lab curriculum
- Generated learning activities and discussion

Finzi Lab **Jan 2011- August 2012**
Undergraduate Research Intern Mentor

- Coordinated up to 7 undergraduate research interns assisting with lab work
- Managed the independent research project of Amanda Alon, senior Biology major

NSF GK-12 GLACIER **June 2011- June 2012**
Teaching Fellow

- Created and taught science and math curriculum for 5th graders for 10 hours per week

OUTREACH

Advocates for Literacy in Environmental Sciences **April 2012-present**
Founding member, Secretary

- Graduate Student Organization Award for Excellence in Student Activities (2013)

Pierce School Climate Change Summit **January 2013**
Moderator

Curley K-8 School Science Fair **January 2012**
Judge

NSF GK-12 GLACIER Garage Sale Fundraiser **September 2011**
Lead Organizer

Summer Pathways Program: Tech Savvy **July 2011**
Program Coordinator

Biology Inquiry & Outreach with Boston University Graduate Students **May 2011**
Student teacher

POSITIONS HELD

- LTER Higher Education Working Group Member (2013-present)
- Harvard Forest Graduate Student Representative (2013-2015)
- BU Biogeosciences Program Digital Media Committee Member (2014-2015)
- BU Biogeosciences Program Outreach Committee Member (2014-2015)
- Ecological Society of America Member (2012-present)
- American Geophysical Union Member (2012-present)

AWARDS

- Howard Hughes Medical Institute Fellowship (2007)
- Boston University Dean's Fellowship (2009)
- NSF EAPSI Fellowship - Japan (2010)
- Amherst College Fellowship for Graduate Study: Forris Jewett Moore Fellowship (2009-2011)
- NSF GK-12 GLACIER Fellowship (2011)
- Graduate Writing Fellowship (waiting list, 2011)
- Boston University Biogeosciences Fellowship Research Award (2013)
- Boston University Teaching Fellowship (2010, 2012, 2013)
- American Geophysical Union Outstanding Student Paper Award (2013)
- Department of Energy Student Travel Fellowship (2014)
- George R. Bernard, Jr. Travel Award (2012, 2013, 2014)
- American Association of University Women Dissertation Fellowship (2014)
- American Geophysical Union Student Travel Grant Award (2012, 2014)
- Boston University Biogeoscience Symposium Outstanding Oral Presentation Award (2015)

SKILLS

- Computer: Git/GitHub, R, Matlab, SAS, SPSS, JMP, STELLA, ArcGIS, RootFly, ImageJ/Fiji, SigmaPlot, Linux
- General: root viewing box and minirhizotron tube design and installation

PUBLICATIONS

Abramoff RZ, Hirota G, Kobori H, Taguchi M (2010) Abundance of dragonfly species and their habitat preferences in urban restored ponds in Yokohama. *The 6th International Workshop on Sustainable Asia. (conference proceeding)*

Abramoff, RZ, Finzi AC (2015) Are above-and below-ground phenology in sync? *New Phytologist*, **205.3**, 1054-1061.

Finzi AF, Abramoff RZ, Darby BA, Spiller KS, Brzostek ER, Phillips RP (2014) Rhizosphere processes are quantitatively important components of terrestrial carbon and nutrient cycles. *Global Change Biology*.

Abramoff RZ, Finzi AF. Seasonality and partitioning of root allocation to rhizosphere soils in a mid-latitude forest (*in prep*)

Abramoff RZ, Finzi AF. Where does the rhizosphere end? Spatially resolved measurements of in situ soil extracellular enzyme activity (*in prep*)

Abramoff RZ, Davidson EA, Finzi AF. A parsimonious modular approach to building a mechanistic belowground carbon and nitrogen model (*in prep*)

SELECTED PRESENTATIONS

Long Term Ecological Research All Scientists' Meeting (2012), September – **Poster: Phenology of belowground carbon allocation in a mid-latitude forest***

American Geophysical Union Fall Meeting (2013), December – **Presentation: Root phenology at Harvard Forest and beyond**

Northeast Natural History Conference (2014), April – **Invited Presentation: Linking above and belowground phenology at Harvard Forest and beyond**

Department of Energy Terrestrial Ecosystem Science PI Meeting (2014), May – **Poster: Seasonality of carbon allocation to roots in a mid-latitude forest**

Boston University (2014), May – **Guest lecture: Measuring C in terrestrial ecosystems**

Ecological Society of America Annual Meeting (2014), August – **Presentation (Organized Session): What is the relationship between aboveground and belowground phenology? A meta-analysis and case study**

American Geophysical Union Fall Meeting (2014), December – **Invited Presentation: A Parsimonious Modular Approach to Building a Mechanistic Belowground C and N Model**

Harvard Forest Ecology Symposium (2015), March – **Invited presentation: The secret lives of roots: Seasonality and partitioning of belowground C to three Harvard Forest stands**